DESIGN AND MODELLING OF PHOTONIC CRYSTALS WITH ANISOTROPIC COMPONENTS

Joaquín Cos Córcoles

ISBN: 978-84-693-9433-5
Dipòsit Legal: T.69-2011

UNIVERSITAT ROVIRA I VIRGILI
DESIGN AND MODELLING OF PHOTONIC CRYSTALS WITH ANISOTROPIC COMPONENTS
Joaquin Cos Córcoles
ISBN:978-84-693-9433-5/DL:T.69-2011

UNIVERSITAT ROVIRA I VIRGILI
Departament d'Enginyeria Electrònica, Elèctrica i Automàtica

Design and modelling of photonic crystals with anisotropic components

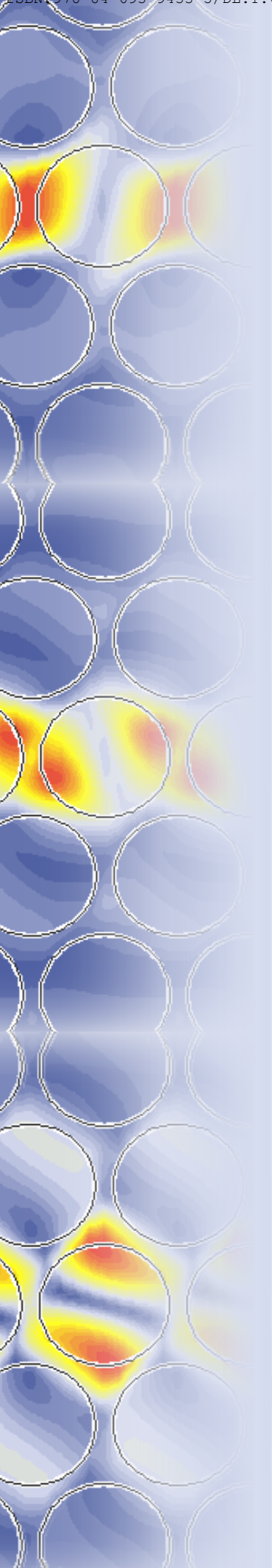

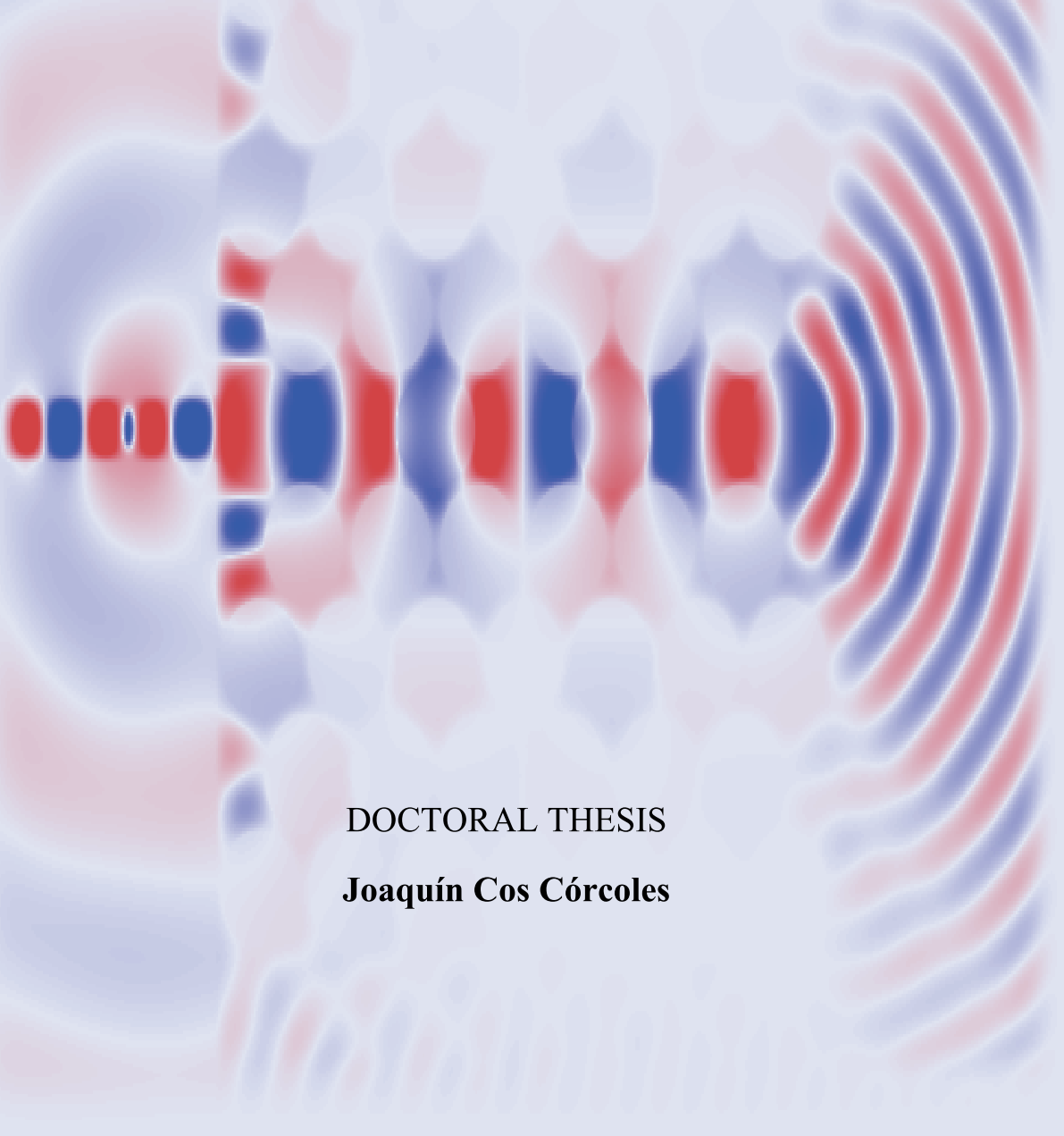

DOCTORAL THESIS

Joaquín Cos Córcoles

UNIVERSITAT ROVIRA I VIRGILI
DESIGN AND MODELLING OF PHOTONIC CRYSTALS WITH ANISOTROPIC COMPONENTS
Joaquin Cos Córcoles
ISBN:978-84-693-9433-5/DL:T.69-2011

UNIVERSITAT ROVIRA I VIRGILI
DESIGN AND MODELLING OF PHOTONIC CRYSTALS WITH ANISOTROPIC COMPONENTS
Joaquin Cos Córcoles
ISBN:978-84-693-9433-5/DL:T.69-2011

Joaquín Cos Córcoles

DESIGN AND MODELLING OF PHOTONIC CRYSTALS WITH ANISOTROPIC COMPONENTS

Doctoral thesis supervised by
Dr. Lluís F. Marsal Garví

Departament d'Enginyeria Electrònica, Elèctrica i Automàtica

UNIVERSITAT ROVIRA I VIRGILI

Tarragona
2010

UNIVERSITAT ROVIRA I VIRGILI
DESIGN AND MODELLING OF PHOTONIC CRYSTALS WITH ANISOTROPIC COMPONENTS
Joaquin Cos Córcoles
ISBN:978-84-693-9433-5/DL:T.69-2011

UNIVERSITAT ROVIRA I VIRGILI
DESIGN AND MODELLING OF PHOTONIC CRYSTALS WITH ANISOTROPIC COMPONENTS
Joaquin Cos Córcoles
ISBN:978-84-693-9433-5/DL:T.69-2011

UNIVERSITAT ROVIRA I VIRGILI
ESCOLA TÈCNICA SUPERIOR D'ENGINYERIA
DEPARTAMENT D'ENGINYERIA ELECTRONICA, ELÈCTRICA I AUTOMÀTICA

Avinguda dels Països Catalans, 26
Campus sescelades
43007 Tarragona
Tel. (977) 55 96 10
Fax (977) 55 96 05
e-mail: secelec@etse.urv.es
http://www.etse.urv.es/DEEEA/

I STATE that the present study, entitled "Design and modelling of photonic crystals with anisotropic components", presented by Joaquín Cos Córcoles for the award of the degree of Doctor, has been carried out under my supervision at the Department of Electrical, Electronic and Automatic Control Engineering of this university, and that it fulfils all the requirements to be eligible for the European Doctorate Award.

Tarragona, 20th September 2010

Doctoral Thesis Supervisor

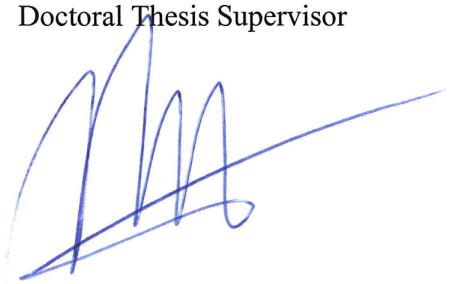

Dr. Lluís Marsal Garví

UNIVERSITAT ROVIRA I VIRGILI
DESIGN AND MODELLING OF PHOTONIC CRYSTALS WITH ANISOTROPIC COMPONENTS
Joaquin Cos Córcoles
ISBN:978-84-693-9433-5/DL:T.69-2011

UNIVERSITAT ROVIRA I VIRGILI
DESIGN AND MODELLING OF PHOTONIC CRYSTALS WITH ANISOTROPIC COMPONENTS
Joaquin Cos Córcoles
ISBN:978-84-693-9433-5/DL:T.69-2011

Acknowledgements

En primer lugar quisiera agradecer a mi director de tesis, Lluís F. Marsal, por darme la oportunidad de desarrollar y difundir este trabajo en su grupo de investigación, por su apoyo y ánimo en los momentos en los que los resultados no eran los esperados, así como las felicitaciones cuando el trabajo daba sus frutos.

Deseo manifestar un especial agradecimiento a Josep Ferré-Borrull por la cantidad de tiempo, paciencia y de folios que ha rellenado con el desarrollo de ecuaciones para dar luz donde yo veía oscuridad. Sin su inestimable ayuda hubiera sido imposible enfrentarme al desarrollo de los modelos computacionales de los métodos numéricos. Gracias a él aprendí que cualquier problema se puede resolver combinando la paciencia con la minuciosidad.

También quiero agradecer a la Universitat Rovira i Virgili, por el soporte económico en forma de beca de investigación sin el que hubiera sido imposible realizar este periodo predoctoral. Por otra parte, no quisiera olvidar el dar las gracias a todos los miembros del Departamento de Ingeniería Electrónica, Eléctrica y Automática (en especial a Josep Pallarès), que de una forma u otra han colaborado para hacer mas fácil mi estancia en este departamento.

UNIVERSITAT ROVIRA I VIRGILI
DESIGN AND MODELLING OF PHOTONIC CRYSTALS WITH ANISOTROPIC COMPONENTS
Joaquin Cos Córcoles
ISBN:978-84-693-9433-5/DL:T.69-2011

A los profesores Lucio Claudio Andreani, Marco Liscidini y Dario Gerace, y en general al *Dipartamento di Fisica "Alessandro Volta"* y la *Universita degli studio di Pavia*, por darme la oportunidad, durante los tres meses de la estancia investigadora con ellos, de desarrollar parte de este trabajo haciéndome sentir parte de su grupo de investigación. También me gustaría agradecerles la atención y rapidez con la que me han atendido antes, durante y después de mi estancia para resolver cualquier duda o gestión que haya sido necesaria.

Quisiera agradecer a los profesores Ignacio Moreno Soriano y María del Mar Sánchez López por hacerme descubrir el fascinante mundo de la investigación, y mantener su interés en mi trabajo pese a ya no estar vinculado a su grupo de investigación. Asimismo, quisiera dar las gracias a mis colegas (y antiguos compañeros de laboratorio) Daniel Puerto y Antonio Martínez, con los que he compartido durante estos años muchas conversaciones (presenciales y telefónicas) relacionadas con nuestro periodo predoctoral o sencillamente sobre nuestra vida.

Me gustaría dar las gracias también a Pilar Formentín y Raquel Palacios por la cantidad de cafés que hemos compartido y que han servido para tener una segunda (y tercera) opinión sobre los avatares del día a día de estos 4 años. Igualmente quiero manifestar mi agradecimiento a Bogdan Nae por la ayuda desinteresada en la corrección del inglés de esta tesis. Por otra parte, no quiero olvidarme de dar las gracias al resto de mis compañeros de grupo (Abel, Jairo, Alejandra, María, Pedro, Victor, Mahbubur, Elisabeth, Lukas, Zdenek y todos aquellos con los que haya compartido el laboratorio) y del resto de grupos del departamento (en especial a Raúl y a Roser) por colaborar en hacer mas agradable este tiempo.

Por último, quisiera agradecer a mi familia por haberme transmitido de forma continua durante 29 años, mediante palabras y el ejemplo de sus actos, que el trabajo es fruto del esfuerzo y la constancia. El cariño, comprensión y apoyo logístico, que de una forma u otra me han brindado durante estos cuatro años, han sido fundamentales durante esta etapa de mi vida.

UNIVERSITAT ROVIRA I VIRGILI
DESIGN AND MODELLING OF PHOTONIC CRYSTALS WITH ANISOTROPIC COMPONENTS
Joaquin Cos Córcoles
ISBN:978-84-693-9433-5/DL:T.69-2011

En especial quisiera agradecer a Elena la cantidad de tiempo y momentos para compartir que ha sido capaz de sacrificar en pos del desarrollo de mi vocación investigadora (espero poder devolvérselos en cómodos plazos), así como la paciencia que ha tenido en los momentos de estrés o concentración absoluta en los que parecía evaporarme. De una forma u otra, parte de este trabajo es gracias a ti.

Por último quiero agradecer a todas aquellas personas que no están incluidas explícitamente en estos agradecimientos y que sin duda, sabrán disculpar que mi mente difusa haya cometido este imperdonable descuido.

Tarragona, a 18 de septiembre de 2010.

This work has been supported by Ministerio de Educación y Ciencia, projects No. TEC2006-06531, TME2008-01343 and TEC2009-09551 and by Generalitat de Catalunya project No. 2009 SGR 549

UNIVERSITAT ROVIRA I VIRGILI
DESIGN AND MODELLING OF PHOTONIC CRYSTALS WITH ANISOTROPIC COMPONENTS
Joaquin Cos Córcoles
ISBN:978-84-693-9433-5/DL:T.69-2011

UNIVERSITAT ROVIRA I VIRGILI
DESIGN AND MODELLING OF PHOTONIC CRYSTALS WITH ANISOTROPIC COMPONENTS
Joaquin Cos Córcoles
ISBN:978-84-693-9433-5/DL:T.69-2011

All truths are easy to understand once they are discovered; the point is to discover them

Galileo Galilei

UNIVERSITAT ROVIRA I VIRGILI
DESIGN AND MODELLING OF PHOTONIC CRYSTALS WITH ANISOTROPIC COMPONENTS
Joaquin Cos Córcoles
ISBN:978-84-693-9433-5/DL:T.69-2011

UNIVERSITAT ROVIRA I VIRGILI
DESIGN AND MODELLING OF PHOTONIC CRYSTALS WITH ANISOTROPIC COMPONENTS
Joaquin Cos Córcoles
ISBN:978-84-693-9433-5/DL:T.69-2011

Publication related to this thesis

Journal articles

J. Cos, J. Ferre-Borrull, J. Pallares, L. F. Marsal, "Tunable Fabry-Perot filter based on one-dimensional photonic crystals with liquid crystal components", *Optics Communications* **282**(6) 1220-1225, (2009).

J. Cos, J. Ferre-Borrull, J. Pallares, L. F. Marsal, "Tunability of a double-cavity Fabry-Perot system based on 1D Photonic Crystals", *Proceedings of the 2009 Spanish Conference on Electron Devices* (*Proceedings Paper*), 364-367, (2009).

J. Cos, J. Ferre-Borrull, J. Pallares, L. F. Marsal, "Double-cavity Fabry-Perot tunable equalizer based on 1D photonic crystals", *International Journal of Numerical Modelling* **23** 400-410, (2010).

J. Cos, J. Ferre-Borrull, J. Pallares, L. F. Marsal, "Analysis of tunable band-gaps in liquid crystal-infiltrated 2D silicon photonic crystals", *Applied Physics B - Lasers and Optics* **100**(4) 833-839, (2010).

UNIVERSITAT ROVIRA I VIRGILI
DESIGN AND MODELLING OF PHOTONIC CRYSTALS WITH ANISOTROPIC COMPONENTS
Joaquin Cos Córcoles
ISBN:978-84-693-9433-5/DL:T.69-2011

J. Cos, J. Ferre-Borrull, J. Pallares, L. F. Marsal, "Optimal tunability of waveguides based on silicon Photonic Crystals infiltrated with Liquid Crystals", *Optics and Quantum Electronic*. Under review

J. Cos, J. Ferre-Borrull, J. Pallares, L. F. Marsal, "Tunable waveguides based on liquid crystal-infiltrated silicon photonic crystals, *Physica Status Solidi C*. Accepted

F. Giorgis, L. Pallavidino, M. Liscidini, A. Virga, A. Chiodoni, E. Descrovi, **J. Cos**, L. C. Andreani, F. Geobaldo, "Synthesis of amorphous silicon/magnesia based direct opals with tunable optical properties", *Chemistry of Materials*. Accepted

J. Cos, M. Liscidini, L. C. Andreani, "Diffraction effects in the optical response of opal photonic crystals in the high-energy region". *Physical Review E*. To be submitted

Communications

J. Cos, L. F. Marsal, J. Pallares, J. Ferre-Borrull , "TE and TM mode analysis for 2D photonic crystals with liquid crystal infiltration", *XVI International Workshop on Optical Waveguide Theory and Numerical Modelling*. Copenague (DINAMARCA). 2007. Poster.

J. Cos, L. F. Marsal, J. Pallares, J. Ferre-Borrull , "Photonic bandgap analysis by transfer matrix method of liquid crystal infiltrated multilayers", *Graduated Student Meeting on Electronic Engineering* (*2007*). Tarragona (ESPAÑA). 2007. Poster.

J. Cos, L. F. Marsal, J. Pallares, J. Ferre-Borrull , "Analysis of tunable 2D silicon photonic crystals", *Graduated Student Meeting on Electronic Engineering* (*2007*). Tarragona (ESPAÑA). 2007. Poster.

J. Cos, L. F. Marsal, J. Pallares, J. Ferre-Borrull , "Análisis de multicapas infiltradas con cristal líquido mediante el método de la matriz de transferencia", *OPTOEL 07. 5ª Reunión Española de Optoelectrónica*. Bilbao (ESPAÑA). 2007. Poster.

J. Cos, L. F. Marsal, J. Pallares, J. Ferre-Borrull, "Design of an optical switch based on 2D tunable photonic crystals", *Graduated Student Meeting on Electronic Engineering* (*2008*). Tarragona (ESPAÑA). 2008. Poster.

UNIVERSITAT ROVIRA I VIRGILI
DESIGN AND MODELLING OF PHOTONIC CRYSTALS WITH ANISOTROPIC COMPONENTS
Joaquin Cos Córcoles
ISBN:978-84-693-9433-5/DL:T.69-2011

J. Cos, L. F. Marsal, J. Pallares, J. Ferre-Borrull, "Analysis of 2D photonic crystals infiltrated with anisotropic materials", *1ª Conferencia Española de Nanofotónica*. Tarragona (ESPAÑA). 2008. Poster.

J. Cos, L. F. Marsal, J. Pallares, J. Ferre-Borrull, "Characterization of 2D anisotropic photonic crystals", *II Barcelona Workshop on Optical Characterisation of Materials*. Barcelona (ESPAÑA). 2008. Poster.

J. Cos, J. Ferre-Borrull, J. Pallares, L. F. Marsal, "Tunability of a double-cavity Fabry-Perot system based on 1D Photonic Crystals", *7th Spanish Conference on Electron Devices*. Santiago de Compostela (ESPAÑA). 2009. Poster.

J. Cos, J. Ferre-Borrull, J. Pallares, L. F. Marsal, "Simple and double cavity Fabry-Perot equalizer", *Graduated Student Meeting on Electronic Engineering* (*2009*). Tarragona (ESPAÑA). 2009. Poster.

J. Cos, J. Ferre-Borrull, J. Pallares, L. F. Marsal, "Modos guiados sintonizables en una guía de onda de cristal fotónico infiltrada con cristales líquidos", *OPTOEL 09, 6ª Reunión Española de Optoelectrónica*. Málaga (ESPAÑA). 2009. Poster.

J. Cos, J. Ferre-Borrull, J. Pallares, L. F. Marsal, "Optimal tunability of waveguides based on silicon Photonic Crystals infiltrated with Liquid Crystals", *XVIII International Workshop on Optical Waveguide Theory and Numerical Modelling*. Cambridge (INGLATERRA). 2010. Oral communication.

J. Cos, J. Ferre-Borrull, J. Pallares, L. F. Marsal, "Tunable Waveguides based on Liquid Crystal-infiltrated Silicon Photonic Crystals", *EMRS*. Estrasburgo (FRANCIA). 2010. Oral communication.

J. Cos, L. F. Marsal, J. Pallares, J. Ferre-Borrull, "Optical characterization of anisotropic porous silicon structures", *2ª Conferencia Española de Nanofotónica*. Segovia (ESPAÑA). 2010. Poster.

J. Cos, J. Ferre-Borrull, J. Pallares, L. F. Marsal, "Analysis of anisotropic photonic crystal waveguides", *Graduated Student Meeting on Electronic Engineering* (*2010*). Tarragona (ESPAÑA). 2010. Oral communication.

UNIVERSITAT ROVIRA I VIRGILI
DESIGN AND MODELLING OF PHOTONIC CRYSTALS WITH ANISOTROPIC COMPONENTS
Joaquin Cos Córcoles
ISBN:978-84-693-9433-5/DL:T.69-2011

UNIVERSITAT ROVIRA I VIRGILI
DESIGN AND MODELLING OF PHOTONIC CRYSTALS WITH ANISOTROPIC COMPONENTS
Joaquin Cos Córcoles
ISBN:978-84-693-9433-5/DL:T.69-2011

Contents

UNIVERSITAT ROVIRA I VIRGILI
DESIGN AND MODELLING OF PHOTONIC CRYSTALS WITH ANISOTROPIC COMPONENTS
Joaquin Cos Córcoles
ISBN:978-84-693-9433-5/DL:T.69-2011

UNIVERSITAT ROVIRA I VIRGILI
DESIGN AND MODELLING OF PHOTONIC CRYSTALS WITH ANISOTROPIC COMPONENTS
Joaquin Cos Córcoles
ISBN:978-84-693-9433-5/DL:T.69-2011

UNIVERSITAT ROVIRA I VIRGILI
DESIGN AND MODELLING OF PHOTONIC CRYSTALS WITH ANISOTROPIC COMPONENTS
Joaquin Cos Córcoles
ISBN:978-84-693-9433-5/DL:T.69-2011

UNIVERSITAT ROVIRA I VIRGILI
DESIGN AND MODELLING OF PHOTONIC CRYSTALS WITH ANISOTROPIC COMPONENTS
Joaquin Cos Córcoles
ISBN:978-84-693-9433-5/DL:T.69-2011

Chapter 1

Introduction and work objectives

The present Communications Age requires more and more efficient devices in terms of speed, consumption and size for the treatment of information. Up to now, the traditional way of transporting and processing large amount of data with Electronic devices has satisfied this demand of the upcoming global information society. However the limits of Moore's law are close to being achieved regarding the scale of transistors with the appearance of Quantum and Short Channel effects. Many of these limitations are expected to be overcome by systems that are based on photons instead of electrons. While in some aspects photonic devices already play a leading role in long-range transmissions through optical fibres, an on-chip manufacturing of photonic circuits is still not achieved at a level mature enough for the market.

The manufacturing of this kind of devices implies the development of the photonic analogs for classical electronic devices such as logical gates, switches, large bandwidth wires, filters,… and therefore many of these photonic devices have to be able to modulate their optical properties.

UNIVERSITAT ROVIRA I VIRGILI
DESIGN AND MODELLING OF PHOTONIC CRYSTALS WITH ANISOTROPIC COMPONENTS
Joaquin Cos Córcoles
ISBN:978-84-693-9433-5/DL:T.69-2011

A combination between nanoscale photonic crystal devices and anisotropic materials is expected to provide a possibility to create electro-optical devices with required characteristics. Within the anisotropic materials, liquid crystal is a serious candidate because its refractive index can be varied either by changing the operating conditions (i.e. temperature) or by applying an external electric field.

In the last decade many efforts have been applied to the theoretical study and development of devices based on photonic crystals with liquid crystal components. For fundamental physical research this means there is a large need for the design and the understanding of systems that can control and manipulate light on small lengthscales, significantly smaller than the wavelength of the light itself.

As the invention of the print was the beginning of the Gutenberg Age, these devices can substitute their conventional optoelectronic analogues and become the beginning of the Optical Age.

The objectives of this work are:

- Development of computer implementations of several numerical methods for the theoretical study of anisotropic structures.
- Analysis of the basic characteristics of one-dimensional (1D) and two-dimensional (2D) structures based on silicon photonic crystals and anisotropic materials, both perfect and with defects.
- Proposal and optimization of functional devices based on these structures, such as optical equalizers or switches.
- Development of a method based on a scattering matrix formalism for the analysis of the optical response of three-dimensional (3D) photonic crystals, which are very suitable for structures for liquid crystal infiltration providing them with tunable conditions.

UNIVERSITAT ROVIRA I VIRGILI
DESIGN AND MODELLING OF PHOTONIC CRYSTALS WITH ANISOTROPIC COMPONENTS
Joaquin Cos Córcoles
ISBN:978-84-693-9433-5/DL:T.69-2011

The thesis is organized as follows:

In chapter 2 an introduction to tunable photonic crystals is given. Firstly, a brief overview of the underlying theory that explains photonic crystal unusual optical properties is presented. Secondly, the physical description of one of the most common optical anisotropic material, the liquid crystal, is given. Finally, different applications of tunable 1D and 2D photonic crystals are presented, in particular, we focus on the applications that have been studied in this work.

Chapter 3 is devoted to the numerical methods. Due to the varied kind of structures it is not efficient to face the study with a single method. Thus we have chosen widely used techniques for the investigation of each kind of photonic crystals (PC). The transfer matrix method is employed for the analysis of one-dimensional photonic crystals, while the plane-wave expansion method and finite-differences time-domain method are employed for the analysis of two-dimensional photonic crystals. For each of the employed methods, the basics of the method are explained, first for a general isotropic case, then the method is extended for our particular case of anisotropic materials and the dimension of the periodicity.

Chapter 4 presents a study of tunable Fabry-Perot interferometer structures composed of alternating layers of silicon and liquid crystal. The dependence of the position in wavelength and the amplitude of resonances with the liquid crystal optical axis orientations are studied for each device by means of the transfer matrix method. Also, a complete characterization of the structures can be obtained in the form of their Jones matrix. From this, an application as optical two-channel equalizer is proposed for each of the devices. The optical two-channel equalizer allows tuning the two resonant wavelengths and their relative amplitude levels by varying the liquid crystal optical axis orientations.

UNIVERSITAT ROVIRA I VIRGILI
DESIGN AND MODELLING OF PHOTONIC CRYSTALS WITH ANISOTROPIC COMPONENTS
Joaquin Cos Córcoles
ISBN:978-84-693-9433-5/DL:T.69-2011

Chapter 5 is dedicated to the study and analysis of tunable filters and waveguide devices based on 2D photonic crystals with anisotropic components. We start our study of the tunable filters by analyzing structures without defects. The studied structures are: a silicon photonic crystal with a triangular lattice of holes infiltrated with liquid crystal and a lattice of silicon rods surrounded by liquid crystal. The second part of this chapter is devoted to the analysis of tunable waveguides. A silicon photonic crystal waveguide, where a line of scatterers filled by liquid crystal acts as the core of the waveguide, is optimized. Finally a methodology for the study of the practical implementation of tunable waveguides is developed, by means of the finite-difference time-domain method and the plane-wave expansion method and the supercell formulation presented in chapter 3 a silicon photonic crystal waveguide with liquid crystal components is studied.

Chapter 6 is devoted to the development of a formalism for the theoretical analysis of opals based on the approximation of each sphere in a stacking of cylinders. The results of this chapter were obtained in collaboration of the Department of Physics "Alessandro Volta" (University of Pavia) during the research stay there.

Chapter 7 completes the thesis with the summary, the discussions and the future work.

UNIVERSITAT ROVIRA I VIRGILI
DESIGN AND MODELLING OF PHOTONIC CRYSTALS WITH ANISOTROPIC COMPONENTS
Joaquin Cos Córcoles
ISBN:978-84-693-9433-5/DL:T.69-2011

Chapter 2

Fundamentals of tunable photonic crystals

Photonic crystals (PC) are materials that consist of periodically varying permittivity and/or permeability. In conventional photonic crystals, the structure of the crystal is fixed at fabrication or design time, which results in designable though not tunable optical properties. There has been a great deal of effort to make photonic crystals tunable.

In this chapter we give an introduction to tunable photonic crystals. We start our description with the basic concepts of photonic crystals and photonic bandgap, linking it with the description of the most common tunable photonic crystals devices. Finally we also describe the physics of one of the most common optical anisotropic materials, the liquid crystal (LC).

UNIVERSITAT ROVIRA I VIRGILI
DESIGN AND MODELLING OF PHOTONIC CRYSTALS WITH ANISOTROPIC COMPONENTS
Joaquin Cos Córcoles
ISBN:978-84-693-9433-5/DL:T.69-2011

2.1 Photonic crystals

Photonic crystals are periodic dielectric or metal-dielectric synthetic structures designed to influence the propagation of electromagnetic waves in the same way as the periodic potential in semiconductor crystals influences the electron motion by defining allowed and forbidden energy bands. The simplest form of the photonic crystal is a one-dimensional periodic structure such as a multilayer film. The propagation of the electromagnetic waves in such structures was first studied by Rayleigh in 1887 [Rayleigh-1887]. It was shown that light propagation is angle dependent and prohibited for a range of frequencies. The possibility to create two- and three-dimensional photonic crystals with two- and three-dimensional forbidden band gaps needed one hundred years more to be proposed almost simultaneously by John and Yablonovich [John-1987; Yablonovitch-1987]. In the last years, several photonic crystal structures with different lengthscale and frequency as been proposed, Schneider *et al.* propose the study of photonic crystals made of coaxial cables that work in the range of the MHz [Schneider-2001], Sánchez-Meroño *et al.* experimentally demonstrate the negative group delay in a photonic crystal made of microstrip dielectric slabs, which work in the range of the GHz [Sánchez-Meroño-2010], finally Torrent *et al.* design a sonic crystal made of elastic cylinders, which is analogue to anisotropic photonic crystal [Torrent-2008].

Fig. 2.1 shows the classification of photonic crystals by the gradually increasing dimension, one-dimensional (1D), two-dimensional (2D) and three-dimensional (3D) photonic crystals depending on whether the periodic variation of the dielectric constant is created in one, two or three dimensions. In each of the cases of the periodicity the spatial period of the elements is called the lattice constant, in analogy with the lattice constant of ordinary crystals composed of a regular array of atoms. In contrast with the case of ordinary crystals, the lattice constant in the photonic crystals case is on the order of the wavelength of the relevant electromagnetic waves for them.

UNIVERSITAT ROVIRA I VIRGILI
DESIGN AND MODELLING OF PHOTONIC CRYSTALS WITH ANISOTROPIC COMPONENTS
Joaquin Cos Córcoles
ISBN:978-84-693-9433-5/DL:T.69-2011

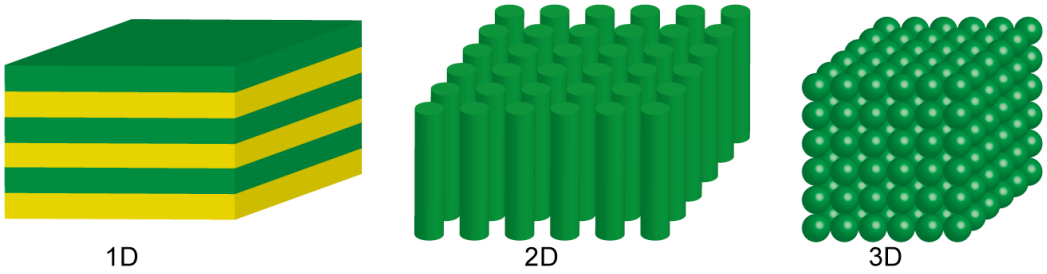

Fig. 2.1 Schematic illustration of one-dimensional (1D), two-dimensional (2D) and three-dimensional (3D) photonic crystals

The one-dimensional photonic crystal are known for several decades [Heavens-1965; Perilloux-2002] in the form of periodic multilayer coatings, consisting of stacked pairs of alternate dielectric or metal-dielectric layers with a large contrast of the dielectric constant along the propagation direction. One-dimensional photonic crystals have a wide range of applications such as stop-band filters, high-reflection mirrors, antireflection coatings, and cavities for distributed feedback lasers.

Two-dimensional photonic crystals consist of a regular array of dielectric or metal-dielectric materials in two directions while the structure is homogeneous and infinite in the other direction. Much of the interest in 2D photonic crystals arises not from the presence of a bandgap alone, but rather from the ability to create localised defect states within the bandgap by introducing a structural defect into an otherwise regular lattice. For example, the removal of a single scatterer from a 2D PC creates a point-like defect or resonant cavity, and the removal of a line of scatterers can create a waveguide that supports propagating modes.

Finally, three-dimensional photonic crystals consist of a regular array of dielectric or metal-dielectric materials in the three directions. This structure is the only one that can exhibit a complete band gap, that is, a frequency range where the propagation of electromagnetic waves is forbidden, irrespective of the propagation direction.

As we commented before, photonic crystals are designed in order to affect the properties of photons in much the same way as ordinary semiconductors affect the properties of electrons. In this way, photonic crystals have forbidden band gaps that

UNIVERSITAT ROVIRA I VIRGILI
DESIGN AND MODELLING OF PHOTONIC CRYSTALS WITH ANISOTROPIC COMPONENTS
Joaquin Cos Córcoles
ISBN:978-84-693-9433-5/DL:T.69-2011

can be compared with the energy gaps between consecutive energy bands of the semiconductors. In order to properly define the concept of the forbidden band gap, we use the definition from [Sakoda-2001].

The following well-known relation between the frequency f, the velocity c, and the wavelength λ_0, of the radiation field in free space is given:

$$c = \lambda_0 f . \tag{2.1}$$

Defining the wave number as $k = 2\pi/\lambda_0$, it can be related with the angular frequency ω as

$$\omega = ck . \tag{2.2}$$

This equation is called the dispersion relation of the radiation field. The density of states of the radiation field in a volume V of free space, $D(\omega)$, is defined by

$$D(\omega) = \frac{\omega^2 V}{\pi^2 c^3} . \tag{2.3}$$

The Eq. (2.3) can be extended for the radiation field in a uniform material with refractive index η, replacing c by $v = c/\eta$. Since the optical properties of atoms and molecules strongly depend on $D(\omega)$, changing the optical properties of atoms and molecules the density of states can be modelled. This is the key idea of photonic crystals where the modification of the distribution of the elements of the structures produces changes in the density of states and the presence of a forbidden band gap for a range of angular frequencies as illustrate the Fig. 2.2:

The one-dimensional photonic crystal case is taken into account by Sakoda [Sakoda-2001] in order to gain an intuitive understanding of the photonic bands and bandgaps. Figure 2.3 shows a schematic view of the structure, where the x axis is taken in the direction perpendicular to the surface of the dielectric layers while y axis is taken in the direction of the polarization. The electric field of the propagated wave in the x direction is denoted by a complex function $E(x,t)$ for convenience. The actual electric field is, of course, a real quantity. It is given by the real part of $E(x, t)$.

UNIVERSITAT ROVIRA I VIRGILI
DESIGN AND MODELLING OF PHOTONIC CRYSTALS WITH ANISOTROPIC COMPONENTS
Joaquin Cos Córcoles
ISBN:978-84-693-9433-5/DL:T.69-2011

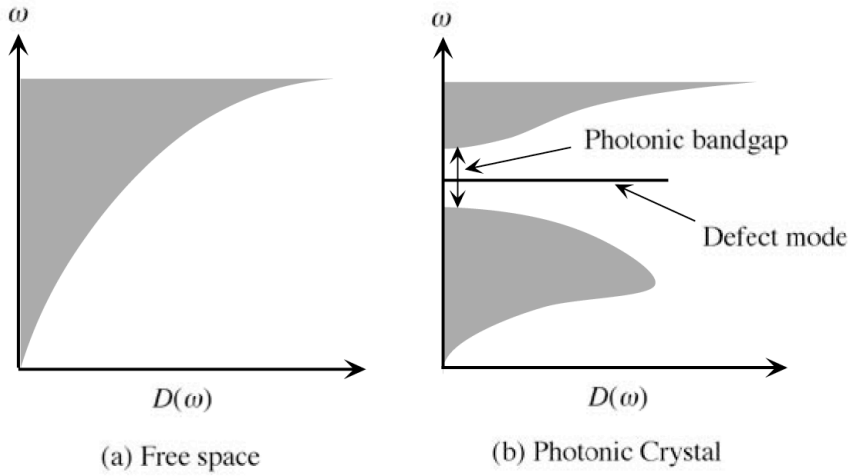

Fig. 2.2 Schematic illustration of the density of states of the radiation field a) in free space and b) in a photonic crystal. In the illustration for the photonic crystal, a photonic bandgap and a localized defect mode with a delta-function like density are included [Sakoda-2001].

Now, the wave equation for $E(x, t)$ is given by

$$\frac{c^2}{\varepsilon(x)}\frac{\partial^2 E}{\partial x^2} = \frac{\partial^2 E}{\partial t^2}, \tag{2.4}$$

where $\varepsilon(x)$ corresponds to the position-dependent dielectric constant of the 1D photonic crystal and the magnetic permeability of the photonic crystal is considered equal to that in free space.

Due to the spatial dependence of the dielectric function, its inverse can be expanded in Fourier series:

$$\varepsilon^{-1}(x) = \sum_{m=-\infty}^{\infty} k_m e^{i\frac{2\pi m}{a}x}, \tag{2.5}$$

where a is the lattice constant, m is an integer and $\{k_m\}$ are the Fourier coefficients.

UNIVERSITAT ROVIRA I VIRGILI
DESIGN AND MODELLING OF PHOTONIC CRYSTALS WITH ANISOTROPIC COMPONENTS
Joaquin Cos Córcoles
ISBN:978-84-693-9433-5/DL:T.69-2011

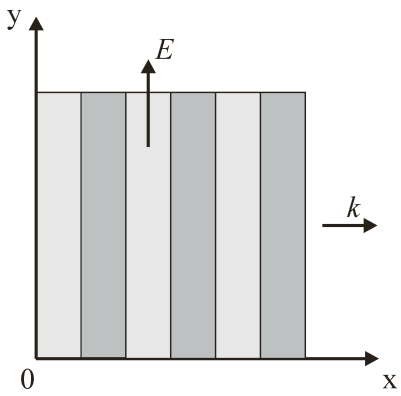

Fig. 2.3 Schematic view of the geometry of the calculation of the photonic band structure, or the dispersion relation, of a 1D photonic crystal.

Since the dielectric constant is assumed to be real, $k_{-m} = k_m^*$ where k_m^* is the complex conjugate of k_m. It is well-known that Bloch's theorem holds for the electronic eigenstates in ordinary crystals because of the spatial periodicity of the potential energy that an electron feels due to the regular array of atomic nuclei [Kittel-1953]. This theorem can be also applied for the case of electromagnetic waves in photonic crystals. Any eigenmode in the one-dimensional crystal is thus characterized by a wave number *k* and expressed as

$$E(x,t) \equiv E_k(x,t) = u_k(x) \cdot e^{i(kx-\omega_k t)}, \tag{2.6}$$

where ω_k denotes the eigenangular frequency and $u_k(x)$ is a periodic function where the period is the lattice constant *a*. Therefore this periodic function can be expanded in Fourier series. As a result, Eq. (2.6) is modified to

$$E_k(x,t) = \sum_{m=-\infty}^{\infty} E_m \cdot e^{i\left[\left(k+\frac{2\pi m}{a}\right)x-\omega_k t\right]}, \tag{2.7}$$

where $\{E_m\}$ are the Fourier coefficients.

In order to simplify the calculations, it is assumed that only components with *m = 0* and *m = ±1* are dominant in the expansion (2.5), and becomes

$$\varepsilon^{-1}(x) \approx k_0 + k_1 e^{i\frac{2\pi}{a}x} + k_{-1} e^{-i\frac{2\pi}{a}x}. \tag{2.8}$$

When we substitute (2.7) and (2.8) into the wave equation (2.4), we obtain

UNIVERSITAT ROVIRA I VIRGILI
DESIGN AND MODELLING OF PHOTONIC CRYSTALS WITH ANISOTROPIC COMPONENTS
Joaquin Cos Córcoles
ISBN:978-84-693-9433-5/DL:T.69-2011

$$k_1\left\{k+\frac{2(m-1)\pi}{a}\right\}^2 E_{m-1}+k_{-1}\left\{k+\frac{2(m+1)\pi}{a}\right\}^2 E_{m+1}\approx\left\{\frac{\omega_k^2}{c^2}-k_0\left(k+\frac{2m\pi}{a}\right)^2\right\}E_m . \quad (2.9)$$

According to the Sakoda assumption that E_0 and E_{-1} are dominant and all others terms can be neglected, the following coupled equations can be obtained:

$$(\omega_k^2-k_0c^2k^2)E_0-k_1c^2\left(k-\frac{2\pi}{a}\right)^2 E_{-1}=0, \quad (2.10a)$$

$$-k_1c^2k^2E_0+\left\{\omega_k^2-k_0c^2\left(k-\frac{2\pi}{a}\right)^2\right\}E_{-1}=0. \quad (2.10b)$$

These linear equations have a nontrivial solution when the determinant of coefficients vanishes:

$$\begin{vmatrix}\omega_k^2-k_0c^2k^2 & -k_1c^2\left(k-\frac{2\pi}{a}\right)^2\\ -k_1c^2k^2 & \omega_k^2-k_0c^2\left(k-\frac{2\pi}{a}\right)^2\end{vmatrix}=0. \quad (2.11)$$

Defining $h = k - \pi/a$, the solutions for the Eq. (2.11) are given by

$$\omega_\pm\approx\frac{\pi c}{a}\sqrt{k_0\pm|k_1|}\pm\frac{ac}{\pi|k_1|\sqrt{k_0}}\left(k_0^2-\frac{|k_1|^2}{4}\right)h^2, \quad (2.12)$$

as long as $|h| << \pi/a$. So, there is no mode in the interval

$$\frac{\pi c}{a}\sqrt{k_0-|k_1|}<\omega<\frac{\pi c}{a}\sqrt{k_0+|k_1|}. \quad (2.10b)$$

This gap disappears when $k_1 = 0$. This result can be interpreted that the modes with $k \approx \pi/a$ and $k \approx -\pi/a$ were mixed with each other in the presence of the periodic modulation of the dielectric constant and this mixing led to a frequency splitting.

UNIVERSITAT ROVIRA I VIRGILI
DESIGN AND MODELLING OF PHOTONIC CRYSTALS WITH ANISOTROPIC COMPONENTS
Joaquin Cos Córcoles
ISBN:978-84-693-9433-5/DL:T.69-2011

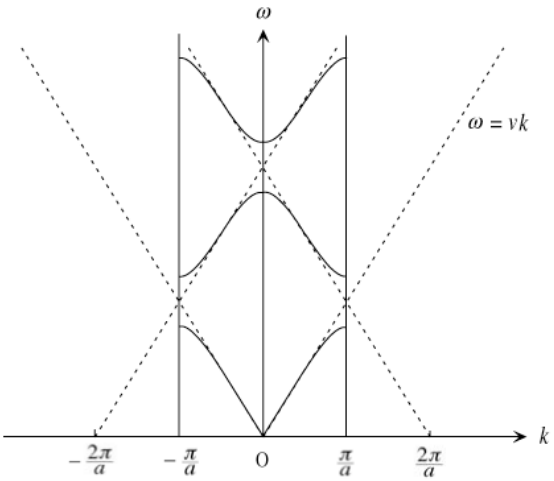

Fig. 2.4 Dispersion relation for a 1D photonic crystal (solid lines). The boundary of the first Brillouin zone is denoted by two vertical lines. The dispersion lines in the uniform material are denoted by dashed lines. They are folded into the first Brillouin zone taking into account the identity of the wave numbers, which differ from each other by a multiple of 2π/a. When two dispersion lines cross, they repel each other and a photonic bandgap appears. [Sakoda-2001].

In general, those wave vectors that differ from each other by a multiple of $2\pi/a$ should be regarded as equal because of the presence of the periodic spatial modulation of the dielectric constant. When the spatial modulation is small, the dispersion relation in the photonic crystal is not so far from $\omega = vk$, but it should thus be expressed with the wave vector in the first Brillouin zone, $[-\pi/a, \pi/a]$. In addition, if two dispersion lines cross each other, a frequency gap appears. All these things are schematically illustrated in Fig. 2.4. There are an infinite number of frequency gaps in the spectrum. However, we should note that this is true only as far as we deal with optical waves travelling in the *x* direction, and that there is no gap when we take into consideration those modes travelling in other directions.

The dispersion relations for 2D and 3D photonic crystals are different from the 1D photonic crystal. The fact that all wave vectors are not parallel to each other in two and three dimensions, however, makes a large difference. Depending on the type of the lattice, the high symmetry points change. Chapter 3 will show more details about it.

UNIVERSITAT ROVIRA I VIRGILI
DESIGN AND MODELLING OF PHOTONIC CRYSTALS WITH ANISOTROPIC COMPONENTS
Joaquin Cos Córcoles
ISBN:978-84-693-9433-5/DL:T.69-2011

2.2 Anisotropic materials: Liquid crystals

Liquid crystals are materials whose molecular structure, in a certain temperature domain, represents an intermediate state of order (mesophase) between the crystalline and the liquid phase. Whereas in crystals the molecules have a three-dimensional long-range order of both position and orientation, liquid molecules do not show any long-range order. In the solid state, the molecules are strongly bound together by attraction forces, each molecule has its well defined place in the crystal lattice (positional order) and the molecular axes are pointing in a specific direction (orientational order), the degree of order is thus very high. In the liquid state, the bounds between molecules are weak, the molecules have high freedom of movement, positionally as well as directionally, and the degree of order is very low. Characteristic for the liquid crystals is thus a degree of order somewhere in between.

Materials changes their molecular phase as a function of their temperature. For a temperature lower than the temperature T_M (melting point) materials are in the crystalline phase. Opposite, for a temperature higher than the temperature T_C (clearing point) materials are in the liquid phase. Between this two temperature limits, T_C and T_M materials are in the liquid crystalline phase and exhibit high viscosity and an opaque appearance. At molecular level, the following happens: at the temperature T_M the molecular bonding forces break down to such an extent that the molecules have more freedom of movement as in the crystalline lattice; they remain however roughly oriented along a common reference axis (the director). Then, when the temperature T_C is reached, the bonding forces between molecules are further weakened, to the extent that the degree of order lowers and the material crosses over into the liquid phase (Fig. 2.5). The liquid crystalline phase, occurring between T_M and T_C , is also known as mesophase.

UNIVERSITAT ROVIRA I VIRGILI
DESIGN AND MODELLING OF PHOTONIC CRYSTALS WITH ANISOTROPIC COMPONENTS
Joaquin Cos Córcoles
ISBN:978-84-693-9433-5/DL:T.69-2011

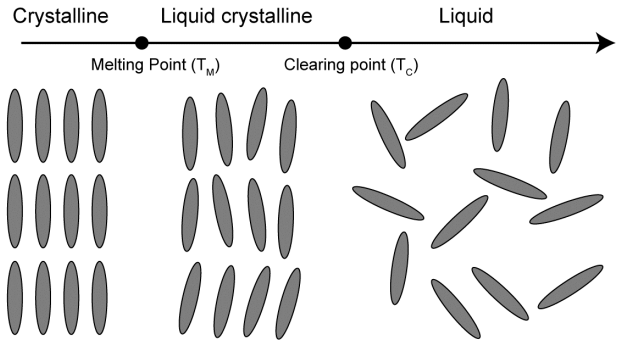

Fig. 2.5. Types of state a material depending on the temperature.

Liquid crystals are soft condensed matter systems of major technological and scientific interest. In liquid crystals the orientational order of the constituent molecules is associated with a reduced or absent translational order. This gives liquid crystalline systems a combination of fluidity (liquid-like properties) and anisotropic electro-optic properties, similar to those of a crystal. Orientational order can be controlled easily by the application of external fields, leading to the spatial switching of bulk properties in response to external stimuli. This provides the basis for a wide range of technological applications, including displays, optical switches, adaptive optics for telescopes and many other electro-optical devices.

The reasons for the formation of a mesophase can be the molecular shape or a microphase separation of amphiphilic compounds. These materials can be classified by chemical structures and physical characteristics (Table 2.1). Generally, molecules of liquid crystalline substances have the following shapes:

- Rod-like molecules, which form calamitic liquid crystals (nematic, smectic and cholesteric phases).
- Disk-like molecules, which form discotic liquid crystals (discoid nematic and discotic phases).
- Amphiphilic compounds, which form layered columnar or cubic phases in the pure state and in solution.

UNIVERSITAT ROVIRA I VIRGILI
DESIGN AND MODELLING OF PHOTONIC CRYSTALS WITH ANISOTROPIC COMPONENTS
Joaquin Cos Córcoles
ISBN:978-84-693-9433-5/DL:T.69-2011

Shape	Rod-like molecules	Disk-like molecules
Phase structure	Calamitic liquid crystals	Discotic liquid crystals
Mesophase units	Thermotropic liquid crystals	Lyotropic liquid crystals
Mesophase origin	Amphiphilic liquid crystals	Monophilic liquid crystals

Table 2.1. Classifications of liquid crystals

In the case of the rod-like molecules, liquid crystals can be at the nematic, smectic and cholesteric phases. The nematic phase (Fig. 2.6) has the lowest degree of order. The nematic phase is the simplest and most widespread liquid crystalline phase [Gennes-1993]. Apart from the common alignment along the director, the molecules have no other positional restriction. The nematic liquid crystals are thus closest to the liquid state, in the case of a temperature raise a nematic liquid crystal crosses over directly into liquid. The nematic phase of a liquid crystal is characterized by a global alignment of the molecules in a direction called the nematic director $n(r)$, and an otherwise translational disorder. In the smectic phase (Fig. 2.6), the degree of order grows and the liquid crystal is closer to the crystalline state. In addition to the alignment along the common director, the molecules show a tendency of arranging themselves in layers. Finally, in the cholesteric phase (Fig. 2.6), the liquid crystal consists of thin layers of nematic molecules, with the director rotating from layer to layer with a small angle.

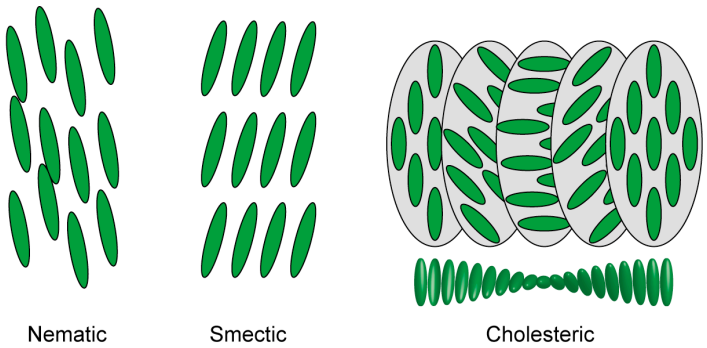

Fig. 2.6. Schematic representation of a liquid crystal sample in the nematic, smectic and cholesteric phases.

UNIVERSITAT ROVIRA I VIRGILI
DESIGN AND MODELLING OF PHOTONIC CRYSTALS WITH ANISOTROPIC COMPONENTS
Joaquin Cos Córcoles
ISBN:978-84-693-9433-5/DL:T.69-2011

The tendency of the liquid crystals molecules, to orient themselves along a preferred direction, causes anisotropy. A number of physical magnitudes are anisotropic in liquid crystals: viscosity, dielectric permittivity, magnetic susceptibility and optical refractive index. The optical anisotropy is one of the most useful properties for the application of liquid crystals in photonic crystal devices; this property is employed in this thesis for the design of several tunable devices. For the sake of simplicity, optical anisotropy will be referred to as anisotropy throughout this thesis.

Optical anisotropy is closely related to the polarization that occurs in a liquid crystal in the presence of an electric field. An external electric field causes a dipole moment per unit volume (due to charge separation on the molecules). This dipole moment per unit volume is called polarization and is composed of summation of elementary dipole moments of each molecule. The optical anisotropy is defined as $\Delta n = n_e - n_o$, where n_e is the extraordinary and n_o is the ordinary refractive index. For nematics phases, n_e corresponds to $n_{\parallel}$ and n_o corresponds to $n_{\perp}$. For $n_{\perp}$ the vibration vector of plane-polarized light is perpendicular to the optical axis (the director), while for $n_{\parallel}$ the vibration vector of plane-polarized light is parallel to the optical axis (the director). For the majority of LCs the value of Δn is positive. Because the refractive index and the dielectric constant are related, the same description of the optical anisotropy can be extended to the dielectric constant. In this way, the orientation of molecules in an electric field is determined by the sign of the dielectric anisotropy ($\Delta\varepsilon = \varepsilon_{\parallel} - \varepsilon_{\perp}$); $\varepsilon_{\parallel}$ and $\varepsilon_{\perp}$ are the dielectric constants measured parallel and perpendicular to the director.

Nematic liquid crystals are widely used as electro-optic switching devices for displays. They have many attractive features, such as large area formation and low driving voltages, with low power consumption. In addition to displays, this material is considered usable for optical devices such as optical switching elements and wavelength variable filters [Hirabayashi-1993]. In particular, the response speed of nematic liquid crystals is on the order of milliseconds. Research toward optical switching at higher speeds has been carried out extensively [Baier-Saip-1995].

UNIVERSITAT ROVIRA I VIRGILI
DESIGN AND MODELLING OF PHOTONIC CRYSTALS WITH ANISOTROPIC COMPONENTS
Joaquin Cos Córcoles
ISBN:978-84-693-9433-5/DL:T.69-2011

2.3 Application of tunable photonic crystals

Photonic crystals offer an important opportunity to design new optical devices and hold a great potential for many significant applications, such as semiconductor lasers and solar cells [Painter-1999], high quality resonator and filters [Meade-1991], and optical fibers [Knight-1998].

Furthermore, lately there are enough endeavours towards the direction of tuning the properties of photonic crystals in order to design switchable devices. Various structures combining photonic crystals with nonlinear or liquid crystal materials have been proposed [Busch-1999; Takeda-2004; Maksymov-2006]. Furthermore, a high-intensity control signal with optical and low frequency outside the bandgap changes the properties of the crystal [Cuesta-Soto-2004].

In this section we explain in detail several applications for tunable 1D and 2D photonic crystals.

2.3.1 One-dimensional photonic crystals

2.3.1.1 Tunable distributed Bragg reflectors

Distributed Bragg reflectors (DBRs) are dielectric multilayers based on the effect of multiple interferences that occur when a light beam is reflected by various dielectric layers. Depending on the number of layers and their size and refraction index for certain range of wavelengths the structure presents a high reflectivity. The most common application of the DBRs is filtering [Fink-1998], but they have also been used as sensors of the light polarization [Schaadt-2007], and as a part of microcavities [Lei-2010] and waveguides [Xifre-2007].

UNIVERSITAT ROVIRA I VIRGILI
DESIGN AND MODELLING OF PHOTONIC CRYSTALS WITH ANISOTROPIC COMPONENTS
Joaquin Cos Córcoles
ISBN:978-84-693-9433-5/DL:T.69-2011

The introduction of anisotropic components like liquid crystals in the structure allows changing the range of wavelengths where the structure presents a high reflectivity. Bowley *et al.* [Bowley-2001] present a tunable distributed Bragg reflector based on polymer and polymer-dispersed liquid crystal (PDLC) layers. By means of the application of voltage the high reflectivity region can be tuned in wavelength or suppressed (if the PDLC refraction index matches with the polymer refraction index).

A similar structure but considering silicon and liquid crystal layers is proposed by Tolmachev *et al.* [Tolmachev-2007]. They theoretically and experimentally study the electro-optical effect on a tunable DBR. In particular, they show that there is a shift of the band edge, which depends on the state (pseudoisotropic or homeotropic) of the liquid crystal.

As an example of application of tunable DBRs, Gilardi *et al.* [Gilardi-2010] propose a planar waveguide with a liquid crystal cell acting as a tunable DBR. The topology of the electrodes allows periodical regions with different liquid crystal directors creating the tunable DBR.

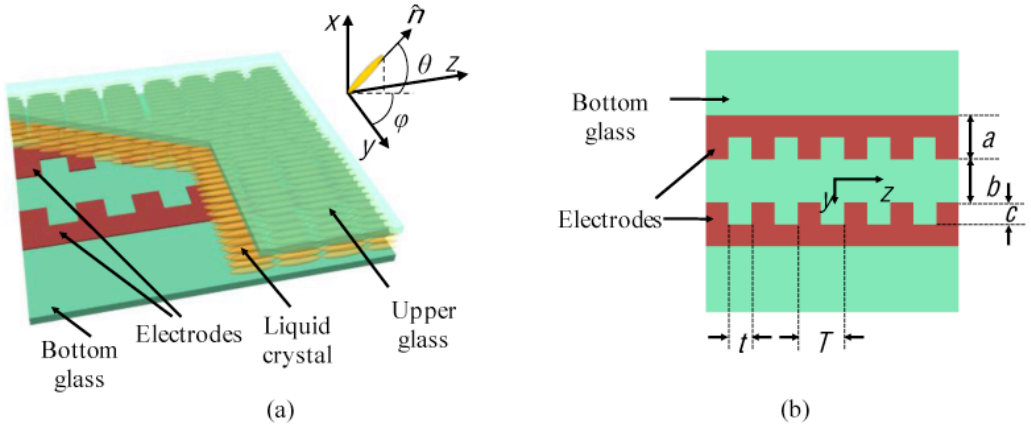

Fig. 2.7. a) 3D sketch of the Bragg reflector and (inset) molecular director, b) top view of the coplanar comb electrode pattern in ITO. [Gilardi-2010]

UNIVERSITAT ROVIRA I VIRGILI
DESIGN AND MODELLING OF PHOTONIC CRYSTALS WITH ANISOTROPIC COMPONENTS
Joaquin Cos Córcoles
ISBN:978-84-693-9433-5/DL:T.69-2011

2.3.1.2 Tunable microcavities

Microcavities consist of two parallel DBRs separated by a spacer layer acting as a cavity, whose refractive index can be the same or different to the ones used for the DBRs. The optical thickness of the cavity is normally equal to the design wavelength, λ, or half of the wavelength, $\lambda/2$. The introduction of this cavity (acting as a defect in the photonic crystal structure) permits that defect states, corresponding to localized modes in the defect, exist in the range of wavelengths of the band gap [Joannopoulus-1995]. Therefore the microcavity transmission spectrum as a function of wavelength exhibits peaks of large transmission corresponding to resonances of the cavity. This kind of devices has applications as band-pass filters with a tuned position of the peak [Mazzoleni-1995], chemical sensors [Karakali-2009], and broadening of photoluminescence peaks [Li-2010].

The active modulation of the resonant peaks provides the foundation for a variety of tunable components. In this way, the resonance peak position and intensity can be controlled by filling one or more layers of the structure with liquid crystal.

Ha *et al.* [Ha-2001] theoretically demonstrates that introducing a liquid crystal layer into a DBR, acts as a defect layer and creates a resonance, which can be tuned by an external applied electric field. This electrical control of the liquid crystal, and consequently of the resonance wavelength position has been experimentally demonstrated by Weiss *et al.* [Weiss-2005]. In their work they present a microcavity based on a porous silicon Fabry-Perot where all the structure is filled by liquid crystal. Applying an electric field or heating the structure the position of the resonance is modulated.

UNIVERSITAT ROVIRA I VIRGILI
DESIGN AND MODELLING OF PHOTONIC CRYSTALS WITH ANISOTROPIC COMPONENTS
Joaquin Cos Córcoles
ISBN:978-84-693-9433-5/DL:T.69-2011

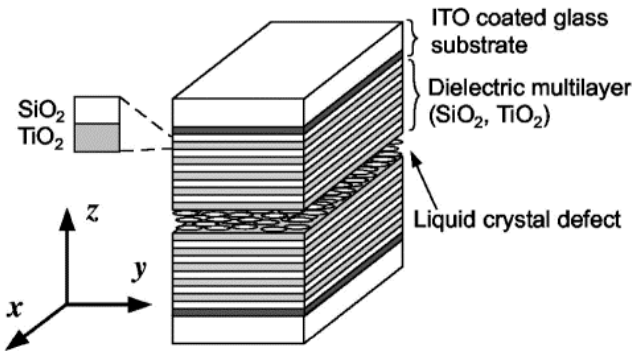

Fig. 2.8. One-dimensional photonic crystal with a liquid defect. [Ozaki-2003]

Several authors propose to place a liquid crystal layer between two DBRs. In this way, Villar *et al.* [Villar-2003] theoretically propose a tunable wavelength filter integrated in a optical fiber, where the application of voltage shifts the position of the resonances into the band gap, providing the structure with the capability of a high finesse filter. Song *et al.* [Song-2007] propose a tunable laser controlled by temperature; they theoretically and experimentally demonstrate that the resonance peak of a liquid crystal layer between two DBRs can be tuned by heating the structure. Finally, Ozaki *et al.* [Ozaki-2003; Ozaki-2005; Ozaki-2007] study microcavities based on DBRs of alternative layers of SiO_2 and TiO_2 and a cavity of liquid crystal. They theoretically and experimentally study the electrical tuning of the wavelength of the resonance; additionally they demonstrate that the structure can be used as a high-speed optical switch with a switch speed of the order of microseconds.

UNIVERSITAT ROVIRA I VIRGILI
DESIGN AND MODELLING OF PHOTONIC CRYSTALS WITH ANISOTROPIC COMPONENTS
Joaquin Cos Córcoles
ISBN:978-84-693-9433-5/DL:T.69-2011

2.3.2 Two-dimensional photonic crystal

2.3.2.1 Tunable waveguides

Photonic crystal waveguides consist of a photonic crystal with a linear defect, which works as the kernel of the waveguide while the rest of the photonic crystal works as the cladding. Guiding light using waveguides is one of the fundamental properties of optics that enables a range of all-optical devices to be created. Additionally to the main objective of guiding the light, waveguides accomplish an important role as tapers [Talneau-2002], junctions [Fan-2001] or polarizers [Liu-2005].

The addition of liquid crystal components to photonic crystal devices would prove advantageous to tuning these devices to some degree in order to enable switching or frequency modulation of the light.

Mingaleev *et al.* [Mingaleev-2004] propose several optical circuits based on the infiltration of individual pores of the photonic crystal. The simplest circuit proposed in that work consists on the infiltration of a line of scatterers, which act as defects, with liquid crystal or polymers. In addition they propose a *90º* waveguide bend, beam splitters and waveguide intersection where the liquid crystal infiltration acts as defect of the structures.

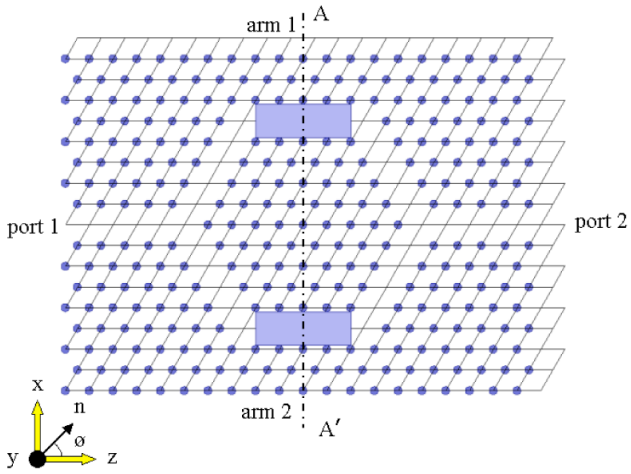

Fig. 2.9. Photonic crystal waveguide Mach-Zehnder interferometer with liquid crystals. Shaded regions, parts infiltrated with liquid crystal waveguides. Diagram at lower left, director of a liquid crystal. [Liu-2004]

UNIVERSITAT ROVIRA I VIRGILI
DESIGN AND MODELLING OF PHOTONIC CRYSTALS WITH ANISOTROPIC COMPONENTS
Joaquin Cos Córcoles
ISBN:978-84-693-9433-5/DL:T.69-2011

Another strategy is proposed by Liu *et al.* [Liu-2006] and consists of the infiltration of a region of scatterers out of the waveguide in order to control a channel drop filter. The resonant modes can be changed by means of the variation of the liquid crystal optical axis orientation by adjusting the applied electric field.

Finally, the third strategy consist on the infilling of all the line of defects of the waveguide. In that way, Takeda *et al.* [Takeda-2003] propose a Y-shaped waveguide where the rotation of the LC optical axis allows controlling the direction of light propagation. A similar idea uses Liu *et al.* [Liu-2004] in order to propose a tunable photonic crystal waveguide coupler.

2.3.2.2 Tunable cavities

Photonic crystal cavities are photonic crystal structures where a point region of the elements is surrounded by the rest of the photonic crystal in order to create a cavity where the light can be confined. As an advantage over classical cavities, photonic crystal cavities are predicted to provide the desired combination of both small mode volume and high quality factor values. The most important application of this kind of cavities is lasers [Painter-1999], although other applications include sensing [Adams-2005] and enhancing the effects of quantum dots [Hughes-2009].

Tuning the optical properties of the cavities makes the structures functional and reconfigurable. In this way, several materials are employed for achieving the tuning. Faraon *et al.* [Faraon-2008] use chalcogenide glasses in order to tune the resonance wavelength by illuminating the chalcogenide glass with light above their band gap. Intoni *et al.* [Intoni-2009] propose achieving the tuning by means of the infiltration of the cavity with water and controlling the evaporation of the water, in this case the tuning of the device being non-reversible.

UNIVERSITAT ROVIRA I VIRGILI
DESIGN AND MODELLING OF PHOTONIC CRYSTALS WITH ANISOTROPIC COMPONENTS
Joaquin Cos Córcoles
ISBN:978-84-693-9433-5/DL:T.69-2011

Several works suggest the infiltration of the photonic crystal cavities with liquid crystal in order to tune the optical properties of the devices. Maune *et al.* [Maune-2005] propose to control the quality factor by means of the infiltration of the photonic crystal cavity with liquid crystal. A photoaddressable polymer (PAP) layer controls the orientation of the liquid crystal. Exciting the photoaddressable polymer layer with a laser, the alignment of the liquid crystal within the defects of the cavity can be different to the alignment of the liquid crystal outside the defects of the cavity, and the quality factor is controlled.

Schuller *et al.* [Schuller-2005] infiltrate a microcavity integrated in a photonic crystal waveguide with liquid crystal in order to control the resonance wavelength by means of small temperature changes. In particular, they compare TE and TM modes resonant positions for the temperature where the liquid crystal changes from ordered nematic phase to disordered isotropic phase.

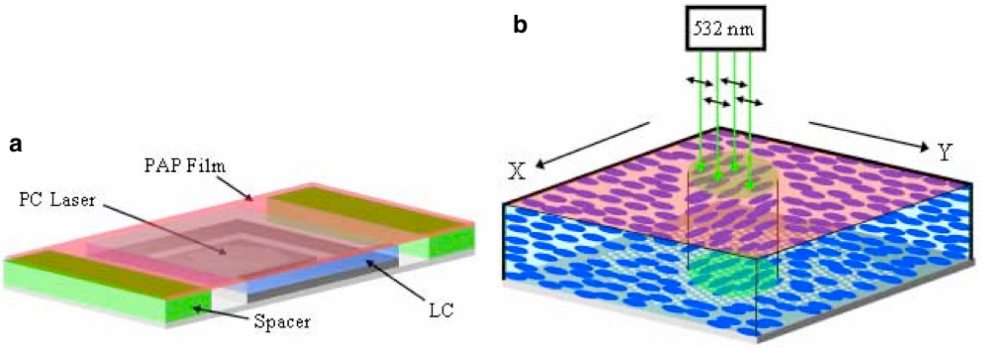

Fig. 2.10. a) Schematic of photonic crystal laser LC/PAP cell. Thickness of LC and PAP films are approximately 5 μm, and 31 ± 1 nm, respectively. Top coverslip is not shown. b) Schematic representation of the LC reorientation via PAP photoinduced alignment. The PAP orients itself orthogonally (along x axis) with respect to the writing laser polarization direction (y axis), which in turn induces a similar alignment in the LC. [Maune-2005]

UNIVERSITAT ROVIRA I VIRGILI
DESIGN AND MODELLING OF PHOTONIC CRYSTALS WITH ANISOTROPIC COMPONENTS
Joaquin Cos Córcoles
ISBN:978-84-693-9433-5/DL:T.69-2011

UNIVERSITAT ROVIRA I VIRGILI
DESIGN AND MODELLING OF PHOTONIC CRYSTALS WITH ANISOTROPIC COMPONENTS
Joaquin Cos Córcoles
ISBN:978-84-693-9433-5/DL:T.69-2011

Chapter 3

Numerical methods for photonic crystals based on anisotropic materials

In this chapter we introduce the numerical methods employed in this thesis for the analysis of photonic crystal structures based on optical anisotropic materials. As we commented previously, when anisotropy appear in the text it is always referring to optical anisotropy. Due to the varied kind of structures it is not possible to face the study up with a single method. Thus we have chosen widely used techniques for the investigation of each kind of photonic crystals (PC).

On one hand, the transfer matrix method (TMM) is a very powerful technique for the analysis of one-dimensional photonic crystals. It is based on the modelling of the wave propagation through the layers and the interference phenomena of these waves in the interface of the layers on stratified structures.

UNIVERSITAT ROVIRA I VIRGILI
DESIGN AND MODELLING OF PHOTONIC CRYSTALS WITH ANISOTROPIC COMPONENTS
Joaquin Cos Córcoles
ISBN:978-84-693-9433-5/DL:T.69-2011

On the other hand, for the analysis of two-dimensional structures we have used two methods, plane-wave expansion method (PWEM), and finite-difference time-domain (FDTD) method. The first of the two methods is a very effective frequency-domain method for obtaining the band structure of a photonic crystal. The second of these methods works in the time domain and it is the most used method for the analysis of the transmission and other related magnitudes of photonic crystal based devices.

The chapter is organized as follows. First, the modelling of the anisotropic materials is presented; this modelling will be common for all the methods in terms of the dielectric tensor. Then, the transfer matrix method will start the description of the numerical methods employed in this Thesis, where the description starts with the general case of isotropic materials and later the method is extended to the anisotropic materials case. The second of the analyzed methods is the plane-wave expansion method, where the description starts with the isotropic formulation and then the method is applied to 2D anisotropic photonic crystals. Finally, a short introduction to the finite-difference time-domain method is given.

3.1 Modelling of anisotropic materials for the theoretical analysis

Anisotropic materials are materials that can split an incident light beam in two (uniaxial) or three (biaxial) linear polarized perpendicular beams. As is commented in the second chapter, liquid crystal (LC) is a kind of anisotropic material where its optical axis, which defines the anisotropy, can be oriented in different angles by means of external fields. In this thesis, we center the study on the uniaxial liquid crystals, where there are two polarization directions corresponding to the ordinary and extraordinary refractive indexes.

UNIVERSITAT ROVIRA I VIRGILI
DESIGN AND MODELLING OF PHOTONIC CRYSTALS WITH ANISOTROPIC COMPONENTS
Joaquin Cos Córcoles
ISBN:978-84-693-9433-5/DL:T.69-2011

In an isotropic medium, the electric field is related proportionally to the electric displacement, the proportionality being a scalar factor (dielectric permittivity),

$$\mathbf{D} = \varepsilon_0 \varepsilon_r \mathbf{E}, \tag{3.1}$$

where ε_0 and ε_r are the dielectric permittivity in vacuum and the relative dielectric permittivity of the medium respectively.

In anisotropic media each component of the electric displacement in the main directions depends on the three components in the main directions of the electric field:

$$D_x = \varepsilon_0 \varepsilon_{xx} E_x + \varepsilon_0 \varepsilon_{xy} E_y + \varepsilon_0 \varepsilon_{xz} E_z, \tag{3.2a}$$

$$D_y = \varepsilon_0 \varepsilon_{yx} E_x + \varepsilon_0 \varepsilon_{yy} E_y + \varepsilon_0 \varepsilon_{yz} E_z, \tag{3.2b}$$

$$D_z = \varepsilon_0 \varepsilon_{zx} E_x + \varepsilon_0 \varepsilon_{zy} E_y + \varepsilon_0 \varepsilon_{zz} E_z. \tag{3.2c}$$

Thus, in anisotropic materials the electric displacement and the electric field are related through a *3x3* tensor:

$$\tilde{\varepsilon} = \begin{pmatrix} \varepsilon_{xx} & \varepsilon_{xy} & \varepsilon_{xz} \\ \varepsilon_{yx} & \varepsilon_{yy} & \varepsilon_{yz} \\ \varepsilon_{zx} & \varepsilon_{zy} & \varepsilon_{zz} \end{pmatrix}. \tag{3.3}$$

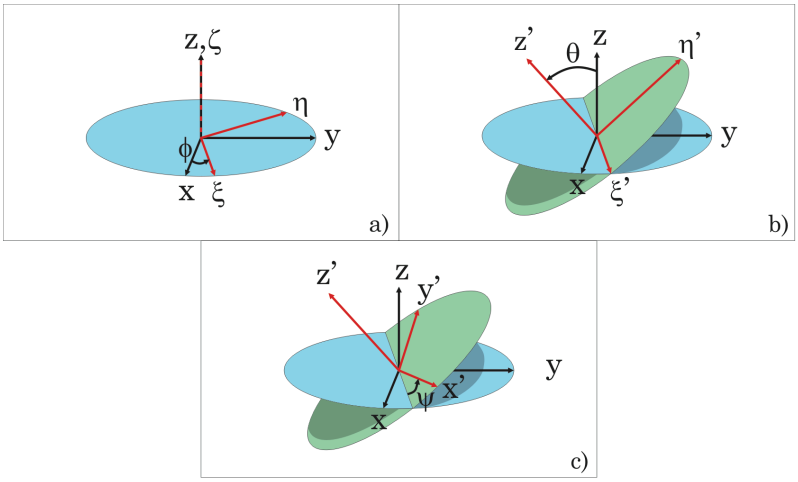

Fig. 3.1 Euler angles for the coordinated rotation matrix. Axes x, y, and z for a fixed space can be rotated to axes x', y', and z' by means of three rotations. a) ϕ Angle. b) θ Angle. c) ψ Angle.

UNIVERSITAT ROVIRA I VIRGILI
DESIGN AND MODELLING OF PHOTONIC CRYSTALS WITH ANISOTROPIC COMPONENTS
Joaquin Cos Córcoles
ISBN:978-84-693-9433-5/DL:T.69-2011

In the particular case of the uniaxial liquid crystals, the anisotropy is characterized by two refractive indexes (or dielectric constants), ordinary and extraordinary and an orientation of the molecules of the liquid crystal.

In order to obtain the dielectric tensor of a LC for a given optical axis orientation we must define a transformation matrix, which depend of the Euler angles ϕ, θ, and ψ, defined in Fig. 3.1, and the dielectric constant tensor:

$$\tilde{\varepsilon} = A\begin{pmatrix} \varepsilon_o & 0 & 0 \\ 0 & \varepsilon_o & 0 \\ 0 & 0 & \varepsilon_e \end{pmatrix} A^{-1}, \tag{3.4}$$

where ε_o and ε_e are the ordinary and extraordinary dielectric constant and A is the coordinated rotation matrix as defined by [Yeh-1979]

$$A = \begin{pmatrix} \cos\psi\cos\phi - \cos\theta\sin\phi\sin\psi & -\sin\psi\cos\phi - \cos\theta\sin\phi\cos\psi & \sin\theta\sin\phi \\ \cos\psi\sin\phi + \cos\theta\cos\phi\sin\psi & -\sin\psi\sin\phi + \cos\theta\cos\phi\cos\psi & -\sin\theta\cos\phi \\ \sin\theta\sin\psi & \sin\theta\cos\psi & \cos\theta \end{pmatrix}. \tag{3.5}$$

By combining Eqs. (3.4) and (3.5) we obtain the dielectric constant tensor defined in Eq. (3.2), which includes the LC's optical axis orientation.

3.2 Transfer matrix method

The transfer matrix method (TMM) is the most widely used method for theoretical study of the light transmission through one-dimensional structures. This method allows obtaining the reflection and transmission spectra [Kitahara-2004], the band diagram [Dubey-2007], and other variables as the density of modes or the polarization state [Mandatori-2003; Mao-1994]. We begin by introducing the method for isotropic materials and then the formalism is extended to the anisotropic case.

UNIVERSITAT ROVIRA I VIRGILI
DESIGN AND MODELLING OF PHOTONIC CRYSTALS WITH ANISOTROPIC COMPONENTS
Joaquin Cos Córcoles
ISBN:978-84-693-9433-5/DL:T.69-2011

3.2.1 Formulation of the transfer matrix method for isotropic structures

In this method, each layer of a stacking is associated to two kinds of matrixes, the dynamical matrix *D* and the propagation matrix *P*. Considering the structure showed in Fig. 3.2 composed of a stacking of *N* kinds of isotropic materials with refractive index and thickness n_i and h_i respectively, the dielectric structure can be defined as

$$n(x)=\begin{cases} n_1, & x_0 < x < x_1 \\ n_2, & x_1 < x < x_2 \\ \vdots & \\ n_N, & x_{N-1} < x < x_N \end{cases}. \tag{3.6}$$

It is considered oblique the incidence of the plane electromagnetic waves with the incidence θ. Thus electric and magnetic fields for TE (3.7a) and TM (3.7b) polarizations can be expressed in the form

$$E(x,z)=E(x)e^{\pm ik_z z}, \tag{3.7a}$$

$$H(x,z)=H(x)e^{\pm ik_z z}, \tag{3.7b}$$

where we assume the plane of propagation is the *xz* plane and k_z is the *z* component of the wave propagation vector. The solutions for electric and magnetic field distribution within the *j-th* layer is composed by two partial waves that describe the incoming and outgoing waves and can be written in the form

$$F_j(x,z)=\left(A_j e^{-ik_{jx}(x-x_j)}+B_j e^{ik_{jx}(x-x_j)}\right)e^{-ik_z z}, \tag{3.8}$$

where *F* replaces the electric field for TE polarization and the magnetic field for TM polarization, A_j and B_j are the amplitudes of the plane wave at the interface $x = x_j$, $k_{jx} = \omega \cdot n_j \cdot \cos(\theta_j)/c$ is the *x* component of the wave vector, ω is the angular frequency, *c* is the vacuum speed of light and θ_j is the ray angle in the *j-th* layer and can be obtained by means of the Snell's law:

$$n_j \sin(\theta_j)=n_{j-1}\sin(\theta_{j-1}). \tag{3.9}$$

UNIVERSITAT ROVIRA I VIRGILI
DESIGN AND MODELLING OF PHOTONIC CRYSTALS WITH ANISOTROPIC COMPONENTS
Joaquin Cos Córcoles
ISBN:978-84-693-9433-5/DL:T.69-2011

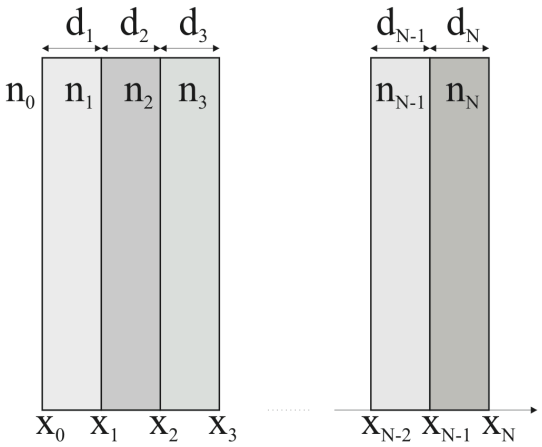

Fig. 3.2 Schematic view of a stratified medium.

Due to the continuity conditions at the interfaces, the plane wave amplitudes at each side of an interface can be related by means of the dynamical matrix D with the following relation:

$$\begin{pmatrix} A_{j-1} \\ B_{j-1} \end{pmatrix} = D_{j-1}^{-1} D_j \begin{pmatrix} A_j \\ B_j \end{pmatrix}, \tag{3.10}$$

where the dynamical matrix has different formulation for TE (Eq. 3.11a) and TM (Eq. 3.11b) modes and can be expressed as

$$D_j^{TE} = \begin{pmatrix} 1 & 1 \\ n_j \cos\theta_j & -n_j \cos\theta_j \end{pmatrix}, \tag{3.11a}$$

$$D_j^{TM} = \begin{pmatrix} \cos\theta_j & \cos\theta_j \\ n_j & -n_j \end{pmatrix}. \tag{3.11b}$$

Finally the propagation matrix P, which describes the propagation in both incoming and outgoing directions through each layer, is defined by

$$P_j = \begin{pmatrix} e^{ik_{jx}d_j} & 0 \\ 0 & e^{-ik_{jx}d_j} \end{pmatrix}. \tag{3.12}$$

UNIVERSITAT ROVIRA I VIRGILI
DESIGN AND MODELLING OF PHOTONIC CRYSTALS WITH ANISOTROPIC COMPONENTS
Joaquin Cos Córcoles
ISBN:978-84-693-9433-5/DL:T.69-2011

Combining Eqs. (3.11) and (3.12) we can define the M_j matrix, which corresponds to the transfer matrix of the *j-th* layer as

$$M_j = D_j^{-1} P_j D_j, \tag{3.13}$$

where D_j and its own inverse are Eq. (3.11a) for TE modes or (3.11b) for TM modes. Consequently the M matrix, which corresponds to the total transfer matrix of a structure composed of N layers, is given by

$$M = \prod_{j=1}^{N} M_j = \begin{pmatrix} M_{11} & M_{12} \\ M_{21} & M_{22} \end{pmatrix}. \tag{3.14}$$

This M matrix expresses the relation between the electric field amplitudes at the beginning of the structure x_0 and the amplitudes at the end of the structure x_N in the following way

$$\begin{pmatrix} A_0 \\ B_0 \end{pmatrix} = \begin{pmatrix} M_{11} & M_{12} \\ M_{21} & M_{22} \end{pmatrix} \begin{pmatrix} A_N \\ B_N \end{pmatrix}, \tag{3.15}$$

and allows us to obtain the Reflectance and Transmittance of the structure as

$$R = |r|^2 = \left| \frac{B_0}{A_0} \Big|_{B_N=0} \right|^2 = \left| \frac{M_{21}}{M_{11}} \right|^2, \tag{3.16a}$$

$$T = \frac{n_N \cos\theta_N}{n_0 \cos\theta_0} |t|^2 = \frac{n_N \cos\theta_N}{n_0 \cos\theta_0} \left| \frac{A_N}{A_0} \Big|_{B_N=0} \right|^2 = \frac{n_N \cos\theta_N}{n_0 \cos\theta_0} \left| \frac{1}{M_{11}} \right|^2. \tag{3.16a}$$

UNIVERSITAT ROVIRA I VIRGILI
DESIGN AND MODELLING OF PHOTONIC CRYSTALS WITH ANISOTROPIC COMPONENTS
Joaquin Cos Córcoles
ISBN:978-84-693-9433-5/DL:T.69-2011

3.2.2 Extension of the method for anisotropic components structures

The TMM was generalized for the case of anisotropic materials by Yeh [Yeh-1979]. This method is based on two kinds of matrixes, the dynamical matrix *D* and the propagation matrix *P*, in contrast to the isotropic case, the matrix size now being *4x4*. As we commented previously, different to the isotropic case, in anisotropic materials the polarization state of a plane wave may vary as it propagates in the medium. Thus, we need to consider these two polarizations and the changes of the plane waves in the analysis of the propagation.

In the isotropic model, we considered two amplitudes to describe the electric or magnetic field (Eq. (3.8)) one corresponding to the wave travelling in the positive direction and another corresponding to the wave travelling in the negative direction. Now, each of these amplitudes must be subdivided into two amplitudes, corresponding to the two main polarization directions. Therefore, the electric and magnetic field in the *j-th* layer can be described as a combination of four partial waves with amplitudes $A_{j\sigma}$, $\sigma = 1,2,3,4$:

$$E_j = \sum_{\sigma=1}^{4} A_{j\sigma}\mathbf{p}_{j\sigma} e^{i[\alpha x+\beta y+\gamma_{j\sigma}(z-z_j)-\omega t]}, \qquad (3.17a)$$

$$H_j = \sum_{\sigma=1}^{4} A_{j\sigma}\mathbf{q}_{j\sigma} e^{i[\alpha x+\beta y+\gamma_{j\sigma}(z-z_j)-\omega t]}, \qquad (3.17b)$$

where α, β, and $\gamma_{j\sigma}$ are the *x*, *y* and *z* propagation components, respectively, $\mathbf{p}$ and $\mathbf{q}$ vectors gives the polarization of each of the four partial waves in the beginning of the *j-th* layer and are described as

UNIVERSITAT ROVIRA I VIRGILI
DESIGN AND MODELLING OF PHOTONIC CRYSTALS WITH ANISOTROPIC COMPONENTS
Joaquin Cos Córcoles
ISBN:978-84-693-9433-5/DL:T.69-2011

$$\mathbf{p}_{j\sigma} = N_{j\sigma}\begin{pmatrix} \left(\left(\frac{\omega}{c}\right)^2\varepsilon_{jyy}-\alpha^2-\gamma_{j\sigma}^2\right)\left(\left(\frac{\omega}{c}\right)^2\varepsilon_{jzz}-\alpha^2-\beta^2\right)-\left(\left(\frac{\omega}{c}\right)^2\varepsilon_{jyz}+\beta\gamma_{j\sigma}\right)^2 \\ \left(\left(\frac{\omega}{c}\right)^2\varepsilon_{jyz}+\beta\gamma_{j\sigma}\right)\left(\left(\frac{\omega}{c}\right)^2\varepsilon_{jxz}+\alpha\gamma_{j\sigma}\right)-\left(\left(\frac{\omega}{c}\right)^2\varepsilon_{jxy}+\alpha\beta\right)\left(\left(\frac{\omega}{c}\right)^2\varepsilon_{jzz}-\alpha^2-\beta^2\right) \\ \left(\left(\frac{\omega}{c}\right)^2\varepsilon_{jxy}+\alpha\beta\right)\left(\left(\frac{\omega}{c}\right)^2\varepsilon_{jyz}+\beta\gamma_{j\sigma}\right)-\left(\left(\frac{\omega}{c}\right)^2\varepsilon_{jxz}+\alpha\gamma_{j\sigma}\right)\left(\left(\frac{\omega}{c}\right)^2\varepsilon_{jyy}-\alpha^2-\gamma_{j\sigma}^2\right) \end{pmatrix}, \quad (3.18)$$

$$\mathbf{q}_{j\sigma} = \frac{c(\alpha e_x+\beta e_y+\gamma_{j\sigma}e_z)}{\mu_0\omega}\times\mathbf{p}_{j\sigma}, \quad (3.19)$$

where μ_0 is the vacuum magnetic permeability with $N_{j\sigma}$ defined as a normalization constant such that $\mathbf{p}_{j\sigma}\,\mathbf{p}_{j\sigma} = 1$.

The propagation constants $\gamma_{j\sigma}$ of the *j-th* layer can be obtained by solving the equation obtained by vanishing the determinant:

$$\begin{vmatrix} \left(\frac{\omega}{c}\right)^2\varepsilon_{jxx}-\beta^2-\gamma_j^2 & \left(\frac{\omega}{c}\right)^2\varepsilon_{jxy}+\alpha\beta & \left(\frac{\omega}{c}\right)^2\varepsilon_{jxz}+\alpha\gamma_j \\ \left(\frac{\omega}{c}\right)^2\varepsilon_{jyx}+\alpha\beta & \left(\frac{\omega}{c}\right)^2\varepsilon_{jyy}-\alpha^2-\gamma_j^2 & \left(\frac{\omega}{c}\right)^2\varepsilon_{jyz}+\beta\gamma_j \\ \left(\frac{\omega}{c}\right)^2\varepsilon_{jzx}+\alpha\gamma_j & \left(\frac{\omega}{c}\right)^2\varepsilon_{jzy}+\beta\gamma_j & \left(\frac{\omega}{c}\right)^2\varepsilon_{jzz}-\alpha^2-\beta^2 \end{vmatrix} = 0. \quad (3.20)$$

Again, due to the continuity conditions at the interfaces, the plane waves at each side of an interface can be related by means of the dynamical matrix *D* in the same way as Eq. (3.10), but now, this dynamical matrix is a *4x4* matrix given by

$$D_j = \begin{pmatrix} e_x\cdot\mathbf{p}_{j1} & e_x\cdot\mathbf{p}_{j2} & e_x\cdot\mathbf{p}_{j3} & e_x\cdot\mathbf{p}_{j4} \\ e_y\cdot\mathbf{q}_{j1} & e_y\cdot\mathbf{q}_{j2} & e_y\cdot\mathbf{q}_{j3} & e_y\cdot\mathbf{q}_{j4} \\ e_y\cdot\mathbf{p}_{j1} & e_y\cdot\mathbf{p}_{j2} & e_y\cdot\mathbf{p}_{j3} & e_y\cdot\mathbf{p}_{j4} \\ e_x\cdot\mathbf{q}_{j1} & e_x\cdot\mathbf{q}_{j2} & e_x\cdot\mathbf{q}_{j3} & e_x\cdot\mathbf{q}_{j4} \end{pmatrix}. \quad (3.21)$$

It is important to mention that for anisotropy orientations where the off-diagonal elements of the matrix of the Eq. (3.3) are zero, the mode coupling disappears and thus the dynamical matrix has to be block diagonalized. This requires that A_1 and A_2 are the amplitudes of the same polarization and propagate in opposite direction each.

UNIVERSITAT ROVIRA I VIRGILI
DESIGN AND MODELLING OF PHOTONIC CRYSTALS WITH ANISOTROPIC COMPONENTS
Joaquin Cos Córcoles
ISBN:978-84-693-9433-5/DL:T.69-2011

Likewise, A_3 and A_4 are amplitudes of the plane waves of the other polarization and propagate in opposite direction each.

The propagation matrix P in *j-th* layer depends on propagation constants and the thickness of this layer:

$$P_j = \begin{pmatrix} e^{-i\gamma_{j1}d_j} & 0 & 0 & 0 \\ 0 & e^{-i\gamma_{j2}d_j} & 0 & 0 \\ 0 & 0 & e^{-i\gamma_{j3}d_j} & 0 \\ 0 & 0 & 0 & e^{-i\gamma_{j4}d_j} \end{pmatrix}. \tag{3.22}$$

With the definition of these two matrixes, we can define the new M matrix, which corresponds to the total transfer matrix of a structure composed of N layers:

$$M = \prod_{j=1}^{N} M_j = \begin{pmatrix} M_{11} & M_{12} & M_{13} & M_{14} \\ M_{21} & M_{22} & M_{23} & M_{24} \\ M_{31} & M_{32} & M_{33} & M_{34} \\ M_{41} & M_{42} & M_{43} & M_{44} \end{pmatrix}. \tag{3.23}$$

Due to the anisotropic components, except for certain configurations, the polarization state of a plane wave varies as it propagates in the medium producing coupling between the plane waves in each polarization in reflection/transmission, therefore it is necessary to introduce four coefficients that define the Jones matrix of the reflection/transmission of the structure, which are related with the matrix from equation (3.23):

$$r_{xx} = \left(\frac{M_{21}M_{33} - M_{23}M_{31}}{M_{11}M_{33} - M_{13}M_{31}} \right)^2, \tag{3.24a}$$

$$r_{xy} = \left(\frac{M_{41}M_{33} - M_{43}M_{31}}{M_{11}M_{33} - M_{13}M_{31}} \right)^2, \tag{3.24b}$$

$$r_{yx} = \left(\frac{M_{11}M_{23} - M_{21}M_{13}}{M_{11}M_{33} - M_{13}M_{31}} \right)^2, \tag{3.24c}$$

$$r_{yy} = \left(\frac{M_{11}M_{43} - M_{41}M_{13}}{M_{11}M_{33} - M_{13}M_{31}} \right)^2. \tag{3.24d}$$

UNIVERSITAT ROVIRA I VIRGILI
DESIGN AND MODELLING OF PHOTONIC CRYSTALS WITH ANISOTROPIC COMPONENTS
Joaquin Cos Córcoles
ISBN:978-84-693-9433-5/DL:T.69-2011

$$t_{xx} = \left(\frac{M_{33}}{M_{11}M_{33} - M_{13}M_{31}} \right)^2, \tag{3.25a}$$

$$t_{xy} = \left(\frac{-M_{31}}{M_{11}M_{33} - M_{13}M_{31}} \right)^2, \tag{3.25b}$$

$$t_{yx} = \left(\frac{-M_{13}}{M_{11}M_{33} - M_{13}M_{31}} \right)^2, \tag{3.25c}$$

$$t_{yy} = \left(\frac{M_{11}}{M_{11}M_{33} - M_{13}M_{31}} \right)^2. \tag{3.25d}$$

From Eqs. (3.24) and (3.25) the reflectance/transmittance of the structure is defined as

$$R_{xx} = \left| r_{xx} \right|^2, \tag{3.26a}$$

$$R_{xy} = \left| r_{xy} \right|^2, \tag{3.26b}$$

$$R_{yx} = \left| r_{yx} \right|^2, \tag{3.26c}$$

$$R_{yy} = \left| r_{yy} \right|^2. \tag{3.26d}$$

$$T_{xx} = \frac{n_N \cos\theta_N}{n_0 \cos\theta_0} \left| t_{xx} \right|^2, \tag{3.27a}$$

$$T_{xy} = \frac{n_N \cos\theta_N}{n_0 \cos\theta_0} \left| t_{xy} \right|^2, \tag{3.27b}$$

$$T_{yx} = \frac{n_N \cos\theta_N}{n_0 \cos\theta_0} \left| t_{yx} \right|^2, \tag{3.27c}$$

$$T_{yy} = \frac{n_N \cos\theta_N}{n_0 \cos\theta_0} \left| t_{yy} \right|^2. \tag{3.27d}$$

UNIVERSITAT ROVIRA I VIRGILI
DESIGN AND MODELLING OF PHOTONIC CRYSTALS WITH ANISOTROPIC COMPONENTS
Joaquin Cos Córcoles
ISBN:978-84-693-9433-5/DL:T.69-2011

3.3 The plane-wave expansion method

Since the method was developed, it has been applied for multiple purposes such as the study of the electric band structures [Yu-2004], acoustics [Li-2005], and photonic band structures [Trifonov-2004].

In the field of the photonic crystals, the aim of the method is to determine the allowed frequencies for a given wave vector **k**. The plane-wave expansion method (PWEM) uses the Bloch theorem [Ashcroft-1976] to obtain the eigensolutions of the Maxwell equations as a superposition of plane waves.

A photonic crystal is composed by dielectric scatterers (layers, rods, holes, opals...) arranged in a periodic photonic lattice generated by one, two or three (1D, 2D, or 3D photonic crystals) base vectors that defines the periodicity direction(s). In the PWEM, instead of using the real space lattice to perform the calculations, its associated reciprocal lattice is used. The reciprocal lattice is generated by one, two or three primitive vectors.

The Brillouin zone (BZ) represents the full symmetry of the lattice in reciprocal space. The irreducible Brillouin zone (IBZ) is the smallest region within the BZ for which the dispersion characteristics of the lattice are not related by symmetry. The behaviour of the entire crystal can be obtained by studying the unit lattice in the IBZ due to periodicity. One cannot obtain independent solutions if the analysis is carried out outside the IBZ. As we will see in a later chapter, the study of the IBZ in anisotropic structures will be determinant for the correct obtaining of the band structures.

UNIVERSITAT ROVIRA I VIRGILI
DESIGN AND MODELLING OF PHOTONIC CRYSTALS WITH ANISOTROPIC COMPONENTS
Joaquin Cos Córcoles
ISBN:978-84-693-9433-5/DL:T.69-2011

3.3.1 Formulation of plane-wave expansion method

In the absence of electric current and free charges, Maxwell equations for nonmagnetic and isotropic media can be written as [Sakoda-2001]:

$$\nabla \cdot \mathbf{D}(\mathbf{r},t) = 0, \tag{3.28a}$$

$$\nabla \cdot \mathbf{B}(\mathbf{r},t) = 0, \tag{3.28b}$$

$$\nabla \cdot \mathbf{E}(\mathbf{r},t) = -\frac{\partial}{\partial t}\mathbf{B}(\mathbf{r},t) = -\mu_0 \frac{\partial}{\partial t}\mathbf{H}(\mathbf{r},t), \tag{3.28c}$$

$$\nabla \cdot \mathbf{H}(\mathbf{r},t) = \frac{\partial}{\partial t}\mathbf{D}(\mathbf{r},t) = \varepsilon_0 \varepsilon(\mathbf{r}) \frac{\partial}{\partial t}\mathbf{E}(\mathbf{r},t), \tag{3.28d}$$

where μ_0 and ε_0 are the permeability and permittivity of the vacuum, respectively.

We can find solutions for the electric and magnetic fields in a time harmonic form:

$$\mathbf{E}(\mathbf{r},t) = \mathbf{E}(\mathbf{r})e^{-i\omega t}, \tag{3.29a}$$

$$\mathbf{H}(\mathbf{r},t) = \mathbf{H}(\mathbf{r})e^{-i\omega t}, \tag{3.29b}$$

where ω is the eigenangular frequency. Combining Eqs. (3.28c), (3.28d) and (3.29) we can express the eigenvalue equations for the electric and magnetic fields:

$$\frac{1}{\varepsilon(\mathbf{r})}\nabla \times \{\nabla \times \mathbf{E}(\mathbf{r})\} = \left(\frac{\omega}{c}\right)^2 \mathbf{E}(\mathbf{r}), \tag{3.30a}$$

$$\nabla \times \left\{\frac{1}{\varepsilon(\mathbf{r})}\nabla \times \mathbf{H}(\mathbf{r})\right\} = \left(\frac{\omega}{c}\right)^2 \mathbf{H}(\mathbf{r}). \tag{3.30b}$$

In both equations the variable that define the structure is the dielectric constant $\varepsilon(\mathbf{r})$. Given that the dielectric constant is periodic, its inverse can be expanded in Fourier series as

$$\frac{1}{\varepsilon(\mathbf{r})} = \sum_G k(\mathbf{G})e^{i\mathbf{G}\mathbf{r}}, \tag{3.31}$$

where $\mathbf{G}$ are the reciprocal lattice vectors.

UNIVERSITAT ROVIRA I VIRGILI
DESIGN AND MODELLING OF PHOTONIC CRYSTALS WITH ANISOTROPIC COMPONENTS
Joaquin Cos Córcoles
ISBN:978-84-693-9433-5/DL:T.69-2011

Considering again the periodicity of the dielectric constant in the reciprocal space the Bloch theorem [Ashcroft-1976] can be applied. Therefore, the eigenstates **E**(**r**) and **H**(**r**) are characterized by a wave vector **k** and a band index *n* and are expressed as

$$\mathbf{E}(\mathbf{r}) = \mathbf{E}_{\mathbf{k}n}(\mathbf{r}) = u_{\mathbf{k}n}(\mathbf{r})e^{i\mathbf{k}\mathbf{r}}, \tag{3.32a}$$

$$\mathbf{H}(\mathbf{r}) = \mathbf{H}_{\mathbf{k}n}(\mathbf{r}) = v_{\mathbf{k}n}(\mathbf{r})e^{i\mathbf{k}\mathbf{r}}. \tag{3.32b}$$

These eigenfunctions can be expanded in Fourier series like the inverse of the dielectric constant in Eq. (3.31) in the following way:

$$\mathbf{E}_{\mathbf{k}n}(\mathbf{r}) = \sum_{\mathbf{G}} \mathbf{E}_{\mathbf{k}n}(\mathbf{G})e^{i(\mathbf{k}+\mathbf{G})\mathbf{r}}, \tag{3.33a}$$

$$\mathbf{H}_{\mathbf{k}n}(\mathbf{r}) = \sum_{\mathbf{G}} \mathbf{H}_{\mathbf{k}n}(\mathbf{G})e^{i(\mathbf{k}+\mathbf{G})\mathbf{r}}. \tag{3.33b}$$

Finally combining Eq. (3.30), (3.31) and (3.33), we obtain the eigenvalue equations for the expansion coefficients of $\mathbf{E}_{\mathbf{k}n}(\mathbf{G})$ and $\mathbf{H}_{\mathbf{k}n}(\mathbf{G})$:

$$-\sum_{\mathbf{G}'} k(\mathbf{G}-\mathbf{G}')\cdot(\mathbf{k}+\mathbf{G}')\times\left[(\mathbf{k}+\mathbf{G}')\times\mathbf{E}_{\mathbf{k}n}(\mathbf{G}')\right] = \frac{\omega_{\mathbf{k}n}^2}{c^2}\mathbf{E}_{\mathbf{k}n}(\mathbf{G}), \tag{3.234a}$$

$$-\sum_{\mathbf{G}'} k(\mathbf{G}-\mathbf{G}')\cdot(\mathbf{k}+\mathbf{G})\times\left[(\mathbf{k}+\mathbf{G}')\times\mathbf{H}_{\mathbf{k}n}(\mathbf{G}')\right] = \frac{\omega_{\mathbf{k}n}^2}{c^2}\mathbf{H}_{\mathbf{k}n}(\mathbf{G}). \tag{3.34b}$$

3.3.2 Two-dimensional photonic crystals with anisotropic components

The previous section has given detailed information about the application of the PWEM to isotropic photonic crystals. In this section we apply this method to the case of two-dimensional photonic crystals with anisotropic components, in particular with liquid crystal components. We consider the *x*-*y* plane as the periodicity plane of the PCs. In order to preserve the two-dimensional condition of the analysis, we consider orientations of the anisotropic components such as TE and TM polarizations can be

UNIVERSITAT ROVIRA I VIRGILI
DESIGN AND MODELLING OF PHOTONIC CRYSTALS WITH ANISOTROPIC COMPONENTS
Joaquin Cos Córcoles
ISBN:978-84-693-9433-5/DL:T.69-2011

decoupled. In these cases TE components are E_x, E_y and H_z while TM components are H_x, H_y and E_z according to Joannopoulus notation [Joannopoulus-1995]. We start from the Maxwell equations for nonmagnetic media (Eqs. (3.28c) and (3.28d)), where the dielectric tensor has the formulation of Eq. (3.2) and are defined by

$$\frac{\partial E_z}{\partial y} = -\mu_0 \frac{\partial H_x}{\partial t}, \tag{3.35a}$$

$$\frac{\partial E_z}{\partial x} = -\mu_0 \frac{\partial H_y}{\partial t}, \tag{3.35b}$$

$$\frac{\partial E_y}{\partial x} - \frac{\partial E_x}{\partial y} = -\mu_0 \frac{\partial H_z}{\partial t}, \tag{3.35c}$$

$$\frac{\partial H_z}{\partial y} = \varepsilon_0 \varepsilon_{xx}(\mathbf{r}) \frac{\partial E_x}{\partial t} + \varepsilon_0 \varepsilon_{xy}(\mathbf{r}) \frac{\partial E_y}{\partial t} + \varepsilon_0 \varepsilon_{xz}(\mathbf{r}) \frac{\partial E_z}{\partial t}, \tag{3.35d}$$

$$\frac{\partial H_z}{\partial x} = -\varepsilon_0 \varepsilon_{yx}(\mathbf{r}) \frac{\partial E_x}{\partial t} - \varepsilon_0 \varepsilon_{yy}(\mathbf{r}) \frac{\partial E_y}{\partial t} - \varepsilon_0 \varepsilon_{yz}(\mathbf{r}) \frac{\partial E_z}{\partial t}, \tag{3.35e}$$

$$\frac{\partial H_y}{\partial x} - \frac{\partial H_x}{\partial y} = \varepsilon_0 \varepsilon_{zx}(\mathbf{r}) \frac{\partial E_x}{\partial t} + \varepsilon_0 \varepsilon_{zy}(\mathbf{r}) \frac{\partial E_y}{\partial t} + \varepsilon_0 \varepsilon_{zz}(\mathbf{r}) \frac{\partial E_z}{\partial t}, \tag{3.35f}$$

where the field notations are simplified as $A_i(\mathbf{r},t) = A_i$.

The decoupling of the TE and TM polarizations is only possible if ε_{xz}, ε_{yz}, ε_{zx}, and ε_{zy} are zero. Therefore, the anisotropic materials must to be in such orientation that the polarizations can be decoupled and that the direction of the extraordinary axes influences the photonic bands. Following [Alagappan-2006], Maxwell's equations can only be decoupled in two cases: i) when the optical axis is oriented along the rods of the 2D photonic crystal (Euler's angles are ϕ = [*0 - 360º*], θ = *0º* and ψ = *0º*), and ii) when the optical axis is perpendicular to the rods (Euler's angles are ϕ = [*0 - 360º*], θ = *90º* and ψ = *0º*). The new dielectric constant tensor of the LC, ε_{LC}, which includes the LC's optical axis orientation, can be expressed in the form of Eq. (3.3) for the first case (Eq. (3.36a)) and for the second case (Eq. (3.36b)) as

UNIVERSITAT ROVIRA I VIRGILI
DESIGN AND MODELLING OF PHOTONIC CRYSTALS WITH ANISOTROPIC COMPONENTS
Joaquin Cos Córcoles
ISBN:978-84-693-9433-5/DL:T.69-2011

$$\varepsilon_{LC}=\begin{pmatrix}\varepsilon_o\cos^2\phi+\varepsilon_o\sin^2\phi & (\varepsilon_o-\varepsilon_o)\cdot\cos\phi\cdot\sin\phi & 0\\ (\varepsilon_o-\varepsilon_o)\cdot\cos\phi\cdot\sin\phi & \varepsilon_o\sin^2\phi+\varepsilon_o\cos^2\phi & 0\\ 0 & 0 & \varepsilon_e\end{pmatrix}=\begin{pmatrix}\varepsilon_o & 0 & 0\\ 0 & \varepsilon_o & 0\\ 0 & 0 & \varepsilon_e\end{pmatrix}, \quad (3.36a)$$

$$\varepsilon_{LC}=\begin{pmatrix}\varepsilon_o\cos^2\phi+\varepsilon_e\sin^2\phi & (\varepsilon_o-\varepsilon_e)\cdot\cos\phi\cdot\sin\phi & 0\\ (\varepsilon_o-\varepsilon_e)\cdot\cos\phi\cdot\sin\phi & \varepsilon_o\sin^2\phi+\varepsilon_e\cos^2\phi & 0\\ 0 & 0 & \varepsilon_o\end{pmatrix}. \quad (3.36b)$$

Furthermore, as can be seen in these equations, only in the second case the direction of the optical axis influences the photonic band structure.

Without coupled modes we can eliminate H_x and H_y from Eqs. (3.35a), (3.35b), and (3.35f) and we can write the following eigenequation for the TM polarization:

$$-\varepsilon_{zz}^{-1}(\mathbf{r})\left(\frac{\partial^2}{\partial x^2}+\frac{\partial^2}{\partial y^2}\right)\mathbf{E}_z(\mathbf{r})=\omega^2\mu_0\varepsilon_0\mathbf{E}_z(\mathbf{r}). \quad (3.37)$$

On the other hand, eliminating E_x and E_y from (3.30c), (3.30d), and (3.30e) we obtain the following eigenequation for the TE polarization:

$$\nabla_{xy}\times\varepsilon_r^{-1}(\mathbf{r})\times\nabla_{xy}\times H_z(\mathbf{r})e_z=\omega^2\mu_0\varepsilon_0 H_z(\mathbf{r})e_z, \quad (3.38)$$

where $\nabla_{xy}=e_x\cdot\partial/\partial x+e_y\cdot\partial/\partial y$ and $\varepsilon_r(\mathbf{r})$ is defined as

$$\varepsilon_r(\mathbf{r})=\begin{pmatrix}\varepsilon_{xx}(\mathbf{r}) & \varepsilon_{xy}(\mathbf{r})\\ \varepsilon_{yx}(\mathbf{r}) & \varepsilon_{yy}(\mathbf{r})\end{pmatrix}. \quad (3.39)$$

In both equations (3.37) and (3.38) the solution $A_z=A(\mathbf{r})e^{-i\omega t}$ is assumed, where ω is the angular frequency.

Applying plane-wave expansion method on Eqs. (3.37) and (3.38) we can obtain a pair of eigenequations for TM and TE respectively [Alagappan-2006]

$$\sum_{\mathbf{G}'}\varepsilon_{z\mathbf{G}\mathbf{G}'}^{-1}(\mathbf{G}-\mathbf{G}')\cdot|\mathbf{k}+\mathbf{G}|\cdot|\mathbf{k}+\mathbf{G}'|F_{z\mathbf{k}}(\mathbf{G}')=(\omega/c)^2F_{z\mathbf{k}}(\mathbf{G}), \quad (3.40a)$$

$$\sum_{\mathbf{G}'}(\mathbf{k}+\mathbf{G})\cdot\varepsilon_{r\mathbf{G}\mathbf{G}'}^{-1}(\mathbf{G}-\mathbf{G}')\cdot(\mathbf{k}+\mathbf{G}')H_{z\mathbf{k}}(\mathbf{G}')=(\omega/c)^2H_{z\mathbf{k}}(\mathbf{G}), \quad (3.40b)$$

UNIVERSITAT ROVIRA I VIRGILI
DESIGN AND MODELLING OF PHOTONIC CRYSTALS WITH ANISOTROPIC COMPONENTS
Joaquin Cos Córcoles
ISBN:978-84-693-9433-5/DL:T.69-2011

where $\varepsilon^{-1}_{zGG'}$ and $\varepsilon^{-1}_{rGG'}$ are, respectively, the Fourier Transform of the inverse of $\varepsilon_{zz}(\mathbf{r})$ and $\varepsilon_r(\mathbf{r})$. It is important to note that $\varepsilon^{-1}_{rGG'}$ is a *2x2* matrix. In order to produce a symmetric eigenvalue problem $F_{z,\mathbf{k}}(\mathbf{G})$ is defined as

$$F_{z\,\mathbf{k}}(\mathbf{G}) = \left|\mathbf{k}+\mathbf{G}\right| \cdot E_{z\,\mathbf{k}}(\mathbf{G}). \tag{3.41}$$

The Fourier components $\varepsilon^{-1}_{zGG'}$ and $\varepsilon^{-1}_{rGG'}$ are defined for two-component systems as:

$$\varepsilon^{-1}(G) = \begin{Bmatrix} (f \cdot \varepsilon_s^{-1} + (1-f)\cdot \varepsilon_b^{-1}) & for\ G = 0 \\ (\varepsilon_s^{-1} - \varepsilon_b^{-1}) \cdot S(G) & for\ G \neq 0 \end{Bmatrix}, \tag{3.42}$$

where ε_s is the element of the dielectric tensor corresponding to the material of the scatterer, ε_b is the same dielectric tensor element corresponding to the background material, f is the filling factor and $S(G)$ is the Fourier transform of the unit cell. It is important to note that $S(G)$ relies only on the geometry of the scatterer and on the lattice structure. Table 3.1 shows the structure factors (Fig. 3.3) and properties for triangular and square lattices [Luan-2001], where a and R are the lattice constant and the rod radius respectively, J_1 is the first-order Bessel function of the first kind and $Q(x)$ is defined as $Q(x) = \dfrac{\sin(x)}{x}$.

It is worth explaining in detail how to obtain ε^{-1}. On one hand, to obtain $\varepsilon^{-1}_{zGG'}$ for a 2D photonic crystal consisting of an isotropic background with holes filled with liquid crystal, and where the liquid crystal optical axis is in the *x-y* plane, ε_s is ε_o and ε_b is the background dielectric constant. Instead, for $\varepsilon^{-1}_{rGG'}$ four elements must be calculated, using each one of the four elements of ε_r as ε_s, in all the cases ε_b is the background dielectric constant. The resulting $\varepsilon^{-1}_{zGG'}$ and $\varepsilon^{-1}_{rGG'}$ can be expressed as:

UNIVERSITAT ROVIRA I VIRGILI
DESIGN AND MODELLING OF PHOTONIC CRYSTALS WITH ANISOTROPIC COMPONENTS
Joaquin Cos Córcoles
ISBN:978-84-693-9433-5/DL:T.69-2011

		Square lattice		Triangular lattice	
		Circular rods	Square rods	Circular rods	Square rods
Base vector	$\mathbf{a}_1$	ae_x	ae_x	ae_x	ae_x
	$\mathbf{a}_2$	ae_y	ae_y	$a\left(\frac{1}{2}e_x+\frac{\sqrt{3}}{2}e_y\right)$	$a\left(\frac{1}{2}e_x+\frac{\sqrt{3}}{2}e_y\right)$
Reciprocal lattice base vector	$\mathbf{b}_1$	$(2\pi/a)e_x$	$(2\pi/a)e_x$	$(2\pi/a)\cdot\left(e_x-\frac{1}{\sqrt{3}}e_y\right)$	$(2\pi/a)\cdot\left(e_x-\frac{1}{\sqrt{3}}e_y\right)$
	$\mathbf{b}_2$	$(2\pi/a)e_y$	$(2\pi/a)e_y$	$(2\pi/a)\frac{2}{\sqrt{3}}e_y$	$(2\pi/a)\frac{2}{\sqrt{3}}e_y$
Filling factor f		$\pi(R/a)^2$	$(R/a)^2$	$\frac{2\pi}{\sqrt{3}}(R/a)^2$	$\frac{1}{2}(R/a)^2$
$S(G)$		$2f\frac{J_1(GR)}{(GR)}$	$fQ\left(\frac{G_xR}{2}\right)Q\left(\frac{G_yR}{2}\right)$	$2f\frac{J_1(GR)}{(GR)}$	$fQ\left(\frac{G_xR}{2}\right)Q\left(\frac{G_yR}{2}\right)$

Table 3.1. Structure factors and properties of square and triangular lattices.

$$\varepsilon_z^{-1}(G)=\begin{Bmatrix}(f\cdot\varepsilon_o^{-1}+(1-f)\cdot\varepsilon_b^{-1}) & for\ G=0\\ (\varepsilon_o^{-1}-\varepsilon_b^{-1})\cdot S(G) & for\ G\neq 0\end{Bmatrix}, \tag{3.43a}$$

$$\varepsilon_{rij}^{-1}(G)=\begin{Bmatrix}(f\cdot\varepsilon_{LCij}^{-1}+(1-f)\cdot\varepsilon_b^{-1}) & for\ G=0\\ (\varepsilon_{LCij}^{-1}-\varepsilon_b^{-1})\cdot S(G) & for\ G\neq 0\end{Bmatrix}, \tag{3.43b}$$

where $i = x, y$ and $j = x, y$.

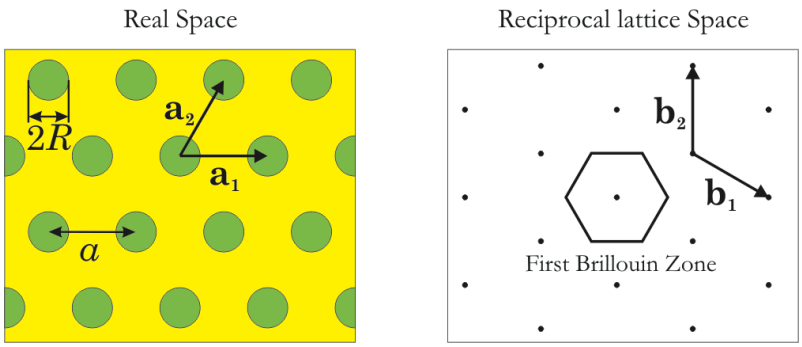

Fig. 3.3 Real and reciprocal lattice space of photonic crystal composed of triangular lattice of circular rods.

UNIVERSITAT ROVIRA I VIRGILI
DESIGN AND MODELLING OF PHOTONIC CRYSTALS WITH ANISOTROPIC COMPONENTS
Joaquin Cos Córcoles
ISBN:978-84-693-9433-5/DL:T.69-2011

On the other hand, to obtain $\varepsilon^{-1}_{zGG'}$ for a 2D photonic crystal consisting of isotropic cylinders surrounded by liquid crystal, and where the liquid crystal optical axis is in the *x*-*y* plane, ε_b is ε_o and ε_s is the cylinder dielectric constant. For $\varepsilon^{-1}_{rGG'}$ four elements must be calculated, using each one of the four elements of ε_r as ε_b, in all the cases ε_s is the cylinder dielectric constant. The resulting $\varepsilon^{-1}_{zGG'}$ and $\varepsilon^{-1}_{rGG'}$ can be expressed as:

$$\varepsilon_z^{-1}(G) = \begin{Bmatrix} (f\cdot\varepsilon_s^{-1} + (1-f)\cdot\varepsilon_o^{-1}) & for\ G=0 \\ (\varepsilon_s^{-1} - \varepsilon_o^{-1})\cdot S(G) & for\ G\neq 0 \end{Bmatrix}, \tag{3.44a}$$

$$\varepsilon_{rij}^{-1}(G) = \begin{Bmatrix} (f\cdot\varepsilon_s^{-1} + (1-f)\cdot\varepsilon_{LCij}^{-1}) & for\ G=0 \\ (\varepsilon_s^{-1} - \varepsilon_{LCij}^{-1})\cdot S(G) & for\ G\neq 0 \end{Bmatrix}, \tag{3.44b}$$

where $i = x, y$ and $j = x, y$.

3.3.3 Supercell formulation for the numerical analysis of defects in photonic crystals

The PWE method is very useful for the computation of eigenstates in photonic crystals. However, the definition of the method assumes the structure is periodic and infinite. The application of the photonic crystal as a material needs the introduction of defects in the perfect periodic infinite structure to create waveguides and optical cavities. The PWEM can still be applied to such structures by studying what is called a supercell: a set of unit cells of the photonic crystal with the defect under study. With this strategy, the PWEM assumes periodicity of the supercell and is accurate provided the supercell contains enough non-defective unit cells of the base photonic crystal.

In contrast with of the classical formulation of the PWEM where only one element of the photonic crystal was defined (and define the main cell) and replicated periodically in the reciprocal directions, in the case of the formulation of the supercell, the main cell is composed by the defect(s) and the neighbour elements. Thus both, the defect and the neighbour elements are replicated periodically in the reciprocal main directions.

UNIVERSITAT ROVIRA I VIRGILI
DESIGN AND MODELLING OF PHOTONIC CRYSTALS WITH ANISOTROPIC COMPONENTS
Joaquin Cos Córcoles
ISBN:978-84-693-9433-5/DL:T.69-2011

In this thesis, we consider 2D photonic crystal consisting of an isotropic background with air holes and defects consisting of some of these air holes filled with liquid crystal.

Therefore we can define two kinds of Fourier Transform of the inverse of the dielectric constant, one for the air rods scatterers (Eq. (3.45a)) and other for the holes filled with liquid crystal scatterers (Eq. (3.45b)).

$$\varepsilon_{air}^{-1}(G)=\begin{Bmatrix}(f\cdot\varepsilon_{air}^{-1}+(1-f)\cdot\varepsilon_b^{-1}) & for\,G=0\\ (\varepsilon_{air}^{-1}-\varepsilon_b^{-1})\cdot S(G) & for\;G\neq 0\end{Bmatrix}, \tag{3.45a}$$

$$\varepsilon_{LC}^{-1}(G)=\begin{Bmatrix}(f\cdot\varepsilon_{LC}^{-1}+(1-f)\cdot\varepsilon_b^{-1}) & for\,G=0\\ (\varepsilon_{LC}^{-1}-\varepsilon_b^{-1})\cdot S(G) & for\;G\neq 0\end{Bmatrix}, \tag{3.45b}$$

where ε_b and ε_{air} are two *2x2* identity matrixes multiplied by the dielectric constant of the isotropic background and air respectively and ε_{LC} is defined in Eq. (3.39).

Equation (3.45) corresponding to each scatterer of the supercell is modulated by the displacement property of the Fourier Transform:

$$\mathrm{TF}\left[f(x-x_0)\right]=F(\omega)e^{-i\omega x_0}. \tag{3.46}$$

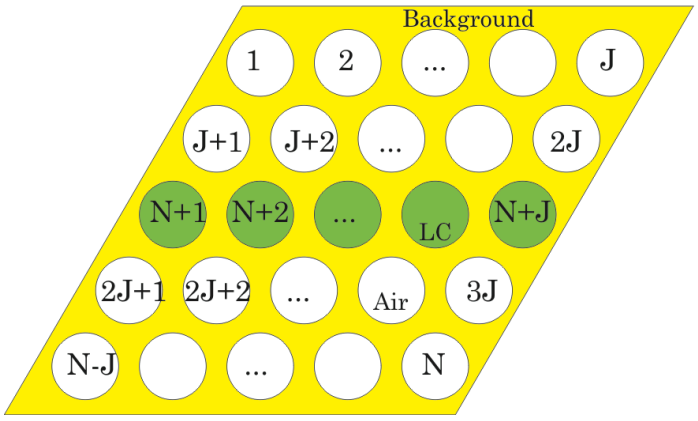

Fig. 3.4 Schematic of a supercell composed of triangular lattice of circular rods where one of the lines of scatterers has been filled by liquid crystal. Numbers indicate the order of the scatterer in the definition of Eq. (3.38).

UNIVERSITAT ROVIRA I VIRGILI
DESIGN AND MODELLING OF PHOTONIC CRYSTALS WITH ANISOTROPIC COMPONENTS
Joaquin Cos Córcoles
ISBN:978-84-693-9433-5/DL:T.69-2011

Therefore, according to the notation of Fig. 3.4, the Fourier Transform of the inverse of the dielectric constant of the supercell is defined as

$$\varepsilon^{-1}_{rGG'} = \sum_{m=1}^{N} \varepsilon^{-1}_{air}(\mathbf{G}-\mathbf{G}') \cdot e^{-i((\mathbf{G}-\mathbf{G}')\mathbf{P}(m))} + \sum_{m=N+1}^{N+J} \varepsilon^{-1}_{LC}(\mathbf{G}-\mathbf{G}') \cdot e^{-i((\mathbf{G}-\mathbf{G}')\mathbf{P}(m))}, \qquad (3.47)$$

where **P(m)** is a vector with the positions of the scatterers in the reciprocal base. It is important to note that in this vector the elements are ordered such as the first *N* elements correspond to the position of the air scatterers and the last *J* elements correspond to position of the defect scatterers.

3.4 Finite-difference time-domain method

The plane-wave expansion method is a solid method to obtain the band structure of a photonic crystal, but the study of other optical properties such as the transmission or the coupling and insertion losses requires an alternative method.

Finite-difference time-domain method [Taflove-2000] is an appropriate method for obtaining these parameters. This method calculates the temporal evolvement of the electromagnetic fields by means of the approximation in finite differences of the time and the space derivates of the time-dependent Maxwell equations. Different to PWEM, in this case, all the calculations are in real space, therefore the definition of the structure becomes easier. However, other parameters or configurations have to be defined, such as the boundary conditions, the initial field state and the data extraction.

From the classical definition of the method [Taflove-2000] for isotropic photonic crystals where the calculations are made for **E** and **H** fields, some considerations have to be taken into account for the efficient calculation of the light wave propagation through an anisotropic photonic crystal.

UNIVERSITAT ROVIRA I VIRGILI
DESIGN AND MODELLING OF PHOTONIC CRYSTALS WITH ANISOTROPIC COMPONENTS
Joaquin Cos Córcoles
ISBN:978-84-693-9433-5/DL:T.69-2011

Starting from the Maxwell equations for anisotropic structures, where the z direction is the direction normal to the plane of periodicity, defined in Eq. 3.35 it is clear to observe the difficulty of calculations in terms of central finite differences because of the dependence of the **H** fields on all the components of the **E** fields. For solving this problem, it is very useful to make the calculations for **D** and **H** fields.

We start calculating the **D** fields in terms of central finite differences of the **H** fields from the equations:

$$\frac{\partial H_z}{\partial y} = \frac{\partial D_x}{\partial t}, \tag{3.48a}$$

$$\frac{\partial H_z}{\partial x} = -\frac{\partial D_y}{\partial t}, \tag{3.48b}$$

$$\frac{\partial H_y}{\partial x} - \frac{\partial H_x}{\partial y} = \frac{\partial D_z}{\partial t}. \tag{3.48c}$$

The values of the electric fields **E** can be deduced from the **D** fields calculated in the last step by means of the inversion of the linear system of the dielectric tensor defined in Eq. (3.3):

$$\begin{pmatrix} E_x \\ E_y \\ E_z \end{pmatrix} = \tilde{\varepsilon}^{-1} \cdot \begin{pmatrix} D_x \\ D_y \\ D_z \end{pmatrix}. \tag{3.49}$$

Finally, **H** fields are calculated in terms of central finite differences of the **E** fields from the equations:

$$\frac{\partial E_z}{\partial y} = -\mu_0 \frac{\partial H_x}{\partial t}, \tag{3.50a}$$

$$\frac{\partial E_z}{\partial x} = -\mu_0 \frac{\partial H_y}{\partial t}, \tag{3.50b}$$

$$\frac{\partial E_y}{\partial x} - \frac{\partial E_x}{\partial y} = -\mu_0 \frac{\partial H_z}{\partial t}. \tag{3.50c}$$

UNIVERSITAT ROVIRA I VIRGILI
DESIGN AND MODELLING OF PHOTONIC CRYSTALS WITH ANISOTROPIC COMPONENTS
Joaquin Cos Córcoles
ISBN:978-84-693-9433-5/DL:T.69-2011

The basis of the FDTD consists on the calculation of the temporal evolvement of the electromagnetic fields by means of the discretization on a simple cubic lattice where space-time points are separated by fixed units of time Δt and distance Δs. The spatial derivatives are approximated at each lattice point by a corresponding centered difference, which gives rise to finite-difference equations.

It is important to see that **D** and **H** fields are defined at different points of the grid (Fig. 3.5), therefore, each value of a component of a field is calculated by the difference of the fields at neighbouring points.

From the set of Eqs. (3.48) and (3.50) according to the procedure from Taflove [Taflove-2000] their respective finite difference equations are

$$D_x^{n+1} = D_x^n + \frac{\Delta t}{\Delta y}(H_z^{y+1} - H_z^y), \tag{3.51a}$$

$$D_y^{n+1} = D_y^n + \frac{\Delta t}{\Delta x}(H_z^{x+1} - H_z^x), \tag{3.51b}$$

$$D_z^{n+1} = D_z^n + \frac{\Delta t}{\Delta x}(H_y^{x+1} - H_y^x) - \frac{\Delta t}{\Delta y}(H_x^{y+1} - H_x^y). \tag{3.51c}$$

$$H_x^{n+1} = H_x^n - \frac{1}{\mu_0}\frac{\Delta t}{\Delta y}(E_z^{y+1} - E_z^y), \tag{3.52a}$$

$$H_y^{n+1} = H_y^n - \frac{1}{\mu_0}\frac{\Delta t}{\Delta x}(E_z^{x+1} - E_z^x), \tag{3.52b}$$

$$H_z^{n+1} = H_z^n - \frac{1}{\mu_0}\left[\frac{\Delta t}{\Delta x}(E_y^{x+1} - E_y^x) - \frac{\Delta t}{\Delta y}(E_x^{y+1} - E_x^y)\right]. \tag{3.52c}$$

The definition of a PML layer [Berenger-1996] for the truncation of the computational window needs the same procedure, that is, the parameters of the PML layer are defined for **D** and **H** fields.

In this thesis we have used a freely available software package [MEEP-2010]. The last releases of this package have included a variable to consider anisotropic materials.

UNIVERSITAT ROVIRA I VIRGILI
DESIGN AND MODELLING OF PHOTONIC CRYSTALS WITH ANISOTROPIC COMPONENTS
Joaquin Cos Córcoles
ISBN:978-84-693-9433-5/DL:T.69-2011

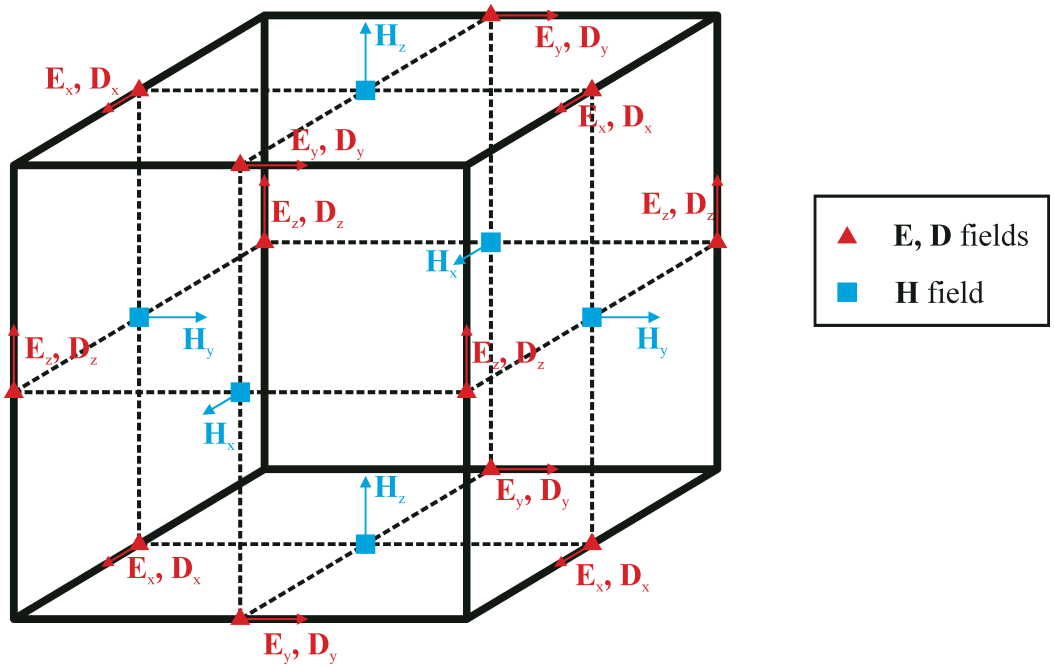

Fig. 3.5 Position of the electric displacement and the electric and magnetic fields vector components about a cubit unit cell of the Yee space lattice.

3.5 Other numerical methods

3.5.1 Finite element method (FEM)

The finite element method was originally devoted to solve structural analysis problems in civil and aeronautical engineering. Despite the origin of the method, nowadays it is used for a wide range of disciplines such as fluid dynamics, heat transfer or modelling of semiconductor devices because its diversity and flexibility as an analysis tool.

FEM is based on the discretization of the computation domain into a number of small regions, therefore the continuity problem, which has an infinite number of unknowns, is transformed in a finite problem with a finite number of unknowns at specified nodes. This method is very suitable for the analysis of photonic crystal because the form of the scatterers can be defined very well by means of discrete elements of different sizes. The meshing grid can have any given form, but for

UNIVERSITAT ROVIRA I VIRGILI
DESIGN AND MODELLING OF PHOTONIC CRYSTALS WITH ANISOTROPIC COMPONENTS
Joaquin Cos Córcoles
ISBN:978-84-693-9433-5/DL:T.69-2011

simplicity reasons it is advisable to use simple polygons. Usually, these subspaces are triangles allowing for a good approximation of circular structures. This kind of mesh brings up two main improvements with respect to e.g. a uniform Cartesian grid:

1) Regions of arbitrary shapes are represented better (no staircase approximation).

2) The FEM mesh can use locally a higher density of nodes in key regions that require it (e.g. narrow veins of high refractive index, typical in photonic crystals), without refining the discretization of the whole domain.

Different to classical plane-wave method, the discontinuous refractive index is handled in real space, therefore FEM does not have convergence problems. Briefly, FEM goes as follows. The photonic crystal structure is divided into homogeneous subspaces where Maxwell equations are solved by accounting for the adjacent subspaces, some interpolation function is chosen and its coefficients are computed for each element and stored as elemental matrices; these matrices are then assembled into global matrices that form an eigenvalue problem whose dimension depends on the number of elements. More details about this method can be found in [Jin-2002].

3.5.2 Korringa-Kohn-Rostoker method (KKR method)

The Korringa-Kohn-Rostoker method of band structure calculations was originally introduced in 1947 by Korringa and in 1954 by Kohn and Rostoker. A characteristic feature of this method applied to semiconductors is the use of multiple scattering theory for solving the Schrödinger equation. For photons the development is similar except for the complications brought about by the full vector character of electromagnetic fields.

The basic idea stems from the fact that the band structure in a periodic array of scatterers is determined by two factors: how a photon is scattered by an isolated scatterer and how the scatterers are distributed in the lattice. The scattering of a single scatterer is determined by the phase shifts of the scattering matrix, while the

UNIVERSITAT ROVIRA I VIRGILI
DESIGN AND MODELLING OF PHOTONIC CRYSTALS WITH ANISOTROPIC COMPONENTS
Joaquin Cos Córcoles
ISBN:978-84-693-9433-5/DL:T.69-2011

distribution of the scatterers is incorporated into a factor called a structure factor (structure constant or form factor).

In this way the problem is broken up into two parts. First, one solves the scattering problem of a single potential in free space. Second, one solves the multiple scattering problem by demanding that the incident wave to each scattering centre should be the sum of the outgoing waves from all other scattering centres. At some point in the calculations, it is assumed that vector field can be expanded, with a reasonable degree of accuracy, by a finite number of spherical harmonics.

The expansion of equations in terms of spherical harmonics is itself an advantage and a limitation at the same time. On the one hand, for systems made of spherical scatterers, the convergence of this method is very fast. Also, the discontinuities of the dielectric functions are accurately represented. On the other hand this method loses its effectiveness when scatterers are not spherical. For example, this method is ideal for colloidal crystals where ordered spheres are significantly apart from each other. However, for close packed arrangements where planes are much more interpenetrated or systems in which spheres are interpenetrated the spherical symmetry is lost. Another disadvantage is the lack of accuracy for high-energy calculations. More details about this method can be found in [Inoue-2004].

3.5.3 Multi-resolution time-domain method (MRTD method)

The multi-resolution time-domain method for the numerical simulation of solutions to Maxwell's electromagnetic equations was initially introduced as an alternative to the popular and, by now, classical finite-difference time-domain method. The basic idea of MRTD is rather simple, as it reduces to a method of moments wherein the spatial basis functions are chosen from a multi-resolution analysis. This choice naturally results in the potential for highly resolved spatial variations of the fields. However, in typical implementations, the realization of this potential is hindered by a low-order (leap-frog)

UNIVERSITAT ROVIRA I VIRGILI
DESIGN AND MODELLING OF PHOTONIC CRYSTALS WITH ANISOTROPIC COMPONENTS
Joaquin Cos Córcoles
ISBN:978-84-693-9433-5/DL:T.69-2011

time stepping procedure. More details about this method can be found in [Bushyager-2006].

UNIVERSITAT ROVIRA I VIRGILI
DESIGN AND MODELLING OF PHOTONIC CRYSTALS WITH ANISOTROPIC COMPONENTS
Joaquin Cos Córcoles
ISBN:978-84-693-9433-5/DL:T.69-2011

UNIVERSITAT ROVIRA I VIRGILI
DESIGN AND MODELLING OF PHOTONIC CRYSTALS WITH ANISOTROPIC COMPONENTS
Joaquin Cos Córcoles
ISBN:978-84-693-9433-5/DL:T.69-2011

Chapter 4

Design and analysis of tunable Fabry-Perot interferometers

In this chapter the study and design of tunable one-dimensional Fabry-Perot (FP) interferometers is presented. We analyze by means of the Transfer matrix method proposed in Chapter 3 two kinds of FP interferometers where, in both cases, resonances can be tuned in their wavelength position and varied in amplitude.

One-dimensional photonic crystals are known for several decades [Heavens-1965; Perilloux-2002] in the form of periodic multilayer coatings, consisting of stacked pairs of alternate dielectric or metal-dielectric layers with a large contrast of the dielectric constant along the propagation direction. Tuning the properties of such structures can be achieved by the infiltration of several layers with liquid crystal (LC), as has been proposed by several authors. In particular, Alagappan *et al.* [Alagappan2-2006] propose alternating anisotropic (E7 LC) and isotropic (silicon) layers and study the bandgap for each polarization. Others authors as Mandatori *et al.* [Mandatori-2003] or Vandenbem *et al.* [Vandenbem-2006] propose photonic crystals that alternate two anisotropic layers with different orientation of the optical axes, and they discuss the

UNIVERSITAT ROVIRA I VIRGILI
DESIGN AND MODELLING OF PHOTONIC CRYSTALS WITH ANISOTROPIC COMPONENTS
Joaquin Cos Córcoles
ISBN:978-84-693-9433-5/DL:T.69-2011

polarization dependence of the transmission. Ha *et al.* [Ha-2001] present the electrical control of the director angle of LC layers alternated with isotropic layers. Finally, Liu *et al.* [Liu-2004] proposed a Mach-Zehnder interferometer in which the phase of light propagation at the two arms can be varied by means of a section in each arm infiltrated with LC, whose optical axes can be varied independently.

Fabry-Perot interferometers are a particular case of one-dimensional multilayer structures that can be seen as a one-dimensional photonic crystal with a defect that acts as a resonant cavity. It is one of the most basic resonant devices, consisting of one (or more) resonant cavities surrounded by high-reflectivity mirrors. The dimensions of these cavities are designed in order to generate resonances in the region of high reflection of the mirrors. Thus, away from resonance, the transmission of the Fabry-Perot device is typically very small.

The sharpness of the resonances and the multiple reflections of the light into the cavity allow the device to be very sensitive to external changes and a good candidate for sensing applications [Guo-2004]. In addition, the FP is an essential device in telecommunication systems such as lasers [Espinosa-1998], wavelength divisors [Ortega-1999] and is a good characteristic that can be exploited for sensors [Spelman-2002], or tunable devices [Ozaki-2007].

Tuning the resonant properties of such structures by the introduction of LC in the defect layer has been reported in the literature. Hirabayashi *et al.* [Hirabayashi-1993] study the application of a tunable FP structure with LC defect for wavelength-division multiplexing (WDM). Ozaki *et al.* [Ozaki-2005] propose this structure to the design and fabrication of tunable lasers. They pay special attention to the estimation of response time for the defect mode switching. In all these works the LC optical axis is varied from a parallel alignment to the layers to a perpendicular alignment.

Studies on the actual practical implementation of the electric-field control of the LC optical axis director have also been published: Zografopoulos *et al.* [Zografopoulos-2007] study the orientation of the LC directors in a one-dimensional photonic crystal slab applying voltage by means of an ITO layer above the slab.

UNIVERSITAT ROVIRA I VIRGILI
DESIGN AND MODELLING OF PHOTONIC CRYSTALS WITH ANISOTROPIC COMPONENTS
Joaquin Cos Córcoles
ISBN:978-84-693-9433-5/DL:T.69-2011

The effect of the introduction of liquid crystal in one of the elements of the Fabry-Perot (cavity or mirrors) is to provide the system of a freedom degree that is used for tuning the resonances. However, in order to control the resonances in amplitude another freedom degree is needed. This supplementary freedom degree can be achieved by means of the introduction of another liquid crystal element in the device. In this thesis, we propose two alternative ways to achieve this control. One of them is a tunable single-cavity FP structure where the LC optical axis can be varied independently at the mirrors and at the cavity. The second one is a double-cavity FP structure where each cavity can vary their liquid crystal optical axis orientation independently. In contrast to previous studies tunability is achieved while maintaining the LC optical axes parallel to the layers.

4.1 Analysis of the optical properties of a single-cavity Fabry-Perot equalizer

The structure we propose is a multilayer Fabry-Perot structure composed of two mirrors surrounding a cavity. Fig. 4.1 shows a schematic view of the structure. The mirrors are composed of a periodic stacking of bilayers, with the high index layer made of silicon and the low index layer of Liquid Crystal, while the cavity is made of LC. The tunability of the filter is achieved allowing the orientations of the LC optical axes at the mirrors and at the cavity to be different. An additional silicon layer must be added to the mirrors to surround the LC cavity and thus to provide mechanical stability to the structure. This additional silicon layer also increases the reflectance maximum value [Hecht-2002]. We have chosen silicon as isotropic material because of its high refractive index at wavelengths with interest in optical communications and because it is compatible with most of the existing fabrication technologies. It is well known that silicon is actually not an isotropic material, however we have considered it as isotropic because the anisotropy is anyway small and to keep the study of the structure simpler.

UNIVERSITAT ROVIRA I VIRGILI
DESIGN AND MODELLING OF PHOTONIC CRYSTALS WITH ANISOTROPIC COMPONENTS
Joaquin Cos Córcoles
ISBN:978-84-693-9433-5/DL:T.69-2011

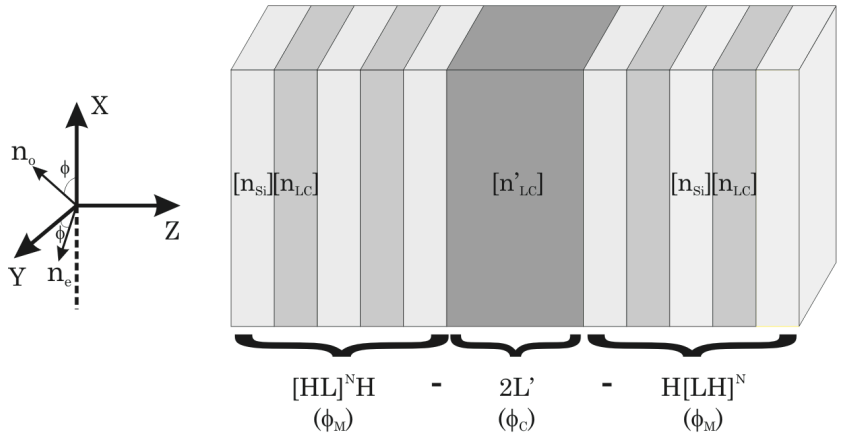

Fig. 4.1 Schematic view of the Fabry-Perot structure composed of two mirrors with N+1 quarter-wave (optical thickness) layers of silicon and N quarter-wave layers of Liquid Crystal separated by a half-wave layer of liquid crystal as cavity. The ϕ_M and ϕ_C indicate the angle of the LC optical axis with the y axis, taking into account that the LC optical axis is parallel to the layers. The prima superscript for the cavity indicates that the angles ϕ_M and ϕ_C can be different. The optical thicknesses are calculated taking the refraction index of the LC in the isotropic state.

As anisotropic material we have considered the E7 LC, since its director angle can be varied with an applied electric field.

We have chosen the dimensions of FP structure so that, when the LC is in its isotropic state, the mirrors are composed of quarter-wave layers of silicon and LC, while the cavity is a half-wave layer of LC, for a wavelength of *1.550 μm*. Thus, the design can be expressed as $[HL]^3$ H-2L'-$H[LH]^3$, where H stands for a quarter-wave layer of the high refractive index material, and L for a quarter-wave layer of the low refractive index material. The prima superscript for the cavity indicates that the LC optical axis direction of the cavity can be different to that of the mirrors. We have considered $n_{si} = 3.4$ as refractive index of silicon and $n_o = 1.522$ and $n_e = 1.704$ as ordinary and extraordinary indexes of E7 LC. The optical axis of the LC in all the layers is kept parallel to the *x-y* plane.

UNIVERSITAT ROVIRA I VIRGILI
DESIGN AND MODELLING OF PHOTONIC CRYSTALS WITH ANISOTROPIC COMPONENTS
Joaquin Cos Córcoles
ISBN:978-84-693-9433-5/DL:T.69-2011

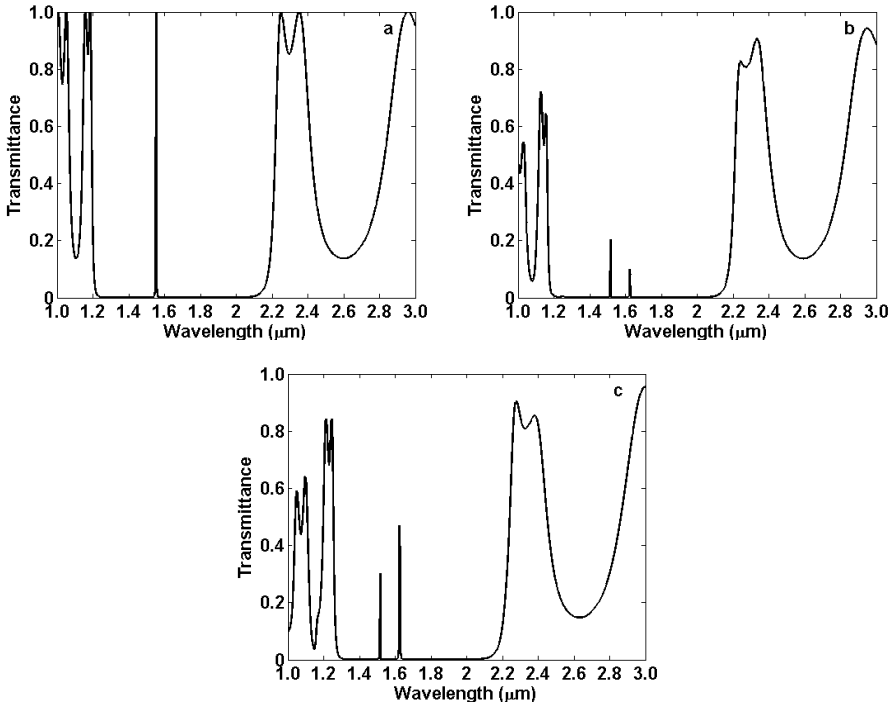

Fig. 4.2 Transmittance spectra for the structure $[HL]^3H\text{-}L'\text{-}H[LH]^3$ a) Isotropic state (n_{isoLC} = 1.585, n_{Si} = 3.4). A resonance for λ = 1.550 μm can be observed. b) $|t_{xx}|^2$ and c) $|t_{yy}|^2$ for the anisotropic state (ϕ_M = 15º, ϕ_C = 45º, n_{oLC} = 1.522, n_{eLC} = 1.704 n_{Si} = 3.4). The resonance present in the isotropic state splits in two, λ_1 = 1.516 μm and λ_2 = 1.625 μm.

As it is commented before, in contrast to previous works with tunable FP filters [Ozaki-2005; Hirabayashi-1993], we propose to tune the filter properties by rotating the LC optical axis in the *x*-*y* plane. With this configuration we have two degrees of freedom: the angle of the optical axis of the LC within the mirrors, ϕ_M, and the angle of the optical axis of the LC within the cavity, ϕ_C. Note that both ϕ_M and ϕ_C are measured with respect to *y* axis. Fig. 4.2 shows the transmission spectra of the structure for the isotropic state of the LC (Fig. 4.2a) and for the anisotropic state with angles $\phi_M = 15^o$ and $\phi_C = 45^o$ for the two main polarizations (Figs. 4.2b and 4.2c). In the isotropic state, the transmittance is polarization-independent, while for the anisotropic state the transmittance spectra $|t_{xx}|^2$ and $|t_{yy}|^2$ (from the structure Jones matrix) are shown. These figures show that the single resonance present in the isotropic state (at wavelength $\lambda = 1.550\ \mu m$) splits in two resonances, $\lambda_1 = 1.516\ \mu m$ and $\lambda_2 = 1.625\ \mu m$. As it can be observed, the transmittance at each of the resonant

UNIVERSITAT ROVIRA I VIRGILI
DESIGN AND MODELLING OF PHOTONIC CRYSTALS WITH ANISOTROPIC COMPONENTS
Joaquin Cos Córcoles
ISBN:978-84-693-9433-5/DL:T.69-2011

wavelengths depends on the polarization. Furthermore, it is worth noting that, in Figs. 4.2b and 4.2c the transmittance at the bandgap edges is not *100%*, in contrast with the isotropic case. This is due to the fact that in the anisotropic case, besides the $|t_{xx}|^2$ and $|t_{yy}|^2$ components, the cross-polarization components $|t_{xy}|^2$ and $|t_{yx}|^2$ are nonzero, even for normal incidence.

These two degrees of freedom mentioned above confer properties to the structure that would not be possible if all the LC optical axes were parallel. In such case, there would be two resonances, due to the interaction of the two main polarizations with the ordinary and extraordinary refractive indices. However, there would not be the possibility of tuning simultaneously these two resonances by changing the optical axis angle in the *x*-*y* plane, since these refractive indices are constant. With the independent variation of the LC optical axes at the mirrors and at the cavities this can be overcome. This tunability is possible due to the existence of the two LC optical axes directions. One of the LC optical axes fixes the main polarization directions, while the second LC optical axis (with angle variable with respect to the first) is the one that actually influences the interaction of the incident light with the ordinary and extraordinary indexes.

The first property that we analyze is the tuning of the resonant wavelengths with the angles ϕ_M and ϕ_C. Since for normal incidence the election of the *x* and *y* axes (the main polarization directions) is free, this reduces the two degrees of freedom in the LC optical axes to a single one consisting of the difference $\phi_M - \phi_C$.

Fig. 4.3 shows the dependence of the two resonant wavelengths with this difference. As it can be seen, varying $\phi_M - \phi_C$ from 0º to 90º the first resonance (λ_1) can be tuned from *1.510 μm* to *1.538 μm* while the second (λ_2) can be tuned simultaneously from *1.630 μm* to *1.604 μm*. Materials with higher anisotropy than E7 LC would enlarge this tuning range [Demus-1998].

UNIVERSITAT ROVIRA I VIRGILI
DESIGN AND MODELLING OF PHOTONIC CRYSTALS WITH ANISOTROPIC COMPONENTS
Joaquin Cos Córcoles
ISBN:978-84-693-9433-5/DL:T.69-2011

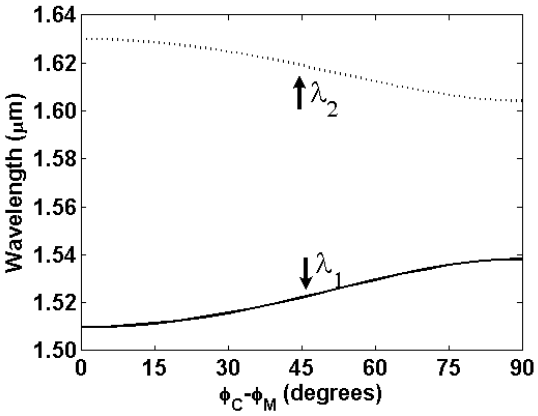

Fig. 4.3 Resonant wavelengths of the structure λ_1 (solid line) and λ_2 (dotted line), versus the difference ϕ_C - ϕ_M.

Fig. 4.4 shows the transmittance properties of the FP structure. The four graphs in Fig. 4.4 correspond to: a) $|t_{xx}|^2$, b) $|t_{xy}|^2$ c) $|t_{yx}|^2$ and d) $|t_{yy}|^2$, calculated for the resonant wavelengths λ_1 and λ_2. The calculations correspond to $\phi_M = 0^o$ (mirror LC optical axis parallel to the *y* axis). The phase of t_{xx}, t_{xy}, t_{yx} and t_{yy} for λ_1 is *0* for all ϕ_C, while for λ_2 the phase of t_{xx} and t_{yy} is *0* and the phase of t_{xy} and t_{yx} is π, also for all ϕ_C. These values (the amplitudes of the transmission coefficient and their phases) describe completely the transmittance properties of the FP structure at the resonant wavelengths, in the form of its characteristic Jones matrix, $J_{FP}(\phi_C;\ \phi_M = 0)$. The transmittance for any combination of angles ϕ_M and ϕ_C can be deduced from these values with the Jones matrix formalism. This is accomplished using the adequate rotation matrixes. Thus, the Jones matrix of the FP system for any two angles ϕ_C and ϕ_M can be written as:

$$J_{FP}(\phi_C,\phi_M) = R^{-1}(\phi_M)J_{FP}(\phi_C;\phi_M = 0)R(\phi_M), \tag{4.1}$$

with $R(\phi_M)$ the rotation matrix:

$$R(\phi_M) = \begin{pmatrix} \cos\phi_M & -\sin\phi_M \\ \sin\phi_M & \cos\phi_M \end{pmatrix}. \tag{4.2}$$

UNIVERSITAT ROVIRA I VIRGILI
DESIGN AND MODELLING OF PHOTONIC CRYSTALS WITH ANISOTROPIC COMPONENTS
Joaquin Cos Córcoles
ISBN:978-84-693-9433-5/DL:T.69-2011

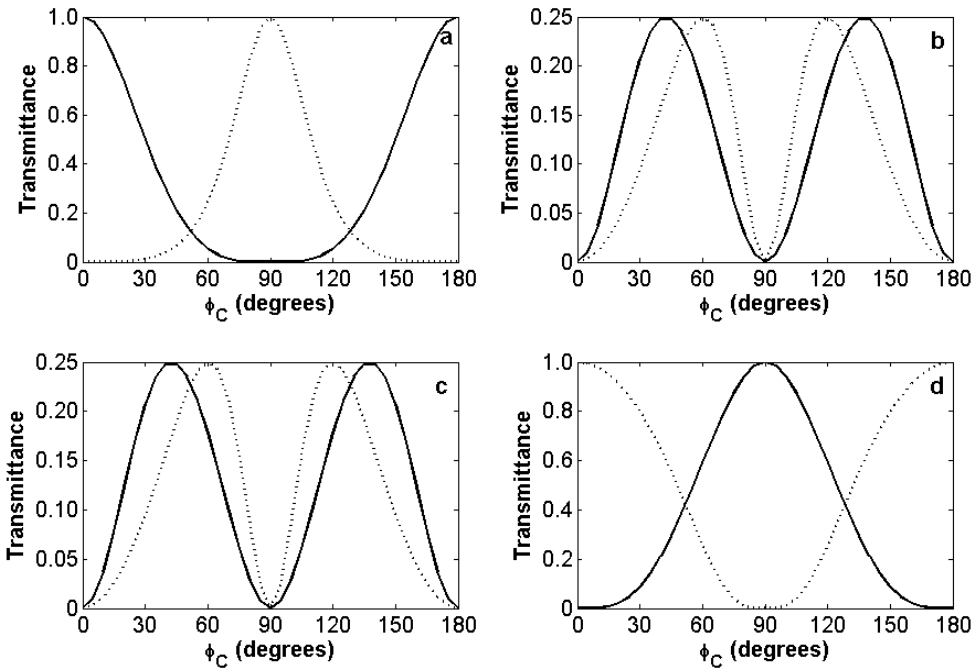

Fig. 4.4 Square modulus of the Jones matrix components of the FP structure at the resonant wavelengths λ_1 (solid lines) and λ_2 (dotted lines), versus the LC optical axis orientation at the cavity ($\phi_M = 0^o$; $\phi_C = [0^o - 180^o]$). a) $|t_{xx}|^2$, b) $|t_{xy}|^2$, c) $|t_{yx}|^2$ and d) $|t_{yy}|^2$.

In order to obtain a working device, it is necessary to complement the FP structure with other optical components that provide it with the desired functionality. By using a polarizer at the input of the device and an analyzer at the output, parallel to the input polarizer, we obtain a two-channel tunable equalizer. This is, a device that can change the resonant wavelengths and the relative transmittance between them as a function of the angles ϕ_C and ϕ_M. With the linear polarizers at the input and at the output of the FP structure oriented with the *x* direction, the transmittance of the device is proportional to the *x*-*x* component of the Jones matrix $J_{FP}(\phi_C; \phi_M)$, $t'_{xx}(\phi_C; \phi_M)$. This component is related by means of Eqs. (4.1) and (4.2) to the components of the $J_{FP}(\phi_C; \phi_M = 0)$ through the expression:

$$t'_{xx}(\phi_C, \phi_M) = t_{xx}\cos^2\phi_M + t_{xy}\cos\phi_M\sin\phi_M + t_{yx}\cos\phi_M\sin\phi_M + t_{yy}\cos^2\phi_M. \qquad (4.3)$$

UNIVERSITAT ROVIRA I VIRGILI
DESIGN AND MODELLING OF PHOTONIC CRYSTALS WITH ANISOTROPIC COMPONENTS
Joaquin Cos Córcoles
ISBN:978-84-693-9433-5/DL:T.69-2011

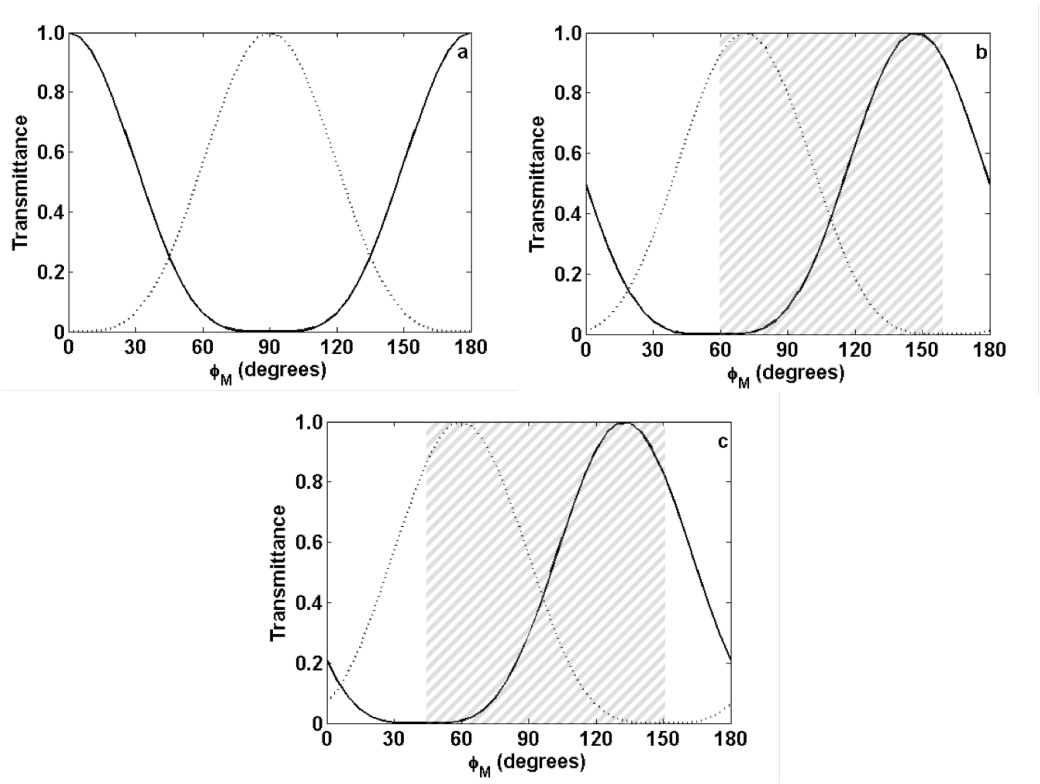

Fig. 4.5 Transmittance at the resonant λ_1 (solid lines) and λ_2 (dotted lines), of the optical two-channel equalizer for three angle differences. a) $\phi_M = \phi_C$, $\lambda_1 = 1.510$ μm and $\lambda_2 = 1.630$ μm. There is complete equalization: the maxima of one resonance correspond with the minima of the other (90° relative shift between the transmittance curves) b) $\phi_C - \phi_M = 30°$, $\lambda_1 = 1.516$ μm and $\lambda_2 = 1.625$ μm. The shift between the two transmittance curves is smaller than 90°. The equalization is not complete. The shaded region corresponds to the range of ϕ_M with the better efficiency. c) $\phi_C - \phi_M = 45°$, $\lambda_1 = 1.522$ μm and $\lambda_2 = 1.619$ μm. This case corresponds to the smallest relative shift between the transmittance curves.

Fig. 4.5 shows the total transmittance of such a device when the LC optical axes are rotated between $\phi_M = 0^o$ to $\phi_M = 180^o$, but with a fixed difference between their director angles. The three plots correspond to differences $\phi_C - \phi_M = 0^o$ (Fig. 4.5a), $\phi_C - \phi_M = 30^o$ (Fig. 4.5b) and $\phi_C - \phi_M = 45^o$ (Fig. 4.5c). For $\phi_C - \phi_M = 0^o$ the resonances are at $\lambda_1 = 1.510$ μm and $\lambda_2 = 1.630$ μm. The transmittance curves for the two resonant wavelengths are equal but shifted 90^o. With this, the first resonance maximum (T = 100%) and the second resonance minimum (T = 0%) appear for $\phi_M = 0^o$ and $\phi_M = 180^o$, while the first resonance minimum and the second resonance maximum appear for $\phi_M = 90^o$. This means that in this configuration and for this pair of resonant

UNIVERSITAT ROVIRA I VIRGILI
DESIGN AND MODELLING OF PHOTONIC CRYSTALS WITH ANISOTROPIC COMPONENTS
Joaquin Cos Córcoles
ISBN:978-84-693-9433-5/DL:T.69-2011

wavelengths, there is *complete* equalization: one channel is completely suppressed while the other is completely transmitted. Another interesting feature in this configuration is that for $\phi_M = 45^o$ and $\phi_M = 135^o$ the transmittance for the two resonant wavelengths intersect and this intersection level is the same for the two values of ϕ_M.

For the case $\phi_C - \phi_M = 30^o$ the resonant wavelengths are now $\lambda_1 = 1.516\ \mu m$ and $\lambda_2 = 1.625\ \mu m$. The transmittances have shifted to the left in a different amount, thus the relative shift between the curves is smaller than in the previous case. This means that in this configuration the transmittance maxima of one resonance do not match with the minima of the other, and consequently the equalization is not complete. However, there are still configurations where one of the channels is completely blocked while the other is still transmitted with transmittance *85.47%* (first resonance blocked, $\phi_M = 60^o$) and *90.39%* (second resonance blocked, $\phi_M = 160^o$). Differently to the previous case, the intersection of the transmittance for the two resonant wavelengths is at different levels: *38.33%* for $\phi_M = 109^o$ and *14.66%* for $\phi_M = 19^o$. Consequently, it is advisable to choose the adequate range of ϕ_M (between $\phi_M = 60^o$ and $\phi_M = 160^o$, indicated by the shaded region in the graph) to achieve a maximum efficiency of the device.

Finally, the case $\phi_C - \phi_M = 45^o$ corresponds to the smallest shift between the transmittance spectra. The resonant wavelengths are now $\lambda_1 = 1.522\ \mu m$ and $\lambda_2 = 1.619\ \mu m$. We include this case because it is the worst case: when one of the channels is blocked the transmittance of the other has the smallest transmittances, which is *78.58%* (first resonance blocked, $\phi_M = 40^o$) and *82.91%* (second resonance blocked, $\phi_M = 150^o$).

UNIVERSITAT ROVIRA I VIRGILI
DESIGN AND MODELLING OF PHOTONIC CRYSTALS WITH ANISOTROPIC COMPONENTS
Joaquin Cos Córcoles
ISBN:978-84-693-9433-5/DL:T.69-2011

4.2 Analysis of the optical properties of a double-cavity Fabry-Perot equalizer

The structure proposed is a multilayer double-cavity Fabry-Perot. Fig. 4.6 shows a schematic view of the structure. The mirrors are composed of a periodic stacking of porous silicon bilayers, with the high index (H) layer of $n = 2.5$ and the low index (L) layer of $n = 1.5$, all of this layers are quarter-wave layers. As in the device of the previous section, an additional H layer has been added to the mirrors in order to increase the reflectance maximum value. The two cavities are half-wave layers of E7 Liquid Crystal (labelled as E layers), while the layer between the two resonant cavities (which we designate as the isolator) is a half-wave layer of low index porous silicon. Thus, the structure can be expressed as $[HL]^3$ H-E_1-2L-E_2-H$[LH]^3$, where the subscript of the E layers indicate that the LC optical axis direction of the two cavities can be different between them.

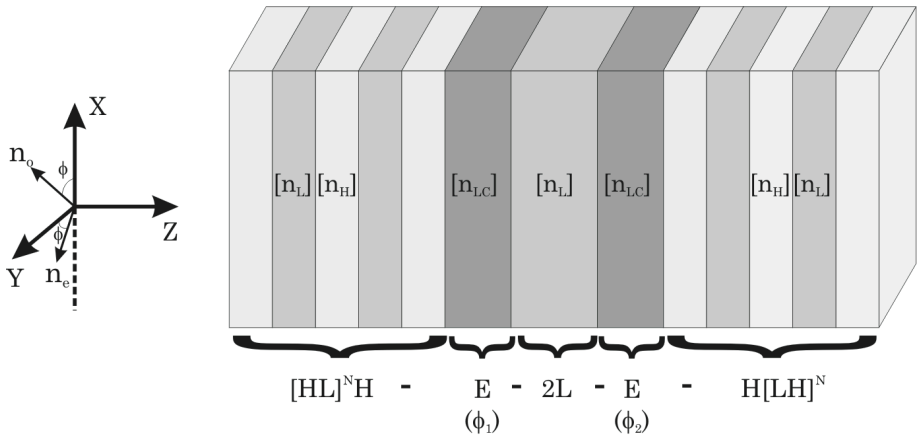

Fig. 4.6 Schematic view of the Fabry-Perot structure composed of two mirrors with N+1 quarter-wave (optical thickness) layers of porous silicon with n = 2.5 (H) and N quarter-wave layers of porous silicon with n = 1.5 (L) and two half-wave layers of liquid crystal (E) as cavities separated by a half-wave layer of porous silicon with n = 1.5 as isolator. The ϕ_1 and ϕ_2 indicate the angle of the LC optical axis with the y axis, taking into account that the LC optical axis is parallel to the layers.

UNIVERSITAT ROVIRA I VIRGILI
DESIGN AND MODELLING OF PHOTONIC CRYSTALS WITH ANISOTROPIC COMPONENTS
Joaquin Cos Córcoles
ISBN:978-84-693-9433-5/DL:T.69-2011

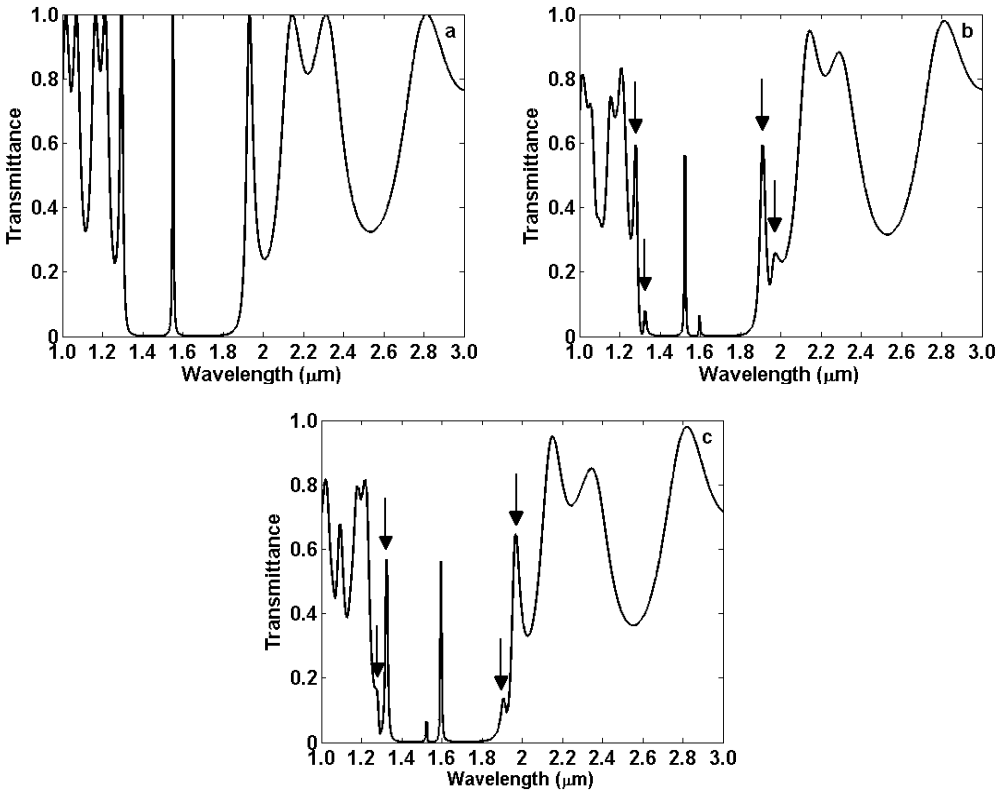

Fig. 4.7 Transmittance spectra for the structure $[HL]^3H$-E_1-$2L$-E_2-$H[LH]^3$ a) Isotropic state (n_{isoLC} = 1.585, n_{Si} = 3.4). A resonance for λ = 1.55 μm can be observed. b) $|t_{xx}|^2$ and c) $|t_{yy}|^2$ for the anisotropic state ($\phi_1 = 20^o$, $\phi_2 = 40^o$, n_{oLC} = 1.522, n_{eLC} = 1.704 n_{Si} = 3.4). The resonance present in the isotropic state splits in two, λ_1 = 1.536 μm and λ_2 = 1.585 μm. Arrows indicate spurious resonances

We have designed the FP structure to have one resonance in *1.550 μm* when the LC is in its isotropic state (Fig. 4.7a). When the liquid crystal is in its anisotropic state, the resonance splits in two new resonances, which have different transmission level in the two main polarizations (Figs. 4.7b and 4.7c).

An alternative structure could be the same but using as isolator a half-wave layer of high index porous silicon instead of a low index layer. Fig. 4.8 shows transmission for the two main polarizations for such a structure. It can be seen that new resonances appear within the bandgap (the low transmission region) of the mirrors, indicated with arrows in the graphs. These spurious resonances are caused by the mismatch between the refractive index of the LC and of the isolator.

UNIVERSITAT ROVIRA I VIRGILI
DESIGN AND MODELLING OF PHOTONIC CRYSTALS WITH ANISOTROPIC COMPONENTS
Joaquin Cos Córcoles
ISBN:978-84-693-9433-5/DL:T.69-2011

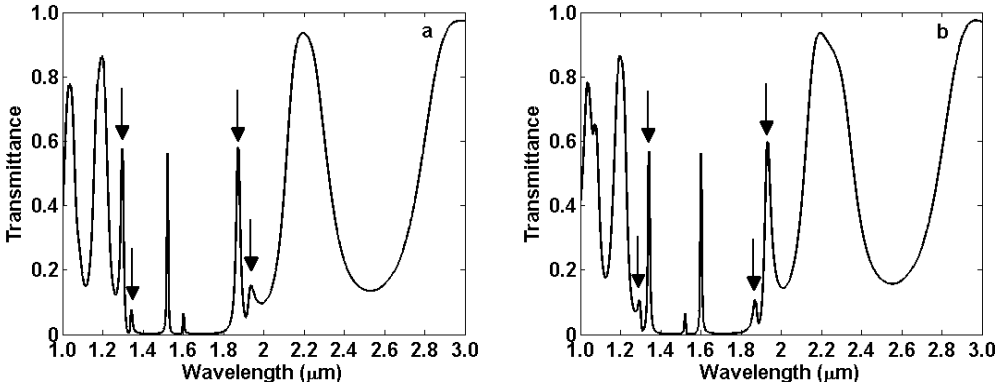

Fig. 4.8 Transmittance spectra for the structure $[HL]^3H$-E_1-$2H$-E_2-$H[LH]^3$ a) $|t_{xx}|^2$ and b) $|t_{yy}|^2$ for the anisotropic state ($\phi_1 = 20^o$, $\phi_2 = 40^o$, $n_{oLC} = 1.522$, $n_{eLC} = 1.704$ $n_{Si} = 3.4$). The undesired resonances are closer to the design wavelength than Fig. 4.8 case. Arrows indicate spurious resonances

The optimal structure would be such that these spurious resonances are cancelled. However, this approach would imply a multilayer design of the isolator, which would increase the device complexity. We have chosen a simpler approach consisting of using the low index porous silicon layer as isolator, since its refractive index is better matched to that of the LC.

The tunability of the filter is achieved by allowing the orientations of the LC optical axes at the two cavities to be different. In the same way as in the previous section, we propose to tune the filter properties by rotating the LC optical axis in the *x*-*y* plane. With this configuration we have two degrees of freedom: the angle of the optical axis at the first cavity (of the LC optical axis with the *y* axis), ϕ_1, and the angle of the optical axis at the second cavity, ϕ_2.

In this structure, the tunability is possible because of the existence of the two LC optical axes directions. One of the LC optical axes fixes the main polarization directions ($\phi_1 = 0^o$), while the second LC optical axis (with angle variable with respect to the first, ($0^o \leq \phi_2 \leq 180^o$) is the one that actually influences the interaction of the incident light with the ordinary and extraordinary indexes.

UNIVERSITAT ROVIRA I VIRGILI
DESIGN AND MODELLING OF PHOTONIC CRYSTALS WITH ANISOTROPIC COMPONENTS
Joaquin Cos Córcoles
ISBN:978-84-693-9433-5/DL:T.69-2011

Fig. 4.9 shows the dependence of the two resonant wavelengths with this difference. As it can be seen, varying (ϕ_2 - ϕ_1) between *0º* and *90º* the first resonance (λ_1) can be tuned from *1.523 μm* to *1.560 μm* while the second (λ_2) can be tuned simultaneously from *1.599 μm* to *1.560 μm*. This tuning range can achieve higher values using any liquid crystal with a higher birefringence than E7 LC [Demus-1998].

To be able to design devices based on this structure, it is necessary to know the transmittance properties at the resonant wavelengths. This is shown in Fig. 4.10 where the four graphs in the figure correspond to the square modulus of the Jones matrix components at the resonant wavelengths as a function of the angle difference. For parallel optical axes (ϕ_2 - ϕ_1 = *0º*) the first resonant wavelength is transmitted with a polarization parallel to the *x* axis while the second resonant wavelength polarized along the *y* axis. Meanwhile for perpendicular axes (ϕ_2 - ϕ_1 = *90º*) the two resonances become degenerated at λ = *1.560 μm* and appear singular transmittance values, that is, transmittance levels are maximum (T = *100%*) for the main polarizations and minimum (T = *0%*) for the cross polarizations. For all cases the phase for λ_1 and λ_2 is *0*. These values (the amplitudes of the transmission coefficient and their phases) describe completely the transmittance properties of the FP structure at the resonant wavelengths, in the form of its characteristic Jones matrix, $J_{FP}(\phi_1 = 0; \phi_2)$. Combining this Jones Matrix with Eq. (4.2) the transmittance for any combination of angles ϕ_1 and ϕ_2 can be deduced.

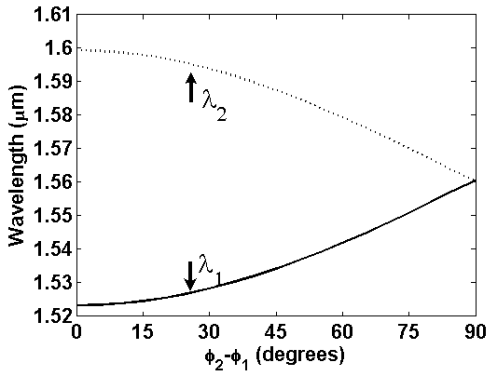

Fig. 4.9 Resonant wavelengths of the structure λ_1 (solid line) and λ_2 (dotted line), versus the difference ϕ_2 - ϕ_1.

UNIVERSITAT ROVIRA I VIRGILI
DESIGN AND MODELLING OF PHOTONIC CRYSTALS WITH ANISOTROPIC COMPONENTS
Joaquin Cos Córcoles
ISBN:978-84-693-9433-5/DL:T.69-2011

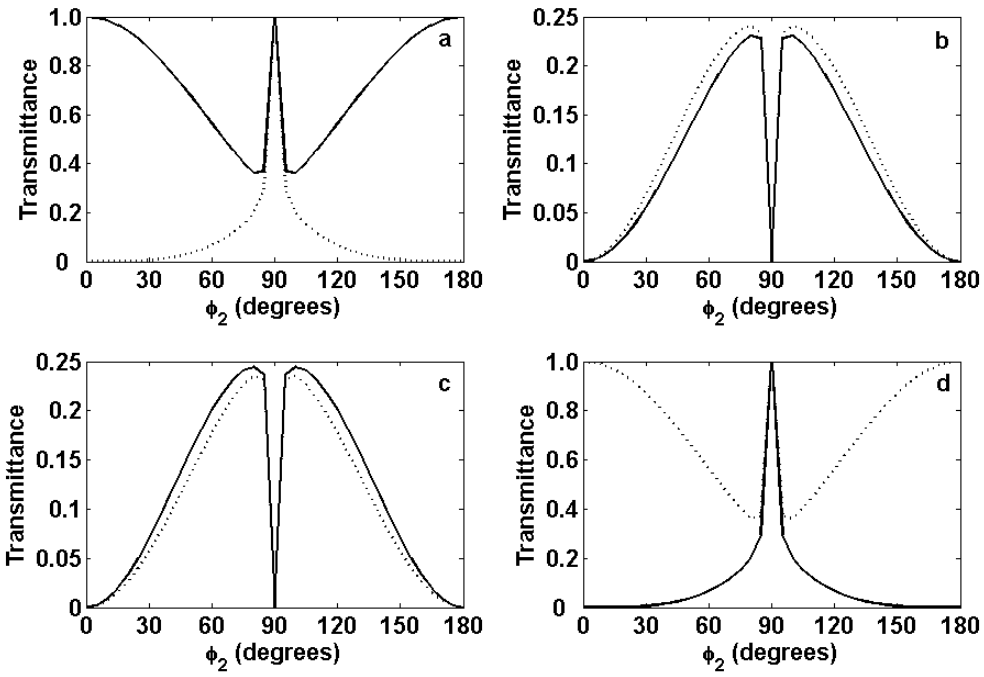

Fig. 4.10 Square modulus of the Jones matrix components of the FP structure at the resonant wavelengths λ_1 (solid lines) and λ_2 (dotted lines), versus the LC optical axis orientation at the second cavity ($\phi_1 = 0^o$; $\phi_2 = [0^o - 180^o]$). a) $|t_{xx}|^2$, b) $|t_{xy}|^2$, c) $|t_{yx}|^2$ and d) $|t_{yy}|^2$.

Up to now we have considered the LC optical orientation of the first cavity, ϕ_1, oriented always in the *y* axis ($\phi_1 = 0^o$) because its LC optical axis was fixing the main polarization directions. However using a linear polarizer at the input of the device and a linear analyzer at the output, parallel to the input polarizer defines the main polarization directions and permits ϕ_1 to be oriented in other directions to obtain different functionalities.

One of such functionalities can be a two-channel tunable equalizer like the one presented in the previous section. This is, a device that can change the resonant wavelengths and the relative transmittance between them as a function of the angles ϕ_1 and ϕ_2. Fig. 4.11 shows the total transmittance of such a device when the polarizer and the analyzer polarize the light along the *x* axis, the LC optical axes are rotated between $\phi_1 = 0^o$ and $\phi_1 = 180^o$, but with a fixed difference between their director angles. The three plots correspond to differences $\phi_2 - \phi_1 = 0^o$ (Fig. 4.11a), $\phi_2 - \phi_1 = 30^o$ (Fig. 4.11b),

UNIVERSITAT ROVIRA I VIRGILI
DESIGN AND MODELLING OF PHOTONIC CRYSTALS WITH ANISOTROPIC COMPONENTS
Joaquin Cos Córcoles
ISBN:978-84-693-9433-5/DL:T.69-2011

and $\phi_2 - \phi_1 = 45^o$ (Fig. 4.11c). For $\phi_2 - \phi_1 = 0^o$ the resonances are at $\lambda_1 = 1.523\ \mu m$ and $\lambda_2 = 1.599\ \mu m$. The transmittance curves for the two resonant wavelengths are equal but shifted 90^o. At $\phi_1 = 0^o$ and $\phi_1 = 180^o$ appear maxima (T = 100%) for the first resonance and minima (T = 0%) for the second resonant wavelength. At $\phi_1 = 90^o$ appear minima for the first resonant wavelength and maxima for the second resonant wavelength. As we can see, at $\phi_1 = 45^o$ and $\phi_1 = 135^o$ the two resonant wavelengths have the same transmittance level (T = 25%).

For $\phi_2 - \phi_1 = 30^o$ the resonances are at $\lambda_1 = 1.528\ \mu m$ and $\lambda_2 = 1.594\ \mu m$. In this case, the two transmittances curves have shifted 15^o with respect to $\phi_2 - \phi_1 = 0^o$ case, therefore the maxima for one resonant wavelength match with the minima for the other resonant wavelength. Again there are two angles ($\phi_1 = 30^o$ and $\phi_1 = 120^o$) where the transmittance levels of the two resonant wavelengths are equal.

Finally, for $\phi_2 - \phi_1 = 45^o$ the resonances are at $\lambda_1 = 1.534\ \mu m$ and $\lambda_2 = 1.587\ \mu m$. In this case, the two transmittances curves have shifted 22.5^o with respect to $\phi_2 - \phi_1 = 0^o$ case, therefore the maxima for one resonant wavelength match with minima for the other resonant wavelength. Again there are two angles ($\phi_1 = 22.5^o$ and $\phi_2 - \phi_1 = 112.5^o$) where the transmittance levels of the two resonant wavelengths are equal.

Different to the device of section 4.1, for the double-cavity Fabry-Perot for all angle differences there is *complete* equalization: one channel is completely suppressed while the other is completely transmitted.

UNIVERSITAT ROVIRA I VIRGILI
DESIGN AND MODELLING OF PHOTONIC CRYSTALS WITH ANISOTROPIC COMPONENTS
Joaquin Cos Córcoles
ISBN:978-84-693-9433-5/DL:T.69-2011

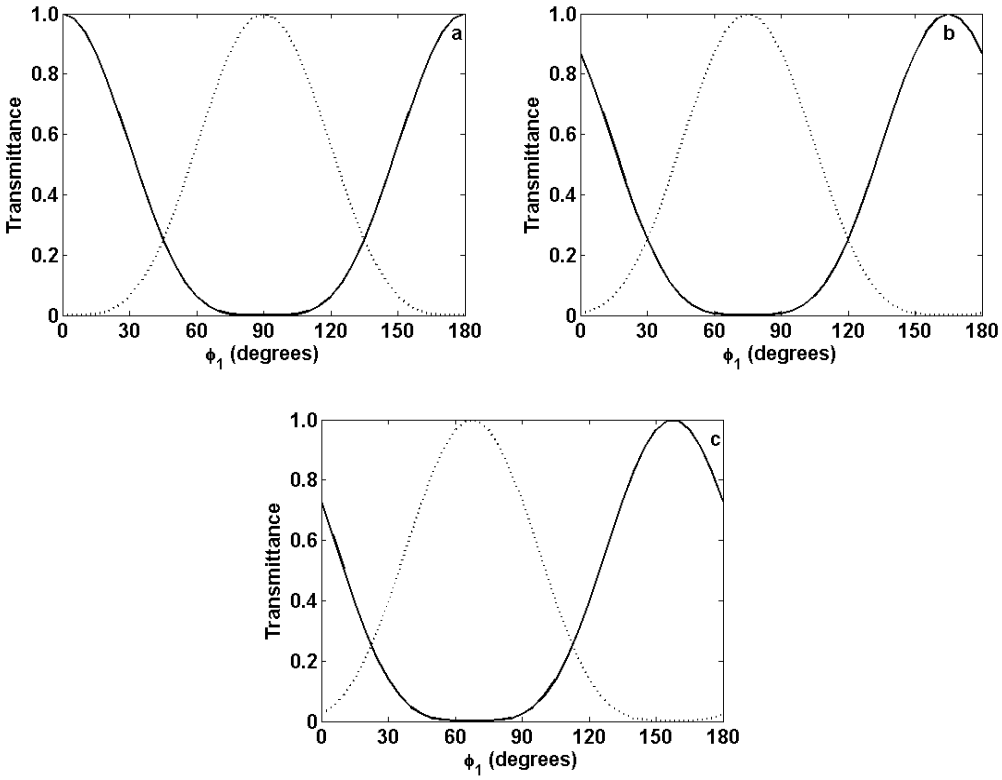

Fig. 4.11 Transmittance at the resonant λ_1 (solid lines) and λ_2 (dotted lines), of the optical two-channel equalizer for three angle differences. a) $\phi_1 = \phi_2$, $\lambda_1 = 1.523$ μm and $\lambda_2 = 1.599$ μm. b) $\phi_2 - \phi_1 = 30°$, $\lambda_1 = 1.528$ μm and $\lambda_2 = 1.594$ μm. c) $\phi_2 - \phi_1 = 45°$, $\lambda_1 = 1.534$ μm and $\lambda_2 = 1.587$ μm.

4.3 Conclusions

We have analyzed the transmittance properties of two tunable Fabry-Perot structures composed of silicon and anisotropic materials, whose optical axes can be varied. The first FP structure (single-cavity FP) is composed of a cavity of anisotropic material surrounded by two mirrors, composed of successive layers of silicon and anisotropic materials. The second FP structure (double-cavity FP) is composed of two cavities of anisotropic material isolated by a low-index silicon layer and surrounded by two mirrors, made of successive layers of high- and low-index porous silicon. We have chosen E7 liquid crystal as anisotropic material because its optical axis can be

UNIVERSITAT ROVIRA I VIRGILI
DESIGN AND MODELLING OF PHOTONIC CRYSTALS WITH ANISOTROPIC COMPONENTS
Joaquin Cos Córcoles
ISBN:978-84-693-9433-5/DL:T.69-2011

electrically varied. In contrast with previous works, we have designed the structures so that the LC optical axes at the mirrors and at the cavities (for the first structure) and at the two cavities (for the second structure) are always parallel to the layers and their direction can be varied independently.

Following the *4x4* transfer matrix method, suited to multilayer structures with anisotropic materials, we are able to obtain the Jones matrix of the structures, and thus completely determine their transmission properties both in amplitude and in phase, and for the two main polarizations.

The FP structures have been designed to have one resonance in the middle of the gap (at *1.550 μm*) when the LC is in its isotropic state. When the LC is in its anisotropic state this resonance splits in two due to the interaction of the light with the ordinary and extraordinary indexes. The tuning of the resonant wavelengths and the associated transmittance is due to the existence of two independent LC optical axes within the mirrors and within the cavity (for the first structure) and within the two cavities (for the second structure).

On the basis of the results obtained in this work, we propose to apply both structures as an optical two-channel equalizer that permits tuning the two resonances and their relative amplitude levels. This application is obtained by placing the FP structures in between two parallel linear polarizers. We have analyzed different relative orientations between the LC optical axes of this equalizer to determine its performance.

For the single-cavity FP, a tuning capability of *28 nm* can be achieved as a function of the relative orientation between the LC optical axes. Thus, for parallel optical axes we obtain *complete* equalization: one channel is completely suppressed (T = *0%*) as the other is completely transmitted (T = *100%*). In this case, we get the largest resonance split *120 nm*. For other relative orientations of the LC optical axes, it is apparent that the transmittances for each of the resonances shift with respect to each other and consequently complete equalization is not achieved. Nevertheless, complete blocking of one channel with respect to the other can be obtained. We have shown that the

UNIVERSITAT ROVIRA I VIRGILI
DESIGN AND MODELLING OF PHOTONIC CRYSTALS WITH ANISOTROPIC COMPONENTS
Joaquin Cos Córcoles
ISBN:978-84-693-9433-5/DL:T.69-2011

worst case corresponds to a difference in the optical axes orientation of *45°*, in which the transmittance of the unblocked channel has a minimum of *78.58%* (first resonance blocked) and *82.91%* (second resonance blocked).

For the double-cavity FP, a tuning capability of *39 nm* can be achieved as a function of the relative orientation between the LC optical axes. For parallel optical axes we obtain complete equalization: one of the resonant wavelengths is completely suppressed (T = *0%*) for one polarization and completely transmitted (T = *100%*) for the perpendicular polarization, at the same time the other resonant wavelength is completely transmitted or suppressed at the opposite polarizations. In this case, we get the largest resonance split of *80 nm*. Oppositely, for perpendicular optical axes, the two resonances become degenerated at *1.560 μm* and both polarizations are completely transmitted (T = *100%*). In contrast with the single-cavity FP, *complete* equalization is achieved for all the orientations of the LC optical axes. However, spurious resonances appear within the gap and they are caused by the mismatch between the refractive index of the LC and of the isolator.

The results presented in this chapter show that both devices can be useful with a good performance in a wide range of resonant frequencies.

UNIVERSITAT ROVIRA I VIRGILI
DESIGN AND MODELLING OF PHOTONIC CRYSTALS WITH ANISOTROPIC COMPONENTS
Joaquin Cos Córcoles
ISBN:978-84-693-9433-5/DL:T.69-2011

UNIVERSITAT ROVIRA I VIRGILI
DESIGN AND MODELLING OF PHOTONIC CRYSTALS WITH ANISOTROPIC COMPONENTS
Joaquin Cos Córcoles
ISBN:978-84-693-9433-5/DL:T.69-2011

Chapter 5

Design of tunable filters and waveguide devices

Tunable photonic crystal (PC) technology is one of the essential technologies for the development of the photonic analogues of classical electronic devices. Several structures combining photonic crystals with nonlinear optical (NLO) materials or liquid crystal (LC) materials have been proposed [Busch-1999; Takeda-2002; Maksymov-2006]. Furthermore, a high-intensity control signal with frequency outside the bandgap changes the properties of the crystal [Cuesta-Soto-2004]. Among available strategies, liquid crystals are recognized as unique materials that combine birefringence and periodic spatial ordering with a pronounced sensitivity to external electric fields [Weiss-2005].

Besides the tuning properties of the liquid crystals, the optical anisotropy is another fundamental property than can be taken as a degree of freedom in the design of applications. In the last years there have been several works that exploit this anisotropy in the theoretical [Kopperschmidt-2001; Arriaga-2008] or the experimental [Schuller-2005; Sun-2007] analysis of photonic crystals. However, only a few studies on

UNIVERSITAT ROVIRA I VIRGILI
DESIGN AND MODELLING OF PHOTONIC CRYSTALS WITH ANISOTROPIC COMPONENTS
Joaquin Cos Córcoles
ISBN:978-84-693-9433-5/DL:T.69-2011

LC-infiltrated 2D photonic structures are devoted to study the gap maps and tunable capabilities as a function of the geometrical parameters of the photonic crystal for direct and inverse structures.

The aim of this chapter is to study and analyze the viability of tunable devices based on liquid crystal and silicon. We start our study with the tunable filters analyzing structures without defects. The studied structures are a silicon photonic crystal (PC) with a triangular lattice of holes infiltrated with liquid crystal and a triangular lattice of silicon rods surrounded by liquid crystal. The second part of this chapter is devoted to the analysis of tunable waveguides, where we optimize, by means of the plane-wave expansion method and the supercell formulation presented in chapter 3, a silicon photonic crystal where a line of scatterers filled by liquid crystal acts as core of the waveguide. Finally, a methodology for the study of the practical implementation of tunable waveguides based on silicon photonic crystals with liquid crystal-infiltrated pores is presented. First, by using the FDTD method, the transmission properties of the waveguide depending on the liquid crystal optical axis orientation are studied. Then by means of the plane-wave expansion method and taking into account the anisotropy of the photonic crystal components and considering adequate supercells, the transmission or rejection of the optical beam are explained.

5.1 Study of the tunability of the bandgap of liquid crystal based photonic crystals

In this section we study and analyze the viability of tunable filters made of photonic crystals without defects based on liquid crystal and silicon. To this end, we study the gap maps as a function of the geometrical parameters of the photonic crystal (radius of the scatterers), the optical axis angle of LC and the PC configuration (holes infiltrated with liquid crystal or rods surrounded by liquid crystal). The knowledge of these properties is important since they have to be taken into account when designing

UNIVERSITAT ROVIRA I VIRGILI
DESIGN AND MODELLING OF PHOTONIC CRYSTALS WITH ANISOTROPIC COMPONENTS
Joaquin Cos Córcoles
ISBN:978-84-693-9433-5/DL:T.69-2011

tunable devices based on liquid crystal-infiltrated photonic crystals. One of the most important aspects in this study is that the optical anisotropy of the liquid crystal component induces a change in the symmetry properties of the photonic crystal lattice. For this reason, an exhaustive study of the irreducible Brillouin zone is necessary.

Due to the anisotropy of the liquid crystal and its influence on the TE polarization commented in chapter 3, the Irreducible Brillouin Zone (IBZ) usually considered for isotropic 2D photonic crystals with triangular lattice is not sufficient to represent the whole First Brillouin Zone (FBZ). In fact, in [Alagappan-2006] it is demonstrated that the IBZ depends on the LC optical axis orientation. Such work provides us with a means for calculating the photonic bandgaps based in choosing the IBZ depending on the LC optical axis orientation and calculating all the **k** points within the IBZ.

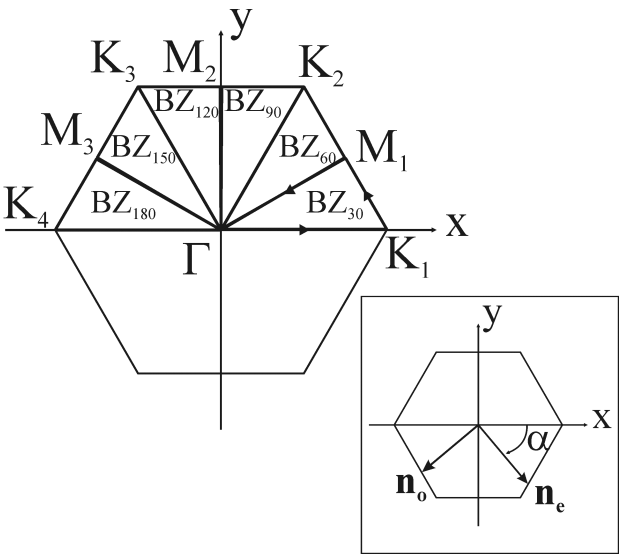

Fig. 5.1 Definition of the BZ sets for the accurate and efficient calculation of the photonic bandgaps of the studied photonic crystals. The inset shows the definition of the angle α that characterizes the LC optical axis orientation with respect x axis (α = 90 - ϕ).

UNIVERSITAT ROVIRA I VIRGILI
DESIGN AND MODELLING OF PHOTONIC CRYSTALS WITH ANISOTROPIC COMPONENTS
Joaquin Cos Córcoles
ISBN:978-84-693-9433-5/DL:T.69-2011

We propose an alternative method to calculate the photonic bandgaps based on calculating the bands along the **k** in the main high symmetry directions of the First Brillouin Zone. With this aim we have divided the upper half of the FBZ in sets of **k** points denominated BZ_{30}, BZ_{60}, BZ_{90}, BZ_{120}, BZ_{150}, and BZ_{180}, as it is shown in Figure 5.1. The set BZ_{30} consists of the **k** points along the path $\mathbf{\Gamma}$-$\mathbf{K}_1$-$\mathbf{M}_1$-$\mathbf{\Gamma}$, the set BZ_{60} to the path $\mathbf{\Gamma}$-$\mathbf{M}_1$-$\mathbf{K}_2$-$\mathbf{\Gamma}$, and analogously for the other sets. Only the upper half is meaningful, since for all orientations of the optical axis the system retains the *180º* rotation symmetry. Taking into account that the symmetry of the photonic crystal is reduced by the fact that the liquid crystal sets a preferential direction on the structure, the maximum and minimum frequencies of the photonic bands will appear at the points along the paths included in the BZ sets. This permits us to obtain the photonic bandgap for TE modes without calculating the photonic bands for all **k** points of the FBZ, resulting in a less time-consuming numerical method. Thus, the photonic bandgap limits and its width are determined by taking the maximum frequency for the lower band and the minimum frequency of the upper band, at the calculated points from each of the sets from BZ_{30} to BZ_{180}.

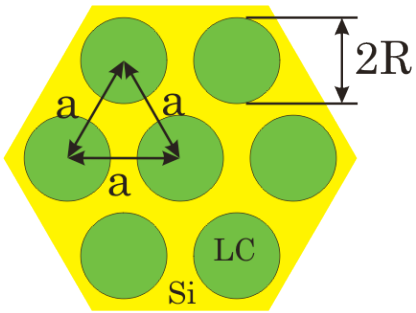

Fig. 5.2 Schematic view of the photonic crystal composed of silicon with a triangular lattice of circular holes with radius R and lattice constant a, infiltrated by E7 liquid crystal.

UNIVERSITAT ROVIRA I VIRGILI
DESIGN AND MODELLING OF PHOTONIC CRYSTALS WITH ANISOTROPIC COMPONENTS
Joaquin Cos Córcoles
ISBN:978-84-693-9433-5/DL:T.69-2011

Using this method we have analyzed the photonic bang gap properties of a photonic crystal composed of silicon (n_{Si} = *3.4* at *0.8 eV*) with a triangular lattice of circular holes with radius *R* and lattice constant *a*, infiltrated by E7 liquid crystal (n_o = *1.522*, n_e = *1.704*). Fig. 5.2 shows a schematic view of the structure. Typical fabricated silicon photonic crystals lattice dimensions are of the order of a few microns [Leonard-2000], with hole diameters of some hundreds of nanometers. On the other hand, the E7 molecule length is about *2-3 nm*, which ensures the mobility of the LC within the hole and thus its control by means of external electric fields.

We have carried the analysis of the gap maps as a function of the hole radius and of the LC director angle α. The gap maps were calculated for α between 0^o and 60^o. We use *529* plane-waves in order to guarantee convergence for the first 8 bands within an error lower than *1%*. Due to the low index contrast between silicon and liquid crystal there exists only one photonic bandgap between the 1st and 2nd modes.

Figure 5.3a shows the gap maps for TE polarization for α = 0^o and α = 30^o, which correspond to the biggest difference between the gap maps. The solid line delimits the area corresponding to the gap map for α = 0^o, while the dashed line corresponds to the gap map for α = 30^o. The gap map for any other angle is included within the gap map for α = 0^o and includes the gap map for α = 30^o. The arrows indicate the radius corresponding to the maximum bandgap width for the two angles i.e. for α = 0^o the maximum bandgap ($\Delta\omega a/2\pi c$ = *0.0581*) is obtained at *R/a = 0.401* while for α = 30^o the maximum bandgap ($\Delta\omega a/2\pi c$ = 0.0521) is obtained at *R/a = 0.395*. Fig. 5.3b shows a detail of the graph in Fig. 5.3a, for the range of *R/a* where the bandgap is maximum. As it can be seen, the change of the gap width with the LC optical axis orientation is small, and it is mainly caused by the decrease of the upper edge of the bandgap with increasing α. In this figure the difference between the radii at which the gap is maximum can be observed. Finally, Fig. 5.3c shows a detail of the gap maps in the range of *R/a* around the value where the gap closes. As it can be seen, the gap closes at different *R/a* for different LC optical axis orientations.

UNIVERSITAT ROVIRA I VIRGILI
DESIGN AND MODELLING OF PHOTONIC CRYSTALS WITH ANISOTROPIC COMPONENTS
Joaquin Cos Córcoles
ISBN:978-84-693-9433-5/DL:T.69-2011

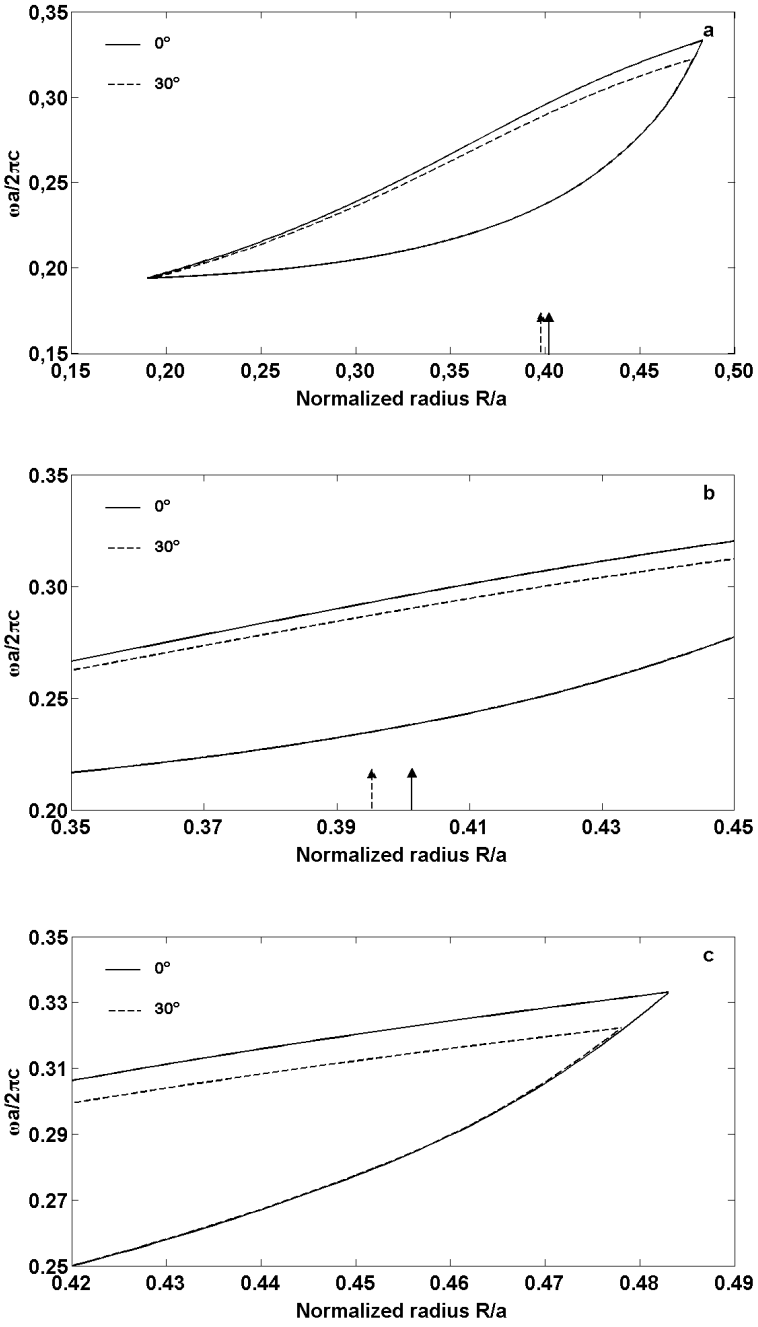

Fig. 5.3 a) Photonic bandgap map for the TE polarization for $\alpha = 0^o$ *(solid line) and* $\alpha = 30^o$ *(dashed line). The arrows indicate the R/a corresponding to the maximum gap width. b) Detail of the region around the maximum gap width. c) Detail of the region of R/a with the biggest difference between the gap maps at* $\alpha = 0^o$ *and* $\alpha = 30^o$.

UNIVERSITAT ROVIRA I VIRGILI
DESIGN AND MODELLING OF PHOTONIC CRYSTALS WITH ANISOTROPIC COMPONENTS
Joaquin Cos Córcoles
ISBN:978-84-693-9433-5/DL:T.69-2011

The dependence of the band gap limits with the LC orientation angle can be explained by the analysis of the H_z component field distribution for the photonic bands corresponding to such limits (Figs. 5.4-5.5). As we commented before, the gap limits are formed by the first and second photonic bands (Fig. 5.4a and 5.5a).

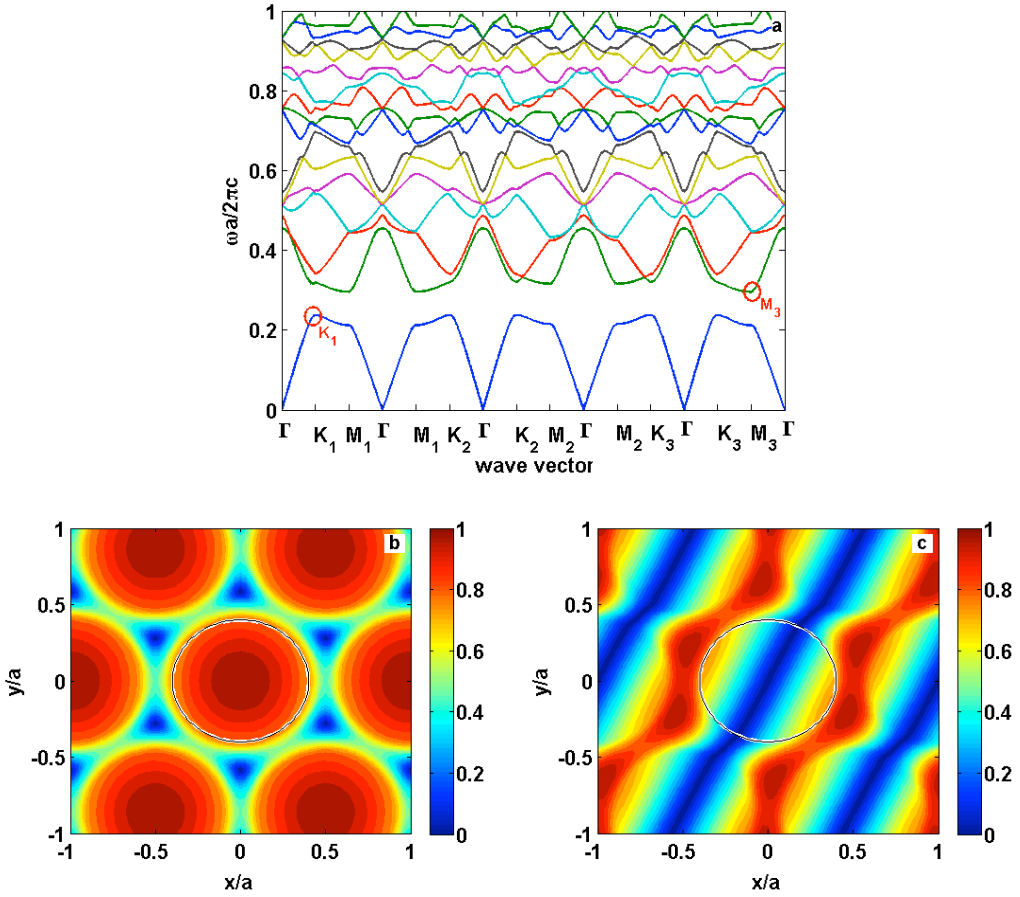

Fig. 5.4 a) Photonic band structures for the TE polarization for $\alpha = 0^o$. *Red circles indicate the k-points where the field distribution (as the modulus of the* H_z *component) is calculated for b) the lower and c) upper limits of the bandgaps.*

UNIVERSITAT ROVIRA I VIRGILI
DESIGN AND MODELLING OF PHOTONIC CRYSTALS WITH ANISOTROPIC COMPONENTS
Joaquin Cos Córcoles
ISBN:978-84-693-9433-5/DL:T.69-2011

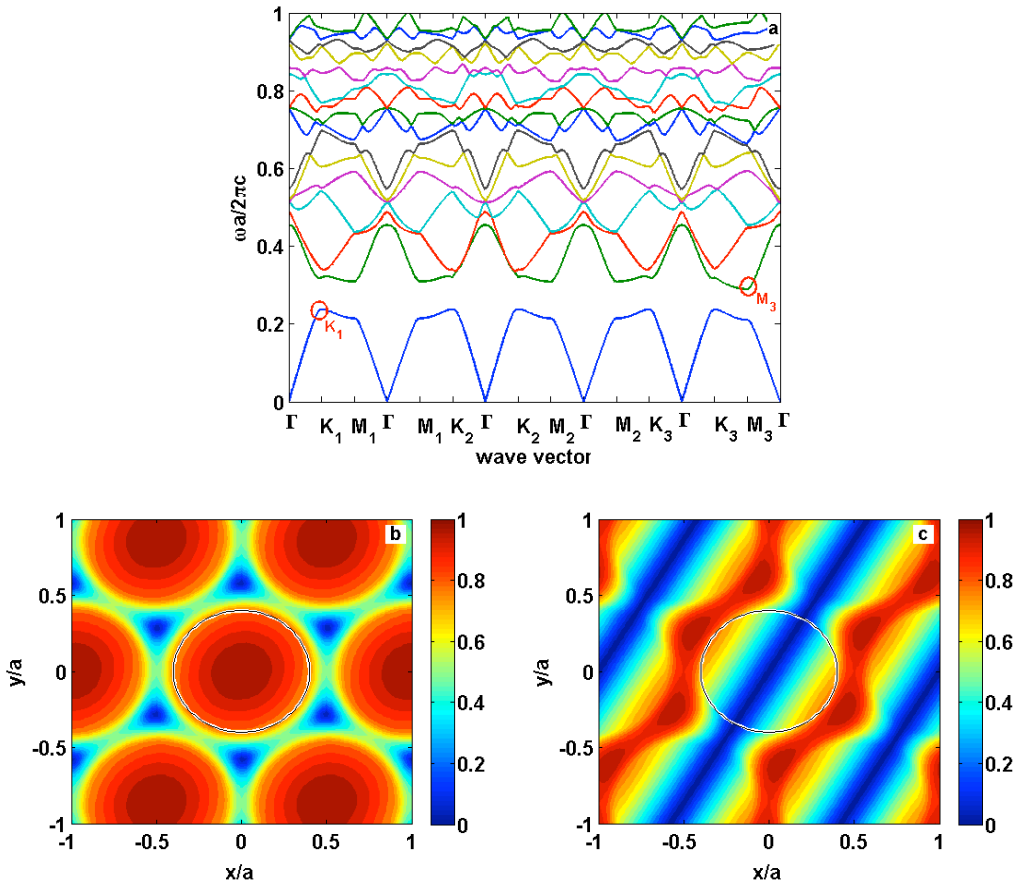

Fig. 5.5 a) Photonic band structures for the TE polarization for $\alpha = 30^o$. *Red circles indicate the k-points where the field distribution (as the modulus of the* H_z *component) is calculated for b) the lower and c) upper limits of the bandgaps.*

The field distribution for the first band shows a strong confinement in the circular holes, with almost circular symmetry for $\alpha = 0^o$ (Fig. 5.4b). When α changes the field distribution for the first band does not change appreciably (Fig. 5.5b). The almost circular symmetry of the first band field distribution causes it to be insensitive to the LC optical axis orientation, and thus the lower band gap limit is constant.

The field distribution for the second band shows a node along one diameter of the circular holes, while the Si shows a high field amplitude for $\alpha = 0^o$ (Fig. 5.4c). When α changes the field distribution for the second band is slightly dependent on α, but the field is manly confined in the Si, thus, even though a corresponding change in the upper band gap limit frequency is observed, it is nevertheless small (Fig. 5.5c).

UNIVERSITAT ROVIRA I VIRGILI
DESIGN AND MODELLING OF PHOTONIC CRYSTALS WITH ANISOTROPIC COMPONENTS
Joaquin Cos Córcoles
ISBN:978-84-693-9433-5/DL:T.69-2011

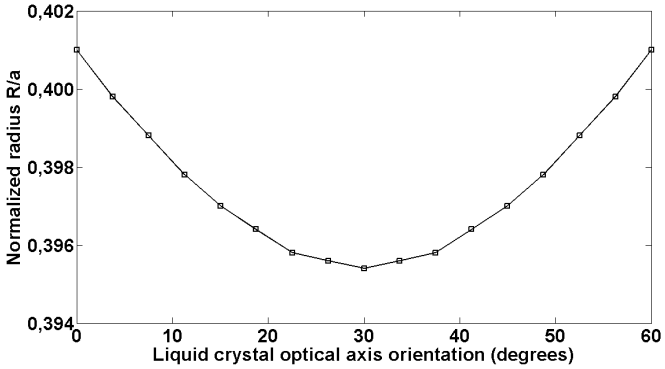

Fig. 5.6 Radius corresponding to the maximum bandgap as a function of the LC optical axis orientation, α.

Figure 5.6 shows the radius corresponding to the maximum bandgap as a function of the LC optical axis orientation, α. As it can be seen, the influence of α is very small: the maximum relative difference between the observed radii in Fig. 5.6 is only *1.4%*. This means that a tunable device based on this structure designed to have the maximum bandgap should have a radius in the range shown in Fig. 5.6. However, an actual device must have a fixed radius, and therefore the bandgap of the device will change with the LC optical axis orientation.

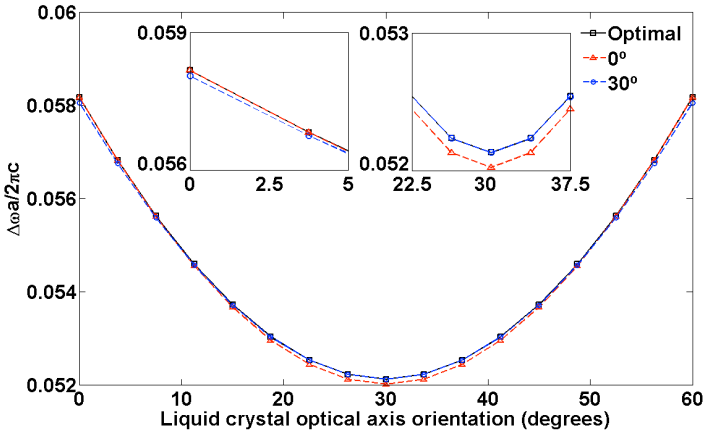

Fig. 5.7 Bandgap width between 1st and 2nd TE modes versus LC optical axis orientation for i) the radius corresponding to the maximum bandgap at each α (black line and square marker), ii) the radius giving the maximum width at α = 0º (red line and triangular marker) and iii) the radius giving the maximum width at α = 30º (blue line and circular marker). The insets show a detail of the ranges of α where the difference between the three curves is maximum.

UNIVERSITAT ROVIRA I VIRGILI
DESIGN AND MODELLING OF PHOTONIC CRYSTALS WITH ANISOTROPIC COMPONENTS
Joaquin Cos Córcoles
ISBN:978-84-693-9433-5/DL:T.69-2011

In Fig. 5.7, the influence of having a fixed radius on the bandgap width is depicted. The graph shows the bandgap width as a function of α. The three curves correspond to: i) the bandgap obtained with the optimal radius at the given LC optical axis orientation (black line and square marker), ii) the bandgap obtained for the fixed radius giving the maximum width for $\alpha = 0^o$, $R/a = 0.401$ (red line and triangular marker) and iii) the bandgap obtained for the fixed radius giving the maximum width for $\alpha = 30^o$, $R/a = 0.395$ (blue line and circular marker). As it can be seen, the bandgap width has a very similar behaviour in the three cases. The insets show a detail of the ranges of α where the difference between the bandgap width for a fixed radius and the optimal width, its difference is lower than *0.2%*. This means that there is a tolerance in the size of the radius of the holes in the photonic crystal structure: the bandgap width dependence with the LC optical axis orientation will be almost invariant as long as the radius lies within the range of optimal radii in Fig. 5.6. Figure 5.7 also shows that, for this range of radius, the bandgap width changes a maximum of an *11.6%* with the LC optical axis orientation.

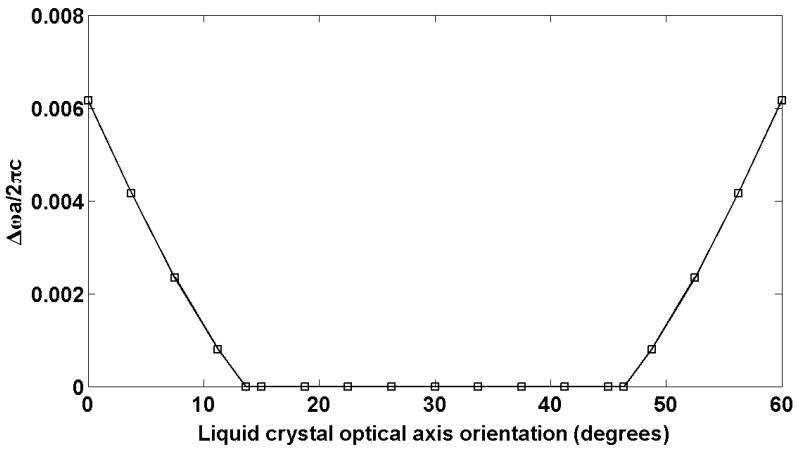

Fig. 5.8 Bandgap width as a function of the LC optical axis orientation for R/a = 0.48.

UNIVERSITAT ROVIRA I VIRGILI
DESIGN AND MODELLING OF PHOTONIC CRYSTALS WITH ANISOTROPIC COMPONENTS
Joaquin Cos Córcoles
ISBN:978-84-693-9433-5/DL:T.69-2011

Another interesting feature of this structure is the fact that the gap can be opened and closed with the LC optical axis orientation. In Figure 5.3c it has been shown that there is a range where, for a given *R/a*, the gap closes at some angle between $\alpha = 0^o$ and $\alpha = 30^o$. By appropriately choosing the radius of the cylinder a photonic crystal can be designed such that its bandgap can be closed or opened up to a certain width, as a function of the LC optical axis orientation. Figure 5.8 shows the gap width as a function of the LC optical axis orientation for $R/a = 0.480$. For this radius the gap is closed for α between 13.64^o and 46.36^o and reaches a maximum gap width of $\Delta\omega a/2\pi c = 0.0062$ for $\alpha = 0^o$ and $\alpha = 60^o$. Changing the scatterer radius results in a change of the maximum gap width and the range of α where the gap closes.

The previous result suggests a structure with a tunable bandgap that can be opened and closed. However, it has a significant drawback: the tolerance of the value of the radius is very small. This can be explained by observing Fig. 5.3c: an increase of *1%* in the *R/a* results in a structure without any bandgap, or a decrease in *1%* in *R/a* results in a structure where the gap never closes. This makes the actual fabrication of a device based on this feature very difficult.

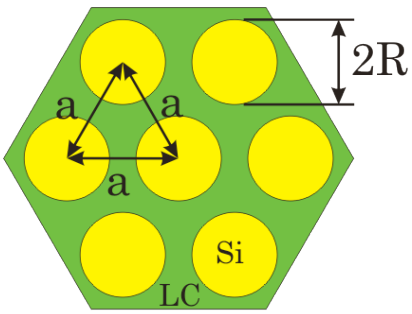

Fig. 5.9 Schematic view of the photonic crystal composed of a triangular array of silicon cylinders surrounded by E7 liquid crystal.

UNIVERSITAT ROVIRA I VIRGILI
DESIGN AND MODELLING OF PHOTONIC CRYSTALS WITH ANISOTROPIC COMPONENTS
Joaquin Cos Córcoles
ISBN:978-84-693-9433-5/DL:T.69-2011

In the following, we study an alternative structure that shows a better fabrication tolerance: a photonic crystal composed of a triangular array of silicon cylinders surrounded by E7 liquid crystal. Figure 5.9 shows a schematic view of the structure. As in the previous case, the liquid crystal optical axis is maintained in the *x*-*y* plane and the structure is tuned by varying the LC optical axis angle with the *y* axis, α. Figure 5.10a shows the gap maps for $\alpha = 0^o$ and $\alpha = 12^o$. The results show that, as the angle α increases, the gap map is reduced until the gap closes for all radius values between $\alpha = 24^o$ and $\alpha = 30^o$. This behaviour is symmetric with respect the angle $\alpha = 30^o$ and repeats every 60^o. The arrow indicates the *R*/*a* corresponding to the maximum width for all α. Figure 5.10b shows a detail of the range of *R*/*a* where the gap is maximum.

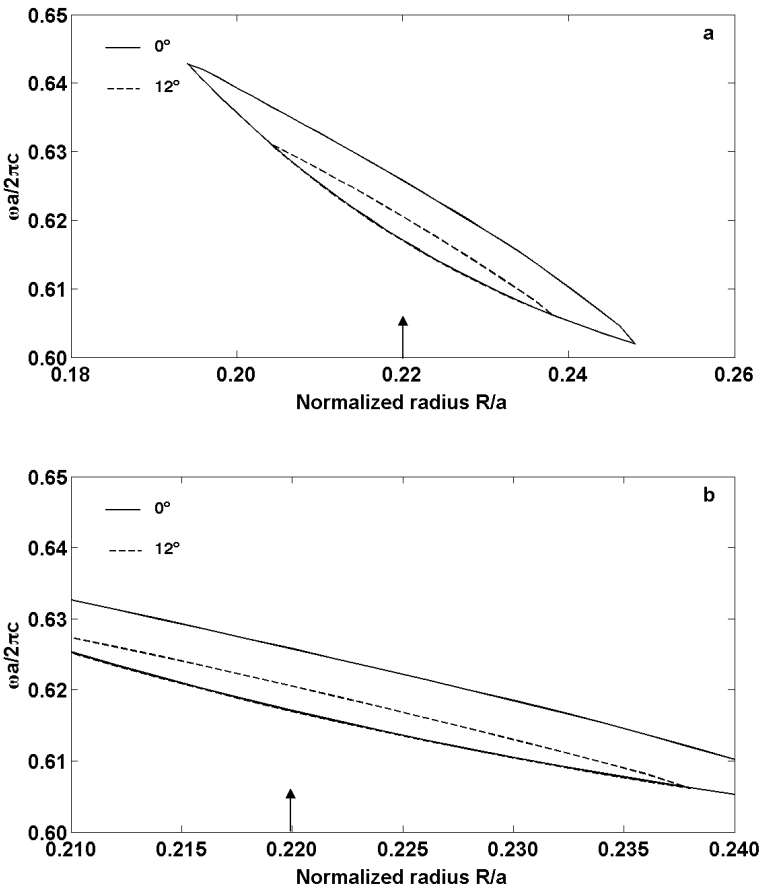

Fig. 5.10 a) Photonic bandgap map for the TE polarization for $\alpha = 0^o$ (solid line) and $\alpha = 12^o$ (dashed line). The arrow indicates the R/a corresponding to the maximum gap width for all α. b) Detail of the region around the maximum gap width.

UNIVERSITAT ROVIRA I VIRGILI
DESIGN AND MODELLING OF PHOTONIC CRYSTALS WITH ANISOTROPIC COMPONENTS
Joaquin Cos Córcoles
ISBN:978-84-693-9433-5/DL:T.69-2011

This dependence of the gap with the optical axis orientation of the LC suggests that it can be applied as a switch. In this case, the radius of the silicon cylinders can be chosen to modulate the duty cycle of the switch, that is: the range of angles where the gap is closed. Choosing the radius also defines the maximum value of the achievable bandgap width and for $R/a = 0.220$ this achievable width is maximum ($\Delta\omega a/2\pi c = 0.009$). Figure 5.11 shows the bandgap width for such radius of the silicon cylinders (squares) as a function of the angle α. For this radius, the corresponding duty cycle is *80%* opened / *20%* closed. If a *50%* duty cycle is desired, the radius should be $R/a = 0.206$. The corresponding bandgap width can be seen in the Fig. 5.11 as well.

Analogue to the previous structure, the dependence of the band gap limits with the LC orientation angle can be again explained by the analysis of the H_z component field distribution for the photonic bands corresponding to such limits (Figs. 5.12-5.13). In this case, the gap limits are between the fourth and fifth photonic bands (Fig. 5.12a and 5.13a).

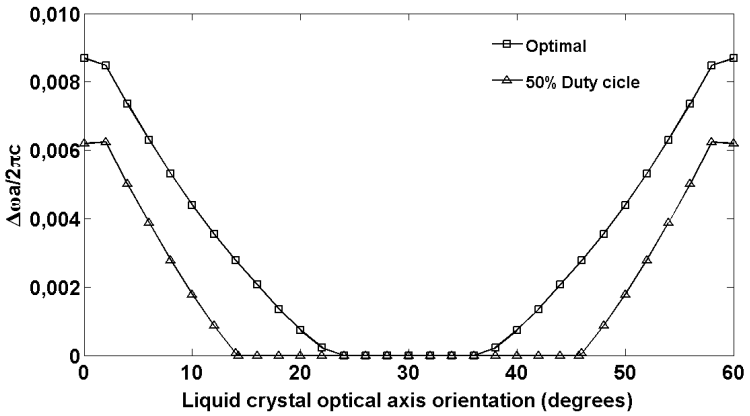

Fig. 5.11 Bandgap width between 4th and 5th TE modes versus LC optical axis orientation for i) the radius corresponding to the maximum bandgap for all α (square marker), ii) the radius giving a 50% duty cycle (triangular marker).

UNIVERSITAT ROVIRA I VIRGILI
DESIGN AND MODELLING OF PHOTONIC CRYSTALS WITH ANISOTROPIC COMPONENTS
Joaquin Cos Córcoles
ISBN:978-84-693-9433-5/DL:T.69-2011

The field distribution for the fourth band for $\alpha = 0^o$ (Fig. 5.12b) shows a strong confinement in the Si, with circular symmetry and an appreciably low amplitude in the LC. The field distribution for the fourth band for $\alpha = 30^o$ (Fig. 5.13b) does not change appreciably. The low band gap limit has not dependence with the LC orientation due to the low field amplitude for the fourth band in the LC. The fifth band for $\alpha = 0^o$ (Fig. 5.12c) shows a dipole shape along a diameter of the Si cylinders in the **Γ-M** direction while the LC region shows field maxima and minima. For $\alpha = 30^o$ (Fig. 5.13c) the field distribution for the fifth band shows a nodal line in the **Γ-K** direction. The remarkable change in the field distribution for the fifth band gives rise to the higher tunability observed for this structure.

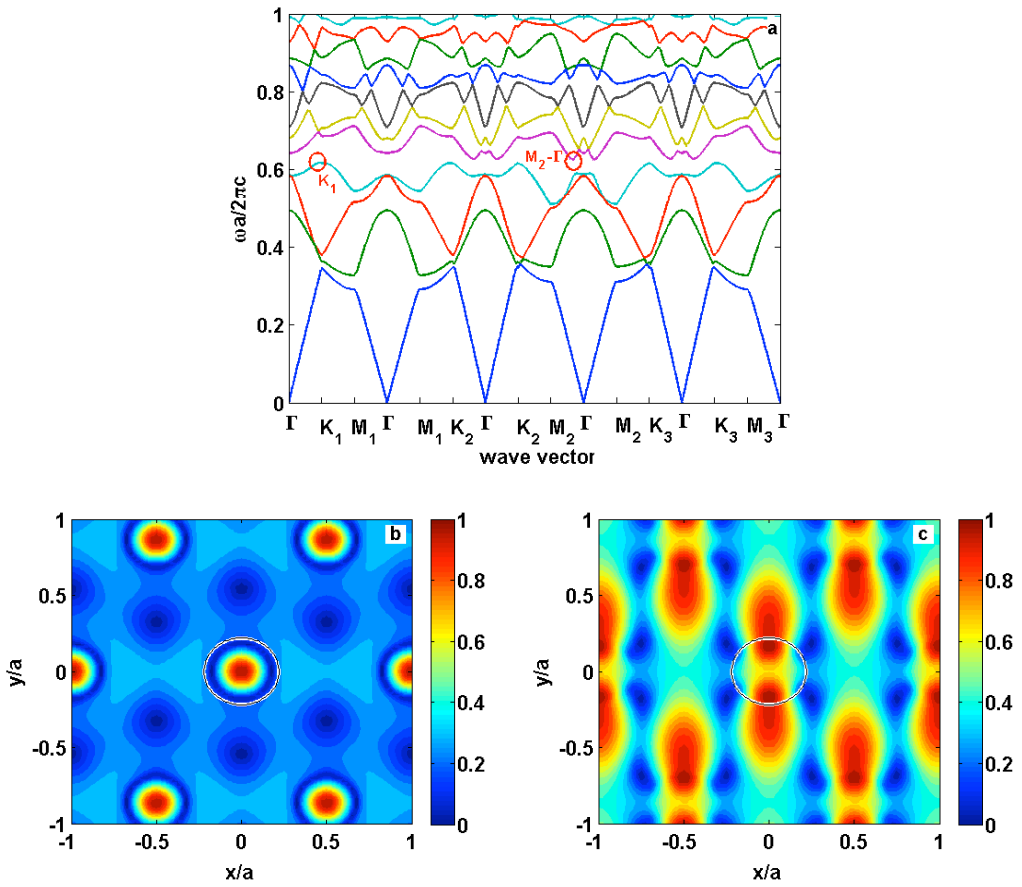

Fig. 5.12 a) Photonic band structures for the TE polarization for $\alpha = 0^o$. Red circles indicate the k-points where the field distribution (as the modulus of the H_z component) is calculated for b) the lower and c) upper limits of the bandgaps.

UNIVERSITAT ROVIRA I VIRGILI
DESIGN AND MODELLING OF PHOTONIC CRYSTALS WITH ANISOTROPIC COMPONENTS
Joaquin Cos Córcoles
ISBN:978-84-693-9433-5/DL:T.69-2011

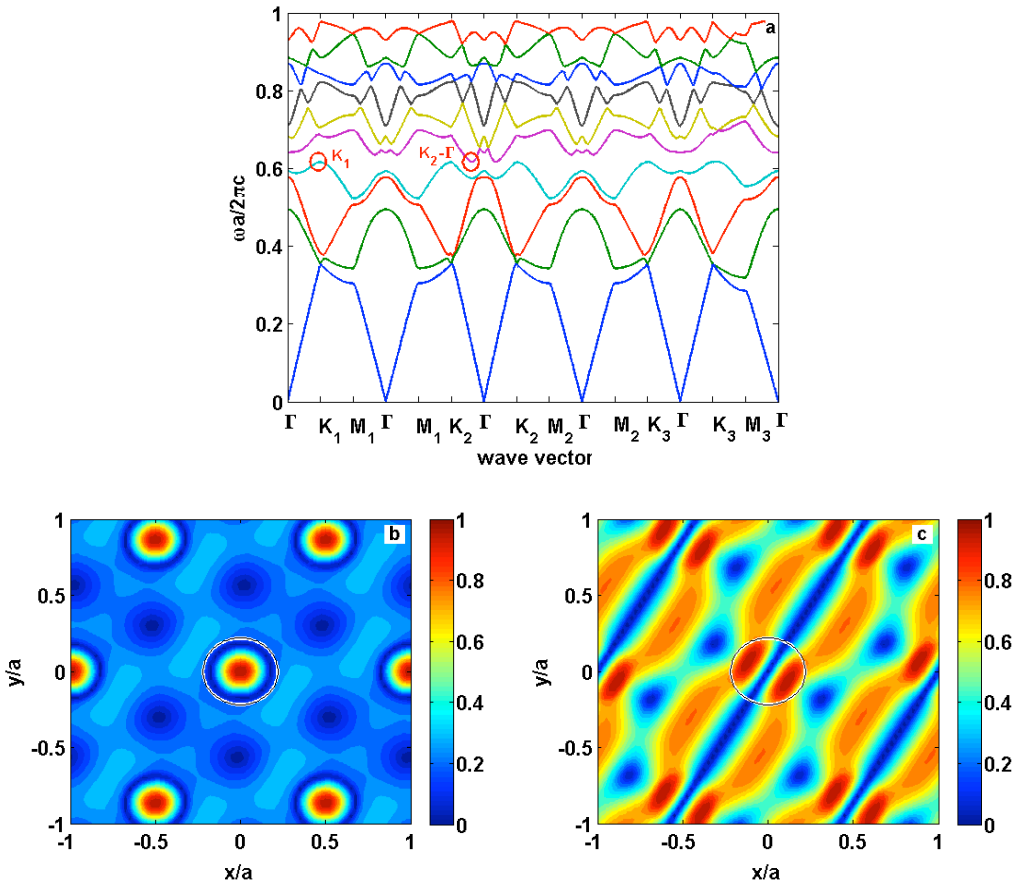

Fig. 5.13 a) Photonic band structures for the TE polarization for $\alpha = 30^{o}$. *Red circles indicate the k-points where the field distribution (as the modulus of the* H_z *component) is calculated for b) the lower and c) upper limits of the bandgaps.*

UNIVERSITAT ROVIRA I VIRGILI
DESIGN AND MODELLING OF PHOTONIC CRYSTALS WITH ANISOTROPIC COMPONENTS
Joaquin Cos Córcoles
ISBN:978-84-693-9433-5/DL:T.69-2011

5.2 Study of the tunability of guided modes of waveguides based on liquid crystal-infiltrated photonic crystals

The inclusion of defects in photonic crystals breaks the crystal symmetry allowing localized states in the photonic band gap. Therefore, cavities (point defect) and waveguides (lineal defect) can be generated. Waveguides based on photonic crystals allows enhancing properties of the classical waveguides [Mekis-1996; Chutinan-2002]. As we commented before, tunability is a necessary feature for many photonic crystal-based devices such as multiplexers or modulators. Among the possibilities for tuning the optical properties of silicon-based photonic crystals, liquid crystals represent a very suitable material for achieving this property for several reasons. On one hand, the easy control of the anisotropy by means of an external applied electric fields provides an easy tuning of the optical properties [Weiss-2005]. On the other hand, there is a good material availability due to its application in the display industry.

However, this infiltration reduces the contrast index with the consequence of a decrease in the performance of the devices. Apart from this index contrast reduction, the liquid crystals usually used in the display industry have a small birefringence in their anisotropic state, which results in an even smaller tunability range. Therefore, an optimal design of the structures is determinant for a proper working of the devices.

In this section we study the optimization of the tunability range in waveguides as a function of the radius of the line of scatterers that defines the waveguide. To this end, we use the plane-wave expansion method and the supercell formulation, presented in chapter 3, to take into account the lattice defects that define the waveguide.

The structure studied (Fig. 5.14) is a two-dimensional silicon photonic crystal with a triangular lattice of circular holes with radius R and lattice constant a, where a line of holes in the direction Γ-K (corresponding to the direction Γ-K_1 of Fig. 5.1) has a different radius R_{def} and is infiltrated by E7 liquid crystal.

UNIVERSITAT ROVIRA I VIRGILI
DESIGN AND MODELLING OF PHOTONIC CRYSTALS WITH ANISOTROPIC COMPONENTS
Joaquin Cos Córcoles
ISBN:978-84-693-9433-5/DL:T.69-2011

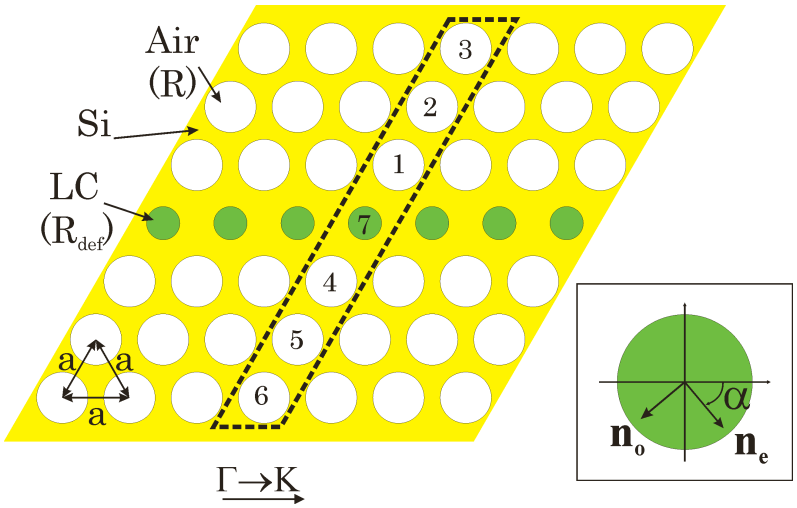

Fig. 5.14 Schematic view of the photonic crystal waveguide. Dotted line and numbers indicates the supercell and the position in the Eq. (5.1). The inset shows the definition of the angle α that characterizes the LC optical axis orientation with respect x axis.

The liquid crystal director is always in the plane of the cylinders, thus guided modes are tuned by changing the angle between the direction **Γ-K** and the LC director, α. The tunability range can be maximized by finding the optimal radius for the infiltrated scatterers, while the radius of the rest of scatterers has been chosen so that the bandgap is maximum (*R/a = 0.440*). We use *1225* plane-waves in order to guarantee convergence for the two guided modes considered within an error smaller than *1%* for radii of the defects bigger than *0.1a*. From Eq. (3.47) of chapter 3, the Fourier Transform of the inverse of the dielectric constant of the waveguide can be expressed as

$$\varepsilon^{-1}_{rGG'} = \sum_{m=1}^{6}\left[\varepsilon^{-1}_{air}(\mathbf{G}-\mathbf{G}')\cdot e^{-i((\mathbf{G}-\mathbf{G}')\mathbf{P}(m))}\right] + \varepsilon^{-1}_{LC}(\mathbf{G}-\mathbf{G}'). \qquad (5.1)$$

Figure 5.15 shows the photonic band structure for TE modes of the photonic crystal without defects. There is a band gap between 1st and 2nd modes in the **Γ-K** direction with a width of $\Delta\omega a/2\pi c = 0.218$ between normalized frequencies $\omega a/2\pi c = 0.511$ and $\omega a/2\pi c = 0.293$.

UNIVERSITAT ROVIRA I VIRGILI
DESIGN AND MODELLING OF PHOTONIC CRYSTALS WITH ANISOTROPIC COMPONENTS
Joaquin Cos Córcoles
ISBN:978-84-693-9433-5/DL:T.69-2011

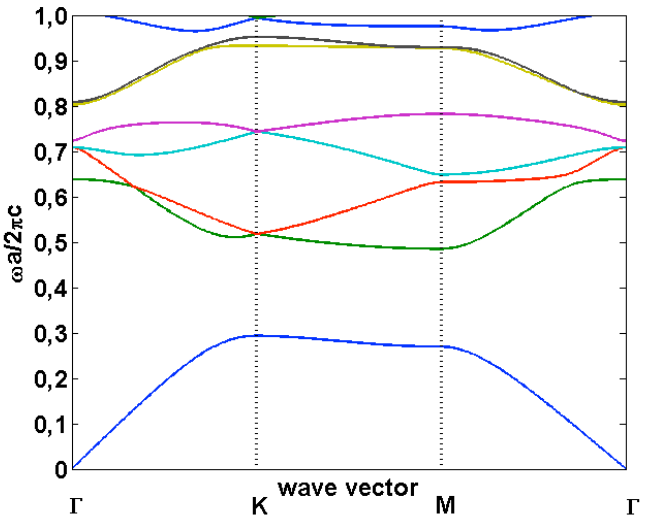

Fig. 5.15 Photonic band structure of a 2D silicon photonic crystal with a triangular lattice of holes (R/a = 0.440).

Figure 5.16 shows, for a waveguide where $R_{def}/a = 0.440$, the dispersion relations for two guided modes for an LC optical axis orientation $\alpha = 0^o$. As can be seen, these two guided modes apparently intersect for a wave-vector between the Γ-point and K-point. In the next section we will demonstrate that, for optical axis orientations different from 0^o, the two guided modes do not intersect while the field distributions correspondent to the two modes swap their shape. Therefore, in order to simplify the notation, we label the two guided modes (and the corresponded field distribution) in the next way, at the Γ-point GM_1 is the lower frequency mode and GM_2 is the higher frequency mode whereas at the K-point GM_1 is the higher frequency mode and GM_2 is the lower frequency mode. Additionally the shadow regions indicate the projected band structure of the periodic structure, that is, the projection of the bands at all the directions of the first Brillouin zone in the Γ-K direction.

UNIVERSITAT ROVIRA I VIRGILI
DESIGN AND MODELLING OF PHOTONIC CRYSTALS WITH ANISOTROPIC COMPONENTS
Joaquin Cos Córcoles
ISBN:978-84-693-9433-5/DL:T.69-2011

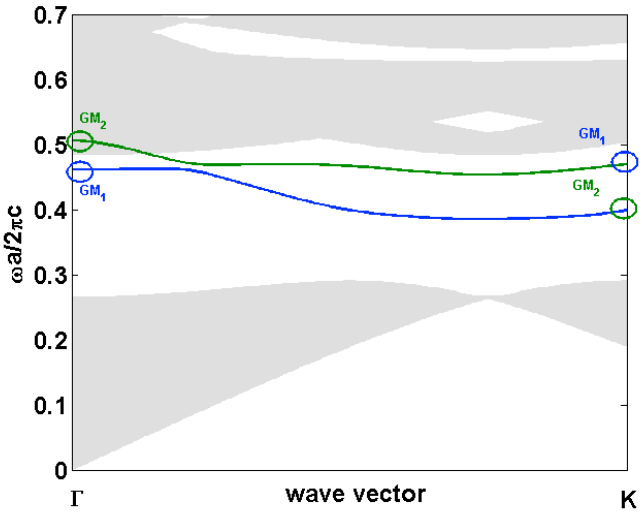

Fig. 5.16 Dispersion relation for two guided modes of a photonic crystal waveguide with defect sizes $R_{def}/a = 0.440$ and a LC optical axis orientation $\alpha = 0^o$. Shadow regions indicate the projected band structure on the Γ-K *direction of the photonic crystal.*

The first property that we analyze is the tuning of the guided modes with the LC optical axis orientation, α. Figure 5.17 shows the dependence of the two guided modes frequency with this angle for a defect radius of $R_{def}/a = 0.440$. As can be seen, for the Γ-point (Fig. 5.17a) varying α from 0^o to 180^o the frequency of GM_1 can be tuned from $\omega a/2\pi c = 0.462$ to $\omega a/2\pi c = 0.443$ while the frequency of GM_2 can be tuned simultaneously from $\omega a/2\pi c = 0.507$ to $\omega a/2\pi c = 0.537$. For the K-point (Fig. 5.17b) GM_1 can be tuned from $\omega a/2\pi c = 0.471$ to $\omega a/2\pi c = 0.454$ while GM_2 can be tuned simultaneously from $\omega a/2\pi c = 0.399$ to $\omega a/2\pi c = 0.422$. It is important to note that there is a periodicity of 180^o and the frequency shows a maximum or a minimum (depending on the mode and the on the wave-vector) at $\alpha = 0^o, 90^o, 180^o$.

UNIVERSITAT ROVIRA I VIRGILI
DESIGN AND MODELLING OF PHOTONIC CRYSTALS WITH ANISOTROPIC COMPONENTS
Joaquin Cos Córcoles
ISBN:978-84-693-9433-5/DL:T.69-2011

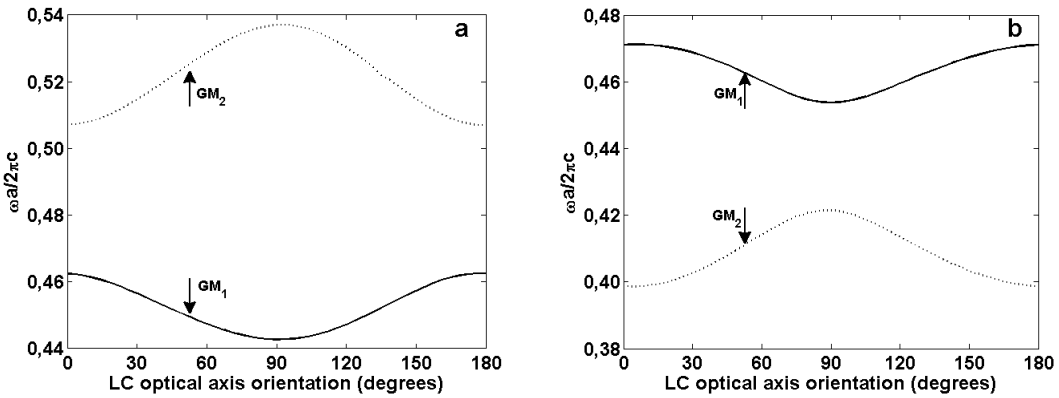

Fig. 5.17 Frequencies of the guided modes GM_1 (solid lines) and GM_2 (dotted lines) of a photonic crystal waveguide with defect sizes $R_{def}/a = 0.440$ versus the LC optical axis orientation at a) Γ-point and b) K-point.

The main goal of this section is to maximize the tunability range optimizing the radius of the line of scatterers that defines the waveguide. This tunability range is defined for each guided mode in the Γ-point or K-point as the difference between the maximum and minimum values of the normalized frequencies. These values can be obtained analyzing the band structure for the angles $\alpha = 0^o$, and $\alpha = 90^o$ for each radius. We have limited the range of the radius analyzed between $R_{def}/a = 0.1$ and $R_{def}/a = 0.5$, since lower values of R_{def}/a requires a higher number of plane-waves to reach the desired precision. Furthermore, for defect radius smaller than $R_{def}/a = 0.1$ the amount of anisotropic material is remarkably small and the resulting tuning range is greatly reduced.

Figure 5.18 shows the tunability range of the two guided modes for defect radius between $R_{def}/a = 0.100$ and $R_{def}/a = 0.500$ at Γ-point and K-point. It is important to note that GM_1 is within the bandgap for all R_{def}/a while GM_2 is within the bandgap between $R_{def}/a = 0.100$ and $R_{def}/a = 0.360$ for the Γ-point and between $R_{def}/a = 0.335$ and $R_{def}/a = 0.500$ for the K-point, for the rest of the radii, the frequency of the mode lies out of the bandgap for some liquid crystal optical axis orientations.

UNIVERSITAT ROVIRA I VIRGILI
DESIGN AND MODELLING OF PHOTONIC CRYSTALS WITH ANISOTROPIC COMPONENTS
Joaquin Cos Córcoles
ISBN:978-84-693-9433-5/DL:T.69-2011

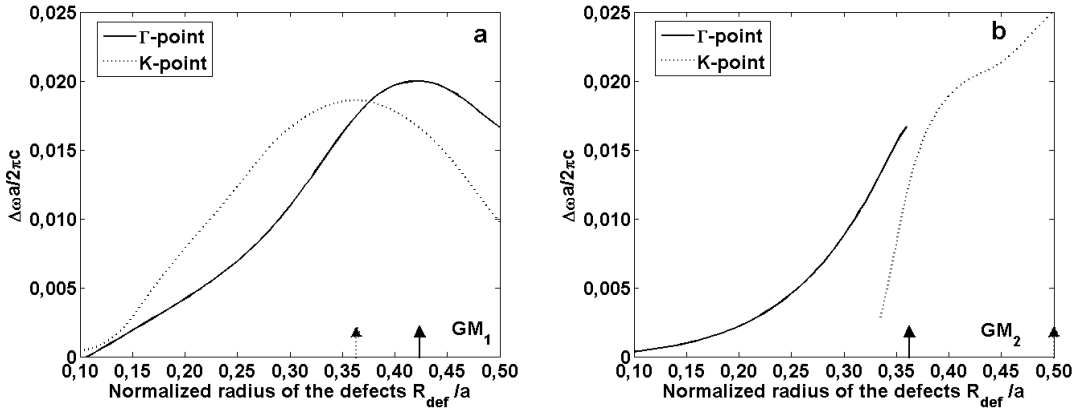

Fig. 5.18 Maximum tunability range of the guided modes versus the defect radius. a) GM_1. b) GM_2.

For GM_1 (Fig. 5.18a) it can be seen that maximum values of the tunability range appear at $R_{def}/a = 0.420$ for the Γ-point and $R_{def}/a = 0.360$ for the K-point. For GM_2 (Fig. 5.18b) a different behaviour of the tunability range can be observed: the tunability range increases with R_{def}/a, thus maximum tunability range appears at the upper limits of R_{def}/a, this is $R_{def}/a = 0.360$ for the Γ-point and $R_{def}/a = 0.500$ for the K-point. This property can be used for the design of optical switches, if the defect radius is designed near of the cut-off radius (slightly above than $R_{def}/a = 0.360$ for the Γ-point or slightly below than $R_{def}/a = 0.335$ for the K-point) the mode is guided only for a range of liquid crystal optical axis orientations.

Finally, the field distributions corresponding to these guided modes at the Γ-point and at the K-point for the defect radius that maximize the tunability range are presented in Figs. 5.19-5.22. Fig. 5.19 shows the amplitude of the H_z field for the first guided mode GM_1 at Γ-point for a photonic crystal with a radius of the defects $R_{def} = 0.420$ and an orientation of the LC optical axis of $\alpha = 0^o$ (Fig. 5.19a), and $\alpha = 90^o$ (Fig. 5.19b). White circles represent a schematic view of the photonic crystal. In these figures it can be observed how the field is confined to the waveguide region due to the photonic gap effect. This guided mode presents one node mainly oriented in the Γ-K direction (corresponding to the direction Γ-K_1 of Fig. 5.1).

UNIVERSITAT ROVIRA I VIRGILI
DESIGN AND MODELLING OF PHOTONIC CRYSTALS WITH ANISOTROPIC COMPONENTS
Joaquin Cos Córcoles
ISBN:978-84-693-9433-5/DL:T.69-2011

Figure 5.20 shows the amplitude of the H_z field for the second guided mode GM_2 at the Γ-point for a photonic crystal with a radius of the defects $R_{def} = 0.360$ and an orientation of the LC optical axis of $\alpha = 0^o$ (Fig. 5.20a), and $\alpha = 90^o$ (Fig. 5.20b). Again, it can be observed how the field is confined in the region of the waveguide due to the photonic gap effect. This guided mode presents a region of high energy between the defect cylinders in the direction Γ-K. It is important to observe that the field distributions for these two optical axis orientations are quite similar, although there are small differences that produce the frequency tuning.

Figure 5.21 shows the amplitude of the H_z field for the first guided mode GM_1 at K-point for a photonic crystal with a radius of the defects $R_{def} = 0.360$ and an orientation of the LC optical axis of $\alpha = 0^o$ (Fig. 5.21a), and $\alpha = 90^o$ (Fig. 5.21b). Again, it can be observed how the field is confined in the region of the waveguide due to the photonic gap effect. This guided mode has the same distribution of the one of Fig. 5.19 because it corresponds to the same guided mode but for a different size of the defects.

Finally, Fig. 5.22 shows the amplitude of the H_z field for the second guided mode GM_2 at K-point for a photonic crystal with a radius of the defects $R_{def} = 0.500$ and an orientation of the LC optical axis of $\alpha = 0^o$ (Fig. 5.22a), and $\alpha = 90^o$ (Fig. 5.22b). Again, it can be observed how the field is confined in the region of the waveguide due to the photonic gap effect. This guided mode has the same distribution as in Fig. 5.20 because it corresponds to the same guided mode but for a different size of the defects. In this case the field distribution for these two LC optical axis orientations show bigger differences than in previous cases because the amount of LC is bigger in this case.

UNIVERSITAT ROVIRA I VIRGILI
DESIGN AND MODELLING OF PHOTONIC CRYSTALS WITH ANISOTROPIC COMPONENTS
Joaquin Cos Córcoles
ISBN:978-84-693-9433-5/DL:T.69-2011

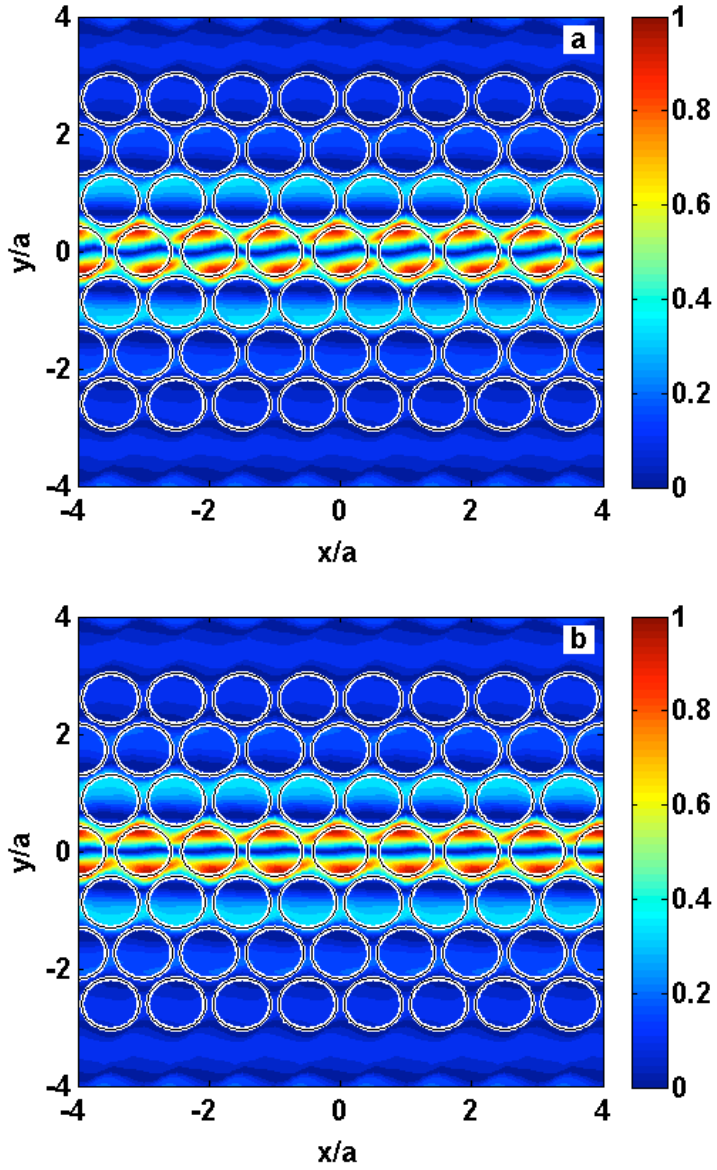

Fig. 5.19 Field distribution for the modulus of the Z-component of the Magnetic Field (H_z) for GM_1 at Γ-point for a photonic crystal waveguide with defect size R_{def} = 0.420 and LC optical axis orientations: a) α = 0º. b) α = 90º.

UNIVERSITAT ROVIRA I VIRGILI
DESIGN AND MODELLING OF PHOTONIC CRYSTALS WITH ANISOTROPIC COMPONENTS
Joaquin Cos Córcoles
ISBN:978-84-693-9433-5/DL:T.69-2011

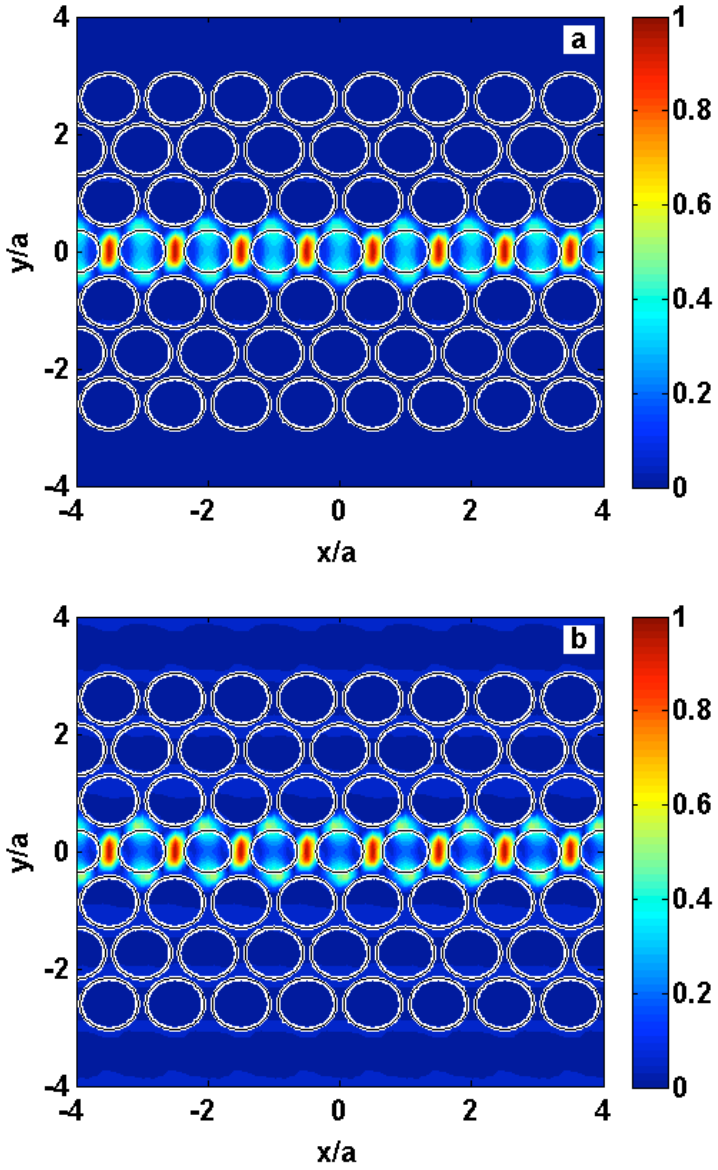

Fig. 5.20 Field distribution for the modulus of the Z-component of the Magnetic Field (H_z) for GM_2 at Γ-point for a photonic crystal waveguide with defect size R_{def} = 0.360 and LC optical axis orientations: a) α = 0º. b) α = 90º.

UNIVERSITAT ROVIRA I VIRGILI
DESIGN AND MODELLING OF PHOTONIC CRYSTALS WITH ANISOTROPIC COMPONENTS
Joaquin Cos Córcoles
ISBN:978-84-693-9433-5/DL:T.69-2011

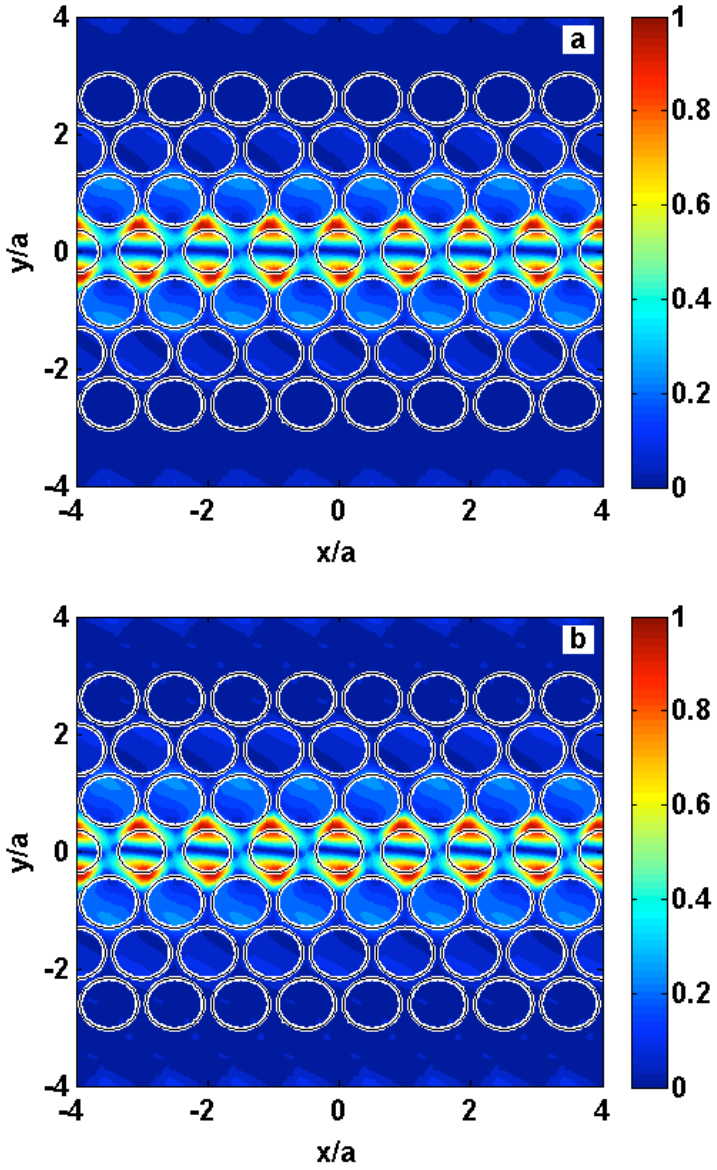

Fig. 5.21 Field distribution for the modulus of the Z-component of the Magnetic Field (H_z) for GM_1 at K*-point for a photonic crystal waveguide with defect size R_{def} = 0.360 and LC optical axis orientations: a) $\alpha = 0^o$. b) $\alpha = 90^o$.*

UNIVERSITAT ROVIRA I VIRGILI
DESIGN AND MODELLING OF PHOTONIC CRYSTALS WITH ANISOTROPIC COMPONENTS
Joaquin Cos Córcoles
ISBN:978-84-693-9433-5/DL:T.69-2011

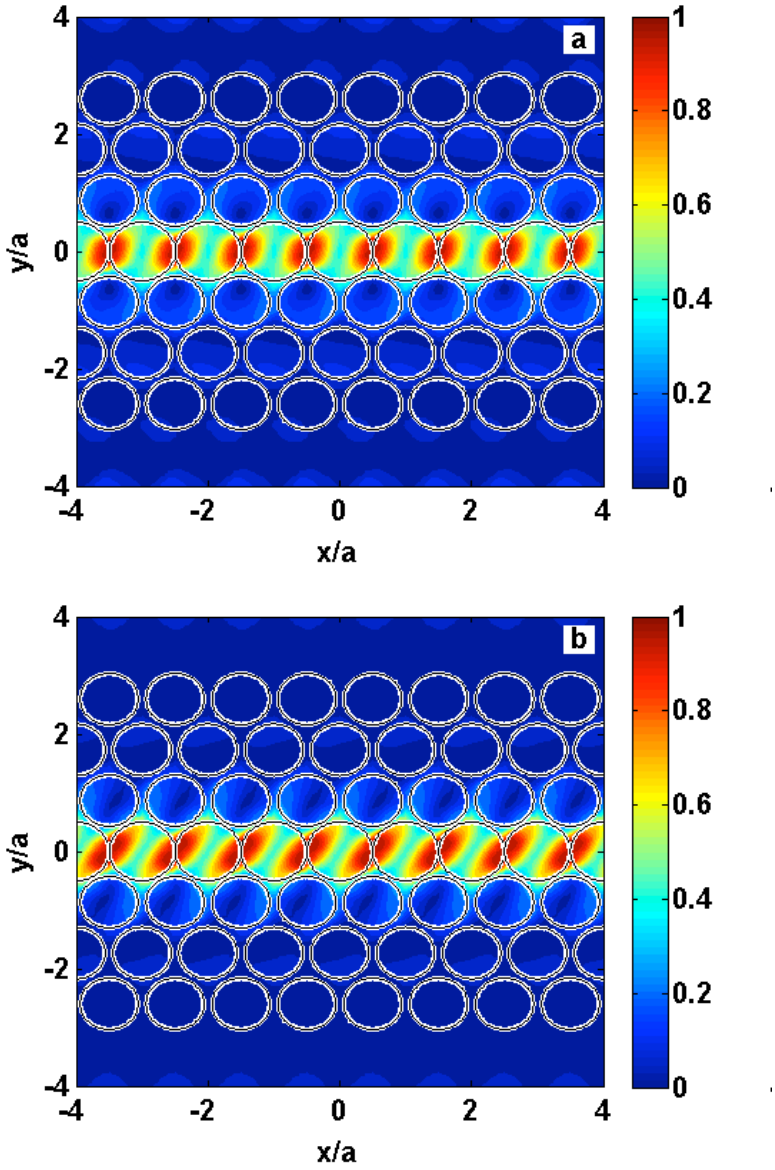

Fig. 5.22 Field distribution for the modulus of the Z-component of the Magnetic Field (H_z) for GM_2 at K*-point for a photonic crystal waveguide with defect size R_{def} = 0.500 and LC optical axis orientations: a) α = 0º. b) α = 90º.*

UNIVERSITAT ROVIRA I VIRGILI
DESIGN AND MODELLING OF PHOTONIC CRYSTALS WITH ANISOTROPIC COMPONENTS
Joaquin Cos Córcoles
ISBN:978-84-693-9433-5/DL:T.69-2011

5.3 Study of the practical implementation of waveguides based on photonic crystals infiltrated with liquid crystals

As we commented in the previous section, tunability is a necessary feature for many photonic crystal-based devices such as multiplexers or modulators. In the case of photonic crystal waveguides the tunability can be applied on the design of couplers [Liu-2004] or Y-shaped waveguides [Takeda-2003]. However, in order to overcome the disadvantages of the use of liquid crystal presented in the previous section, an optimal design of the structures is determinant for a proper working of the devices.

The aim of this section is to establish a method for the analysis of the practical implementation of tunable silicon photonic crystal waveguides. The waveguides are composed of a silicon photonic crystal with air scatterers, where one of the rows is filled with liquid crystal. By means of FDTD we are able to obtain the transmission properties of the structure. Then, the properties are related to the waveguide modes obtained with the plane-wave expansion method and a supercell formulation. With this, an explanation of the tunability of the transmission properties in terms of modal dispersion relations can be obtained. FDTD simulations were performed using a freely available software package [MEEP-2010].

The studied structure is a two-dimensional silicon photonic crystal with a triangular lattice of circular holes (scatterers) with radius R and lattice constant a, where a line of scatterers in the direction Γ-K is infiltrated by E7 liquid crystal. The liquid crystal director is always in the plane of the cylinders, thus guided modes are tuned by changing the angle between the direction Γ-K and the LC director, α. For this configuration, only the TE modes (Magnetic field parallel to the axis of the holes) depend on the optical axis orientation.

UNIVERSITAT ROVIRA I VIRGILI
DESIGN AND MODELLING OF PHOTONIC CRYSTALS WITH ANISOTROPIC COMPONENTS
Joaquin Cos Córcoles
ISBN:978-84-693-9433-5/DL:T.69-2011

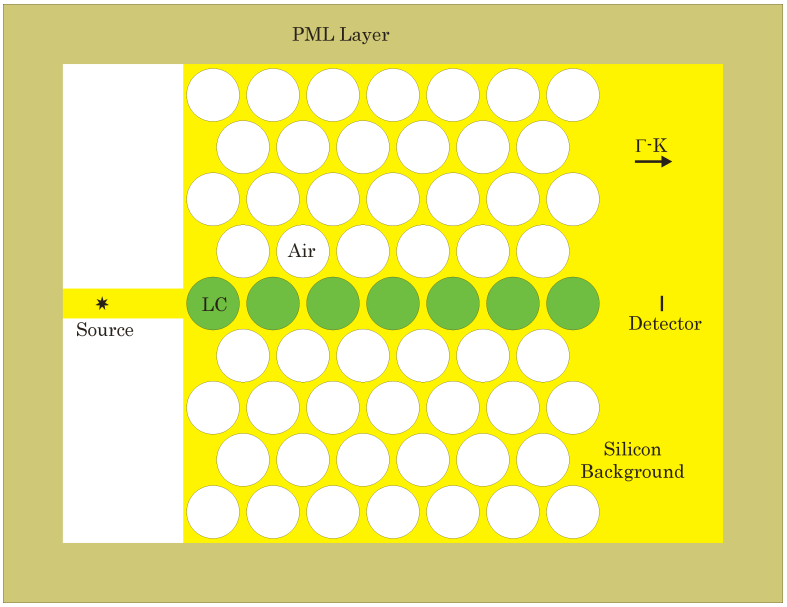

Fig. 5.23 Schematic view of the structure.

In order to evaluate the transmission of light through the waveguide, a section of the photonic crystal with the LC-infiltrated holes is considered, as depicted in Fig. 5.23. The incident light is coupled to the waveguide by means of a step-index monomode waveguide (to the right of the structure) and a point source is placed at the centre of the step index waveguide thus providing a common source for all the studied configurations. In the analysis, two kinds of sources are considered. The first one is a wideband source with a Gaussian time profile and a spectral range that covers the photonic band gap of the silicon photonic crystal. In order to analyze with higher precision the transmittance properties of the structure as a function of the LC orientation angle, a monochromatic source is also used. In both cases the generated field is TE-polarized. The spectrum of the transmitted light is evaluated by placing a detector at the right of the waveguide. This detector is composed by a line of points where the electric field flux is evaluated. The computational domain is surrounded by a Perfectly Matching Layer.

In order to evaluate the tunability range for each frequency, we propagate a wideband pulse of the same width of the detector for all the optical axis orientations between 0^o and 90^o. Then, we study the dependence with the LC optical axis

UNIVERSITAT ROVIRA I VIRGILI
DESIGN AND MODELLING OF PHOTONIC CRYSTALS WITH ANISOTROPIC COMPONENTS
Joaquin Cos Córcoles
ISBN:978-84-693-9433-5/DL:T.69-2011

orientation of a monochromatic pulse and the results are compared with the modal dispersion obtained with the plane-wave expansion method and a *7x1* supercell formulation.

Figure 5.24 shows the maximum and the minimum values of the transmission of a wide-band pulse through the waveguide for each frequency and for all angles α. Two regions with a maximum difference between the maximum and minimum transmission can be observed. The first region corresponds to the frequencies near $\omega a/2\pi c = 0.357$ while a second region corresponds to frequencies near $\omega a/2\pi c = 0.412$.

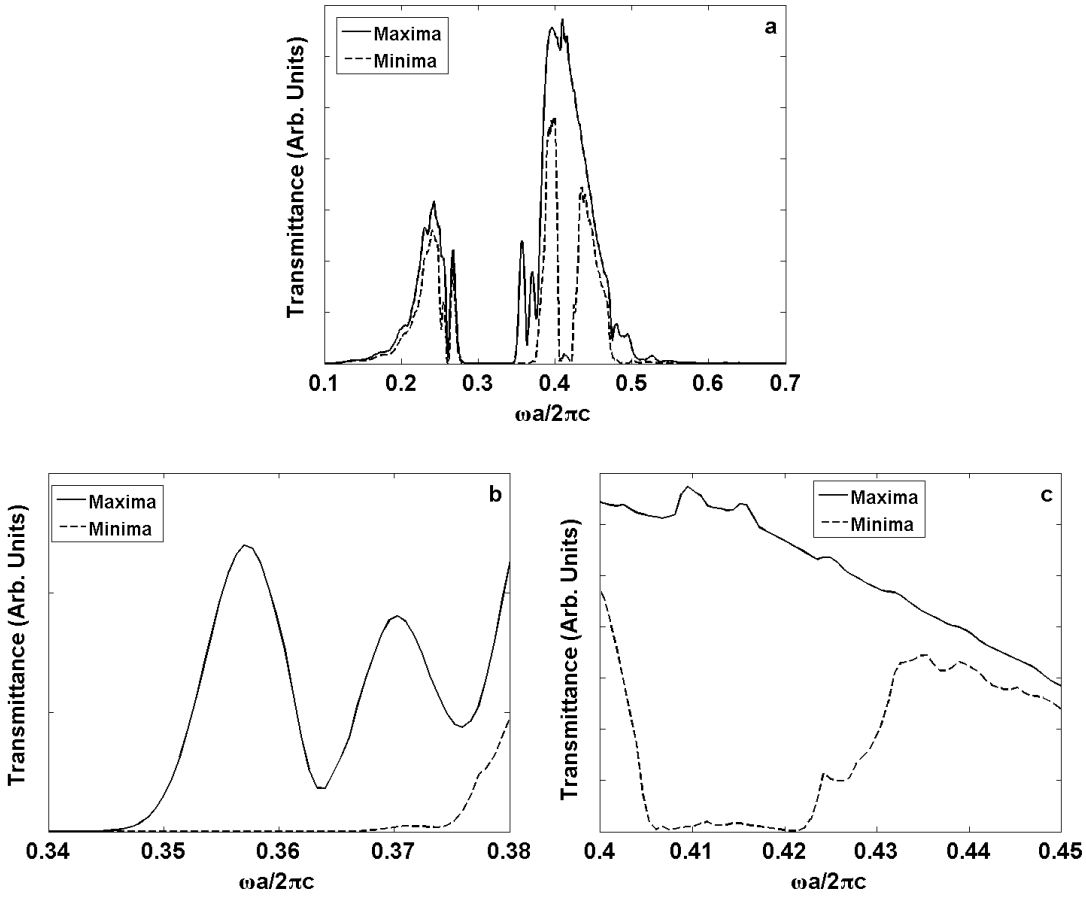

Fig. 5.24 a) Maximum and minimum transmission of a wide-band pulse through the waveguide for each frequency and for all angles. b) Detail of the region near $\omega a/2\pi c = 0.357$ with a maximum difference between the maximum and minimum transmission. c) Detail of the region near $\omega a/2\pi c = 0.412$ with a maximum difference between the maximum and minimum transmission.

UNIVERSITAT ROVIRA I VIRGILI
DESIGN AND MODELLING OF PHOTONIC CRYSTALS WITH ANISOTROPIC COMPONENTS
Joaquin Cos Córcoles
ISBN:978-84-693-9433-5/DL:T.69-2011

Figure 5.25 shows the transmission spectra for four different LC orientation angles. From these spectra it can be seen that for the region near $\omega a/2\pi c = 0.412$ the structure works as a switch, allowing or rejecting the transmission depending on the optical axis orientation.

In order to study more in detail the switching effect, the transmission of a monochromatic pulse of frequency $\omega a/2\pi c = 0.412$ is calculated as a function of the LC orientation. The calculations are carried out with the same geometry as in Fig. 5.23 with a monochromatic source and propagating the wave a time long enough to reach a steady state.

Figure 5.26a shows a region between 30^o and 55^o where the pulse is rejected, while for the rest of orientations the pulse is transmitted. The H_z field distributions shown in the inset confirm this behaviour, furthermore it can be seen that for $\alpha = 0^o$ (Fig. 5.26b) the field distribution inside the structure correspond to a guided mode with an even symmetry (with alternate maxima and nodes along the Γ-K direction), while for $\alpha = 50^o$ (Fig. 5.26c) the incident light is not coupled to any waveguide mode and it is extinguished along the waveguide.

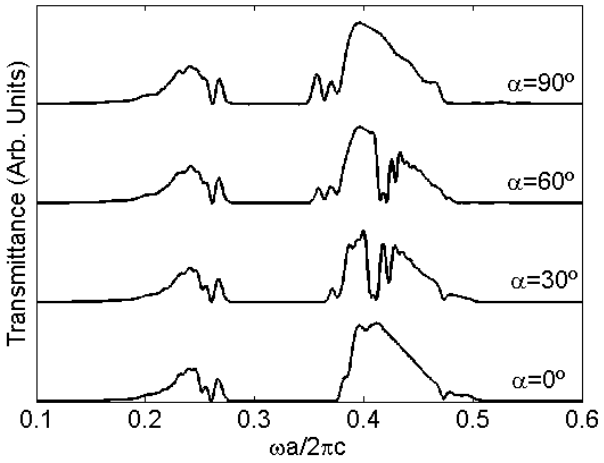

Fig. 5.25 Transmission spectra for different optical axis orientations.

UNIVERSITAT ROVIRA I VIRGILI
DESIGN AND MODELLING OF PHOTONIC CRYSTALS WITH ANISOTROPIC COMPONENTS
Joaquin Cos Córcoles
ISBN:978-84-693-9433-5/DL:T.69-2011

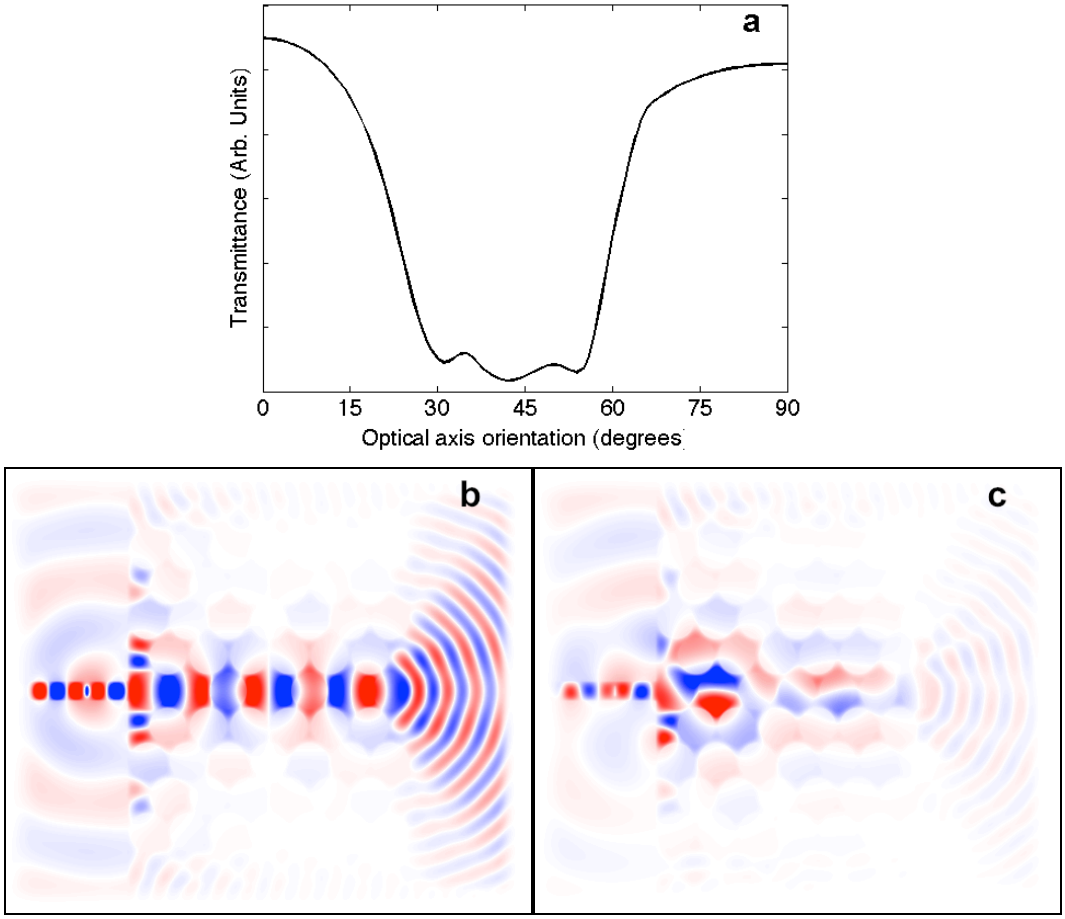

Fig. 5.26 a) Transmittance of a monochromatic pulse of frequency $\omega a/2\pi c = 0.412$ *through the waveguide versus the liquid crystal optical axis orientation.* H_z *field distributions for b)* $\alpha = 0^o$ *and c)* $\alpha = 50^o$ *after a computation time long enough to reach a steady state.*

This behaviour can be explained in terms of the dispersion relations of the guided modes obtained with the plane-wave expansion method and a supercell formulation. Figure 5.27 shows the dispersion relations of the waveguide modes for $\alpha = 0^o$ and $\alpha = 50^o$, the shadow regions indicate the projected band structure for the photonic crystal structure without infiltration of liquid crystal.

UNIVERSITAT ROVIRA I VIRGILI
DESIGN AND MODELLING OF PHOTONIC CRYSTALS WITH ANISOTROPIC COMPONENTS
Joaquin Cos Córcoles
ISBN:978-84-693-9433-5/DL:T.69-2011

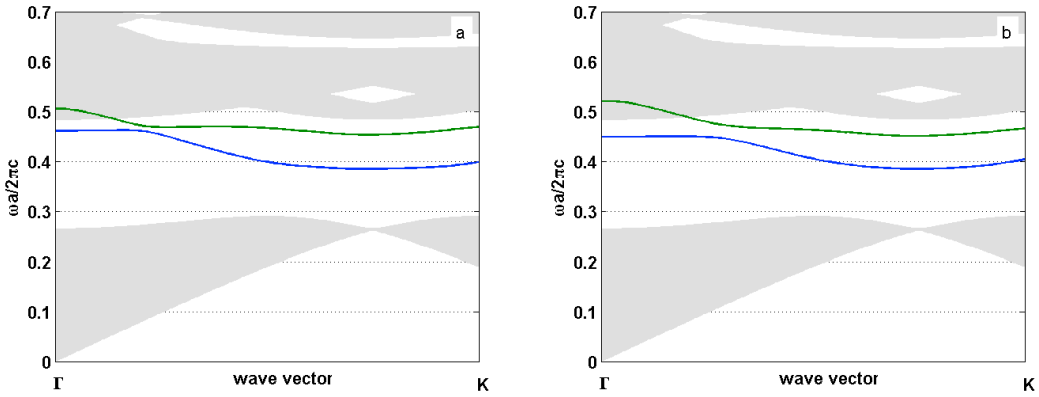

Fig. 5.27 Dispersion relation for two guided modes of the photonic crystal waveguide with a LC optical axis orientation a) α = 0º and b) α = 50º. Shadow regions indicate the projected band structure of the structure without defects.

In order to better understand the behaviour of the field corresponding to these guided modes, in Fig. 5.28 and Fig. 5.29 the amplitudes of the H_z field for such modes at different points in the First Brillouin Zone and for the angles $\alpha = 0^o$ and $\alpha = 50^o$, respectively, are shown. It can be observed that the two modes correspond to an even and an odd field distribution: at the **Γ**-point the lower mode shows an odd distribution (with a nodal line along the **Γ**-**K** direction) while the upper mode shows an even distribution. Oppositely, at **K**-point the lower mode is even while the upper mode is odd. Figures 5.28 and 5.29 show the field distribution for the **k** point in the First Brillouin Zone in which the two modes show a minimum frequency difference. For $\alpha = 0^o$ it can be seen that the two modes are degenerate and thus, there is no frequency gap between them. Instead, for $\alpha = 50^o$, the degeneracy is broken as an effect of the liquid crystal orientation. The difference of the two distributions is significant, and this opens a gap between the two modes.

Taking into account that the mode introduced by the input waveguide is even (as the source is a point source placed at the symmetry axis of the waveguide), the existence of the gap observed above explains the behaviour shown in Fig. 5.26: the incoming wave will only be able to couple to the even mode in the waveguide, however, for a given range of LC orientations, the frequency will lie within the gap and

UNIVERSITAT ROVIRA I VIRGILI
DESIGN AND MODELLING OF PHOTONIC CRYSTALS WITH ANISOTROPIC COMPONENTS
Joaquin Cos Córcoles
ISBN:978-84-693-9433-5/DL:T.69-2011

the wave will not be able to couple. This also explains the existence of frequencies where the tunability is small (see Fig. 5.24), since for any LC orientation there exist an even mode with such frequency.

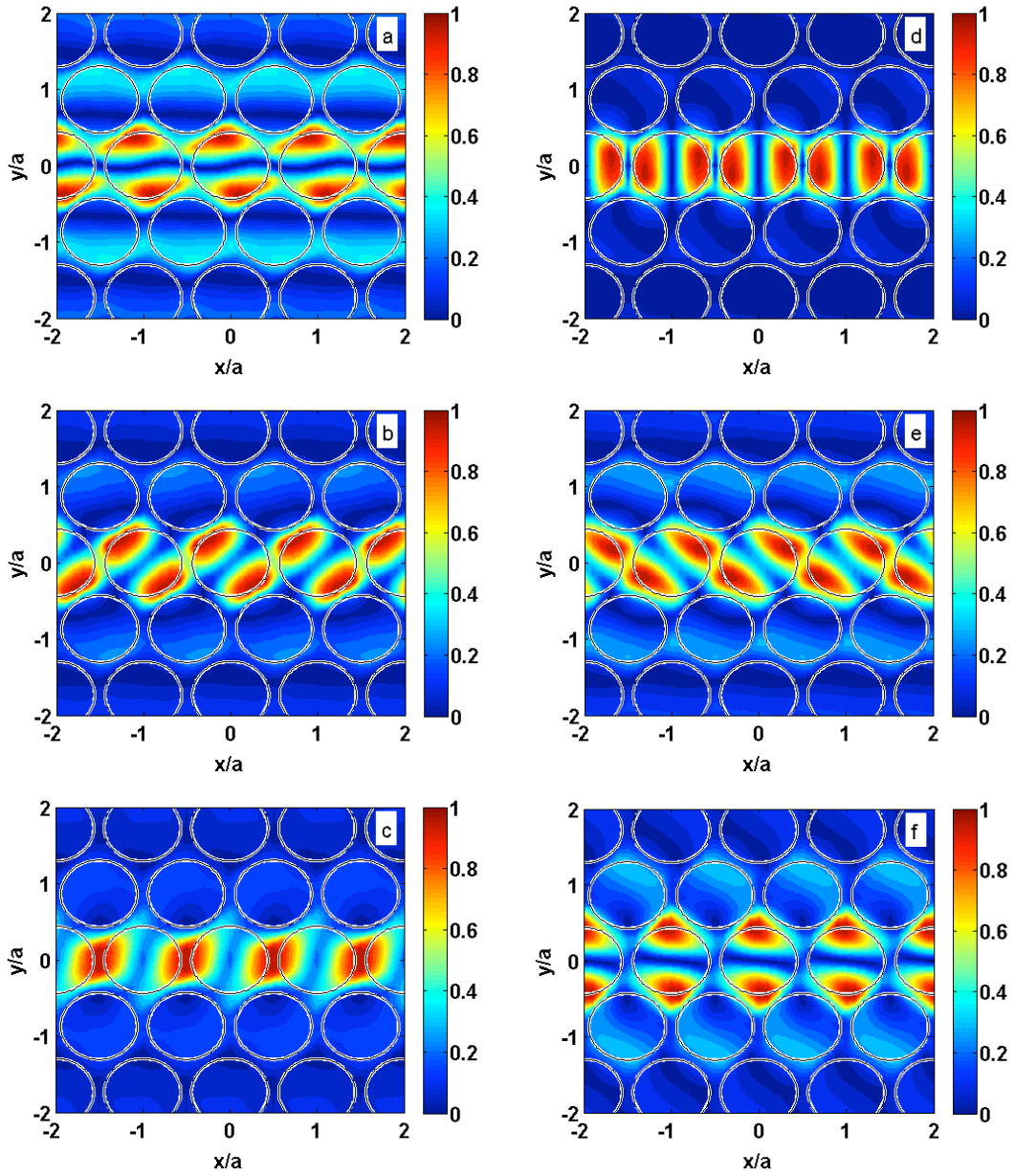

Fig. 5.28 Field distribution of the modulus of the Z-component of the Magnetic Field (H_z) for the lower mode at a) Γ-point b) a point in the region where these two guided modes are nearest and c) K-point and for the upper mode at d) Γ-point e) a point in the region where these two guided modes are nearest and f) K-point. In all the cases the optical axis orientation is $\alpha = 0^o$.

UNIVERSITAT ROVIRA I VIRGILI
DESIGN AND MODELLING OF PHOTONIC CRYSTALS WITH ANISOTROPIC COMPONENTS
Joaquin Cos Córcoles
ISBN:978-84-693-9433-5/DL:T.69-2011

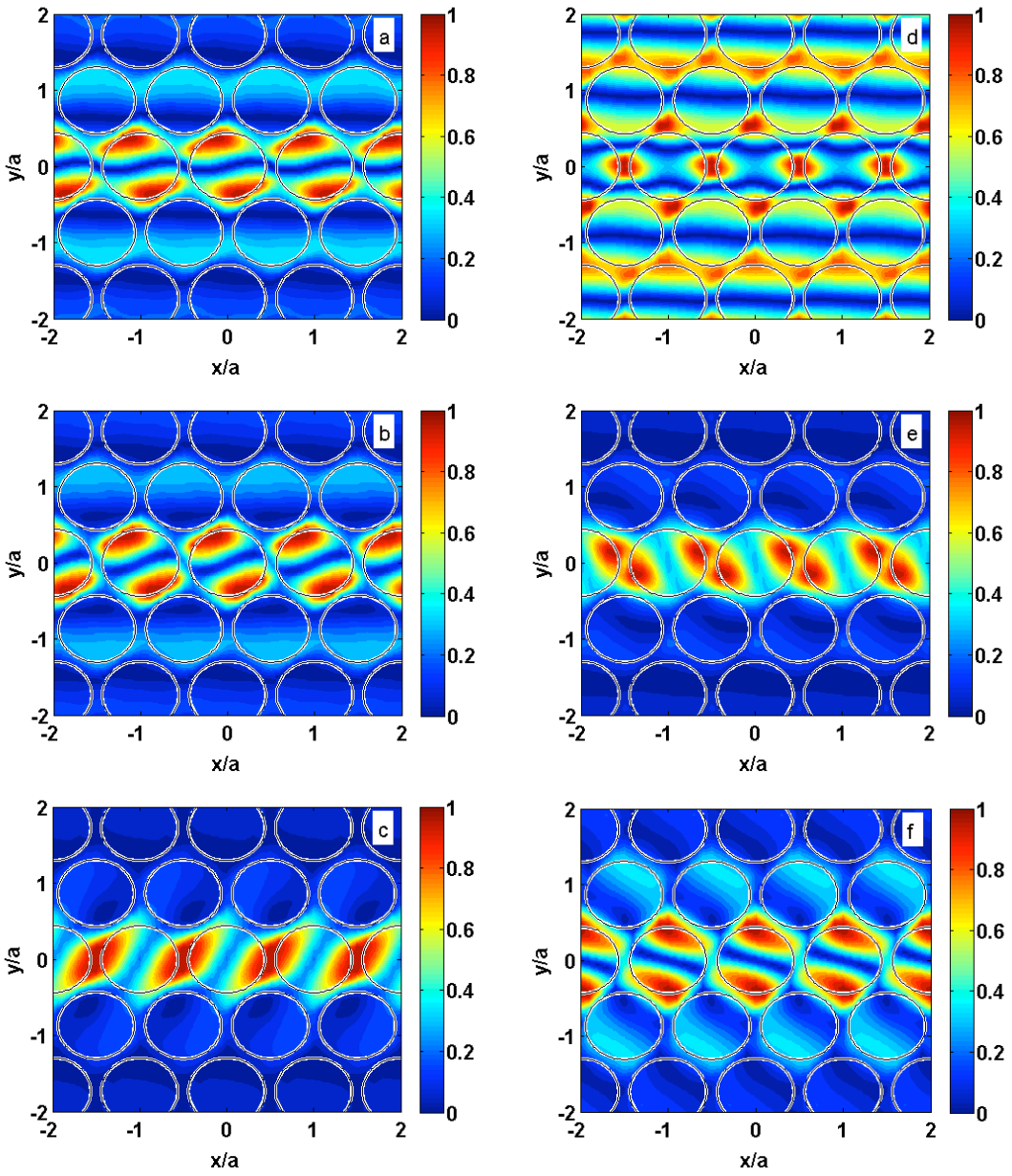

Fig. 5.29 Field distribution of the modulus of the Z-component of the Magnetic Field (H_z) for the lower mode at a) Γ-point b) a point in the region where these two guided modes are nearest and c) K-point and for the upper mode at d) Γ-point e) a point in the region where these two guided modes are nearest and f) K-point. In all the cases the optical axis orientation is $\alpha = 50^o$.

UNIVERSITAT ROVIRA I VIRGILI
DESIGN AND MODELLING OF PHOTONIC CRYSTALS WITH ANISOTROPIC COMPONENTS
Joaquin Cos Córcoles
ISBN:978-84-693-9433-5/DL:T.69-2011

5.4 Conclusions

We have studied and analyzed several structures based on two-dimensional silicon photonic crystals with liquid crystal infiltration. The first structure consists of a tunable filter, where, by filling the air holes in a silicon background with liquid crystal or surrounding the silicon rods with liquid crystal tunable properties are obtained. The second and the third part of this chapter were devoted to the tunable photonic crystal waveguides. On one hand, we study the optimization of the device by changing the defect cylinder radius filled with liquid crystal that composes the core of the waveguide. On the other hand, a methodology for the study of the practical implementation of tunable waveguides based on Silicon Photonic Crystals with liquid crystal-infiltrated pores is presented.

First, we have studied the photonic bandgap tunability properties of 2D photonic crystal tunable filters based on silicon and liquid crystal components. The orientation of the liquid crystal is such that the optical axis lies in the plane of periodicity of the photonic crystal. In this configuration the Maxwell equations can be decoupled in TE and TM modes and the optical axis orientation only influences the TE bands. We have studied two different structures: i) a triangular lattice of E7 liquid crystal cylinders in a silicon background and ii) the inverse structure i.e. triangular array of silicon cylindrical rods in an E7 liquid crystal background.

The anisotropy of the liquid crystal causes that the Irreducible Brillouin Zone is different depending on the liquid crystal optical axis orientation. In order to obtain an accurate value for the bandgap limits, it was necessary to define a method to calculate the bandgaps of the structures based on the plane-wave expansion and on the calculation of the bands along paths of high symmetry in the First Brillouin Zone.

For the first structure, the TE bandgap appears between the 1st and 2nd bands and it has a 60^o periodicity with the LC optical axis orientation, α. Results show that the variation of the obtained bandgap is very small (*1.4%*) and the largest bandgap ($\Delta\omega a/2\pi c = 0.0581$) is obtained for $\alpha = 0^o$. For angles increasing up to $\alpha = 30^o$ the bandgap width decreases because of the decrease of the upper limit. However, from

UNIVERSITAT ROVIRA I VIRGILI
DESIGN AND MODELLING OF PHOTONIC CRYSTALS WITH ANISOTROPIC COMPONENTS
Joaquin Cos Córcoles
ISBN:978-84-693-9433-5/DL:T.69-2011

$\alpha = 30^o$ to $\alpha = 60^o$ there is a symmetrical behaviour and the bandgap increases with an increasing α. Results also show that the maximum bandgap depends very slightly on the radius of the LC cylinders. This demonstrates that using any radius in the range of optimal radii, variation of the bandgap width does not show a significant dependence with α.

In contrast, the second structure i.e. silicon rods surrounded with LC presents a bandgap that is opened between $\alpha = 0^o$ and $\alpha = 24^o$ and it is closed between $\alpha = 24^o$ and $\alpha = 30^o$. For $R/a = 0.220$, we obtain the maximum bandgap ($\Delta\omega a/2\pi c = 0.0087$). Thus, switches with a desired duty-cycle can be designed by adjusting the radius of cylinder appropriately, at the cost of having a narrower maximum bandgap.

The dependence of the band gap limits with the LC orientation angle has been explained by the analysis of the field distribution of the photonic bands corresponding to such limits. The results show that the change in the band gap limits depends not only on the field confinement in the LC but also on the field distribution symmetry.

Second, we have studied the tunability range of a Si-based photonic waveguide with a triangular lattice where a line of scatterers in the direction Γ-K has been infiltrated with E7 liquid crystal. By means of the plane-wave expansion method and the definition of a *7x1* supercell we have studied the optimization of this structure varying the size of the defect scatterers and studying the position in frequency of two guided modes. Also, the field distribution of these two guided modes has been studied.

The calculation reveals that maximum and minimum values of the frequency of the guided modes appear for liquid crystal optical axis orientations of $\alpha = 0^o$ and $\alpha = 90^o$. Therefore, studying the difference between the frequencies of each guided mode for these two orientations, the tunability range can be estimated for each defect size. For the first guided mode there are maxima in the tunability range for $R_{def}/a = 0.420$ for the Γ-point and $R_{def}/a = 0.360$ for the K-point. For the second guided mode there are maxima in the tunability range for $R_{def}/a = 0.360$ for the Γ-point and $R_{def}/a = 0.500$ for the K-point.

UNIVERSITAT ROVIRA I VIRGILI
DESIGN AND MODELLING OF PHOTONIC CRYSTALS WITH ANISOTROPIC COMPONENTS
Joaquin Cos Córcoles
ISBN:978-84-693-9433-5/DL:T.69-2011

The study of the field distribution shows a good confinement of the modes in the waveguide and high field concentration in the regions of high refractive index, corresponding to the silicon. Additionally, the guided modes show the same field distribution of the high energy regions at **Γ**-point and **K**-point for all the cases.

This structure can be used for the design of optical switches selecting the radius of the defects near of the cut-off radius (slightly above than $R_{def}/a = 0.360$ for the **Γ**-point or slightly below than $R_{def}/a = 0.335$ for the **K**-point). That way, the mode is within the bandgap, and consequently it is guided only for a range of liquid crystal optical axis orientations.

Finally, we have described a methodology for a proper understanding of the transmission properties of a silicon-based photonic crystal waveguide where a line of air scatterers in the **Γ**-**K** direction is filled by E7 liquid crystal. First, by means of the FDTD method the propagation of a wide-band pulse is calculated in order to obtain the maximum and minimum transmission values for each frequency as a function of the liquid crystal optical axis orientation. Next, by means of a monochromatic pulse of frequency $\omega a/2\pi c = 0.412$ the dependence of the transmission with the angle can be obtained with accuracy, in order to study in detail the switching effect. The monochromatic pulse is rejected for optical axis orientations between 30^o and 55^o while the monochromatic pulse is transmitted for the rest of orientations. These transmission properties can be explained in terms of the dispersion relations of the guided modes in the same structure. The low or high transmission of a given frequency depends on the aperture or closure of a gap between the two guided modes. For $\alpha = 0^o$ it can be seen that the two modes are degenerated and thus, there is no frequency gap between them. Instead, for $\alpha = 50^o$, the degeneracy is broken as an effect of the liquid crystal orientation. The difference of the two distributions is significant, and this opens a gap between the two modes.

UNIVERSITAT ROVIRA I VIRGILI
DESIGN AND MODELLING OF PHOTONIC CRYSTALS WITH ANISOTROPIC COMPONENTS
Joaquin Cos Córcoles
ISBN:978-84-693-9433-5/DL:T.69-2011

UNIVERSITAT ROVIRA I VIRGILI
DESIGN AND MODELLING OF PHOTONIC CRYSTALS WITH ANISOTROPIC COMPONENTS
Joaquin Cos Córcoles
ISBN:978-84-693-9433-5/DL:T.69-2011

Chapter 6

Theoretical study of the optical response of opals

A three-dimensional photonic crystal is the only material capable of presenting a complete band gap in their photonic band structure when the dielectric contrast is high enough. Within three-dimensional photonic crystals, nature offers a good model to be reproduced, the opal. Opals are iridescent semi-precious gems whose microstructure consists of silica spheres about *150 nm* to *300 nm* in diameter, which are tightly packed into repeating hexagonal or cubic arrangements. Synthetic opals use this same pattern, although they can be made from different materials. Synthetic opals have been the subject of a number of investigations [Andreani-2008; Santamaria-2008] in the recent years because of the advent of fabrication techniques, which takes advantage of the self-assembling properties of spherical colloidal particles in the micrometer scale.

Three-dimensional models of the numerical methods used in the analysis of this kind of structures require to define mesh models composed by N^3 points for each field, which produces a high increase of the computational cost compared to two-dimensional models where mesh models are composed by N^2 points for each field.

UNIVERSITAT ROVIRA I VIRGILI
DESIGN AND MODELLING OF PHOTONIC CRYSTALS WITH ANISOTROPIC COMPONENTS
Joaquin Cos Córcoles
ISBN:978-84-693-9433-5/DL:T.69-2011

Therefore, in order to reduce that cost, two-dimensional approximations of the structures seem to be a good election. For this, Balestreri *et al.* [Balestreri-2006] have characterized the optical properties of an opal photonic crystal by means of a scattering-matrix approach based on approximating each sphere by cylindrical slices.

Although this thesis is devoted to anisotropic photonic crystals, the isotropic structures and the analytical method used in this chapter can be related to anisotropic structures by two points. First, inverse opals are very suitable structures for infiltrate liquid crystal, several of the first works [Busch-1999; Yoshino-1999] on liquid crystal photonic tunable bandgap employed this kind of structures. Second, the idea of considering the spheres of the opal structure as a stacking of cylinders can be extended to anisotropic spheres, Liscidini *et al.* [Liscidini-2008] have applied this treatment of the scattering matrix method for the analysis of a 2D birefringent media.

The complexity of the analysis of anisotropic three-dimensional structures by means of 2D model approximations requires establishing a previous point, which is the develop of a 2D model approximation for the characterization of isotropic opals. This work represents this previous point for a future work on the analysis of anisotropic three-dimensional structures.

In this chapter, the optical response of opals is analyzed by means of another scattering matrix formalism that is suitable for any unit cell geometry [Liscidini-2008]. We start our description with the basic concepts of opal photonic crystals summarizing the most important techniques of fabrication, and some of the their applications. Next, we describe the numerical method and the structure description employed and study several parameters in order to guarantee the convergence. Finally we show the results obtained in this work, first the study of the diffraction effects in the optical response of opal photonic crystals in the high-energy region, and second, the characterization of amorphous silicon/magnesia based direct opals with tunable optical properties.

UNIVERSITAT ROVIRA I VIRGILI
DESIGN AND MODELLING OF PHOTONIC CRYSTALS WITH ANISOTROPIC COMPONENTS
Joaquin Cos Córcoles
ISBN:978-84-693-9433-5/DL:T.69-2011

6.1 Opal photonic crystals

Opal photonic crystals consist of a dense packing of submicron diameter monodisperse spheres arranged in a close-packed face-centered-cubic (fcc) or hexagonal-closed-packing (hcp). As it is commented above, for opals with a high dielectric contrast there is a complete bandgap. Synthetic opals are tightly packed into repeating hexagonal or cubic arrangements that the advantage of being made from different materials.

One of the advantages of opals is the simplicity of the fabrication process of high quality opals with monodisperse building blocks in shape and size. As periodicity for such crystals must be of the order of microns, the kind of particles used as building blocks are among those known as colloidal particles. Under certain conditions colloids may spontaneously self-assemble forming ordered lattices. The most important fabrication techniques are gravity sedimentation, centrifugation, vertical deposition, electrophoresis, template deposition, and controlled drying.

The existence of a complete photonic band gap could provide the opals with a number of unique technological applications, including optical waveguides with sharp bends [Mekis-1996], photonic integrated circuits [Chutinan-2004], single-mode light-emitting diodes [Yablonovitch-1993], and light trapping for solar cell [Knabe-2010].

UNIVERSITAT ROVIRA I VIRGILI
DESIGN AND MODELLING OF PHOTONIC CRYSTALS WITH ANISOTROPIC COMPONENTS
Joaquin Cos Córcoles
ISBN:978-84-693-9433-5/DL:T.69-2011

6.2 Theoretical method

6.2.1 Scattering matrix method

The scattering matrix method is a numerical method based on the definition of the scattering matrix (or s-matrix) for each layer of an arbitrary patterned multilayer structure.

In the scattering matrix method, according to the notation of Fig. 6.1 the s-matrix relates the amplitudes of the outgoing waves (A_N, B_0) at the surface and in the substrate to those of the incoming waves (A_0, B_N) on either side of the structure in the following way:

$$\begin{pmatrix} A_N \\ B_0 \end{pmatrix} = \begin{pmatrix} S_{11} & S_{12} \\ S_{21} & S_{22} \end{pmatrix} \begin{pmatrix} A_0 \\ B_N \end{pmatrix}. \tag{6.1}$$

Therefore, the procedure for the method of the patterned multilayer structure consists of solving the band structure in each layer and constructs the electric and magnetic fields in each layer from these solutions. Finally, the s-matrix is constructed relating the amplitudes of the incoming and outgoing waves of those fields. It is important to note that compared to the transfer matrix method (TMM), where the amplitudes are related in pairs of the same layer, the scattering matrix method is more stable when evanescent waves are involved [Ko-1988].

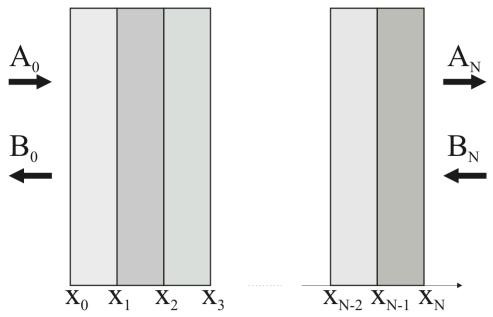

Fig. 6.1 Schematic view of a stratified medium. X_0 and X_N correspond, respectively, to the surface and the substrate.

UNIVERSITAT ROVIRA I VIRGILI
DESIGN AND MODELLING OF PHOTONIC CRYSTALS WITH ANISOTROPIC COMPONENTS
Joaquin Cos Córcoles
ISBN:978-84-693-9433-5/DL:T.69-2011

In this thesis, the Fortran-based code of the scattering matrix formalism previously developed by Liscidini [Liscidini-2008] is used and adapted in order to define our opal description model.

6.2.2 Structure description

The structure we consider is a direct opal composed of dielectric spheres arranged in a close-packed face-centered-cubic (fcc) lattice of period *a*. Despite the opal structure has to be stacked on a substrate (glass) in order to provide mechanical stability to the structure, in several cases during this work we will consider air as a substrate. Fig. 6.2a shows a schematic view of the structure, where the reference system is chosen such that the *z* axis is along the {111} direction. As it can be seen in Fig. 6.2b the structure can be viewed as a stack of spheres' layers in a close-packed lattice where each spheres' plane is shifted in the *x* direction by $d/\sqrt{3}$ with respect to the previous one, according to the sequence ABC, ABC, etc.... In each layer, the spheres are arranged in a triangular lattice of period $d = a/\sqrt{2}$, which is the sphere's diameter. Along the {111} direction the distance between two consecutive spheres' layers is $d_{111} = \sqrt{2}/3d$, thus there exists an interpenetration region of thickness $H_{cap} = (1-\sqrt{2}/3)d$ for two consecutive layers.

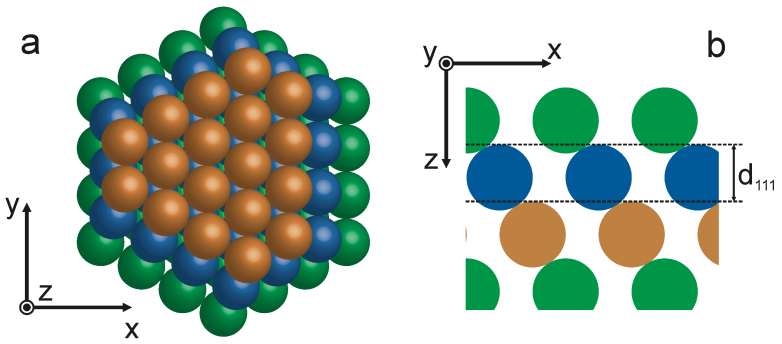

Fig. 6.2 Schematic illustration of the opaline structure. a) Top view and b) front view of several consecutive layers arranged in the ABC order along the {111} direction.

UNIVERSITAT ROVIRA I VIRGILI
DESIGN AND MODELLING OF PHOTONIC CRYSTALS WITH ANISOTROPIC COMPONENTS
Joaquin Cos Córcoles
ISBN:978-84-693-9433-5/DL:T.69-2011

As we commented before, Balestreri *et al.* [Balestreri-2006] showed that the optical properties of an opal can be studied by means of the scattering matrix method in the Whittaker and Culshaw formulation that allows for the description of periodically patterned multilayers [Whittaker-1999]. This method requires subdividing the structure in layers that are homogeneous in the *z* direction, so that each sphere is approximated with a stack of concentric cylinders arranged in a periodic lattice [Balestreri-2006]. In particular, an important feature of the strategy proposed in [Balestreri-2006] is to mimic the interpenetration region between two consecutive spheres' planes by means of one layer of cylinders arranged in a graphite lattice, according to the symmetry that one has by taking a horizontal section in the center of such a region. If one wants to improve the accuracy of the numerical simulation, one must increase the number of subdivisions in this overlap region. In general, a horizontal section of this region is characterized by a borum-nitride lattice (Fig. 6.3a), thus lacking in inversion symmetry. This prevents the description of such a system using the method in [Whittaker-1999] that requires inversion symmetry of the unit cell.

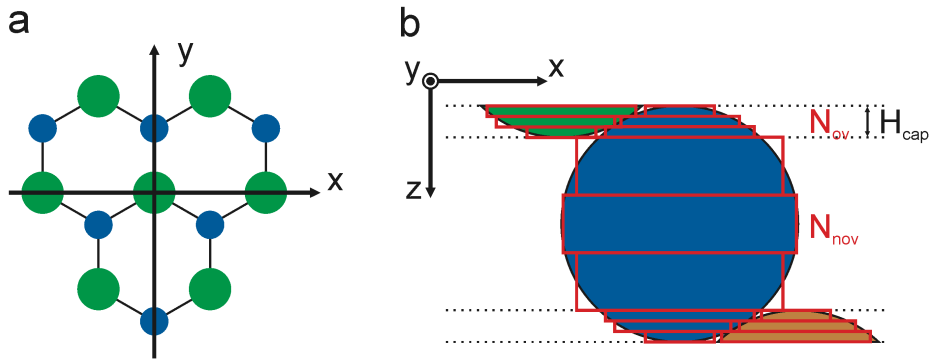

Fig. 6.3 Schematic view of the sphere discretization. a) Borum-Nitride lattice. b) Front view of the spheres discretization in the overlapping and non-overlapping regions, red rectangles indicate the dimensions of the cylinders.

UNIVERSITAT ROVIRA I VIRGILI
DESIGN AND MODELLING OF PHOTONIC CRYSTALS WITH ANISOTROPIC COMPONENTS
Joaquin Cos Córcoles
ISBN:978-84-693-9433-5/DL:T.69-2011

Recently, Liscidini *et al.* [Liscidini-2008] proposed a formulation of the scattering matrix formalism that is suitable for any unit cell geometry. Thus we are able to vertically subdivide the opal in an arbitrary large number of layers. In particular, each sphere is divided in $N_S = N_{nov} + 2 \cdot N_{ov}$ cylinders, where N_{nov} and N_{ov} are the numbers of subdivisions in the non-overlapping and overlapping regions, respectively (Fig. 6.3b). The heights of the cylinders are $h_{ov} = H_{cap}/N_{ov}$ in the overlapping region and $h_{nov} = (1 - 2 \cdot H_{cap})/N_{nov}$ in the non-overlapping region. Each radius is chosen such that the cylinder' volume is that of the corresponding sphere section. This automatically guarantees that the total fraction of dielectric material is preserved.

6.2.3 Convergence optimization

Our studies include the opal response in the high-energy region, therefore it is important to choose the calculation parameters that guarantee its convergence in this region. In this regard, there are essentially two important parameters: the number of plane waves *NPW* and the number of sphere subdivisions $N_S = N_{nov} + 2 \cdot N_{ov}$. Here, the convergence test is done in the high-energy region for a polystyrene opal of 15 spheres' layers. We also include a treatment of the disorder by considering absorption ($\varepsilon_i = 0.02$) as previously suggested by Dorado *et al.* [Dorado-2007].

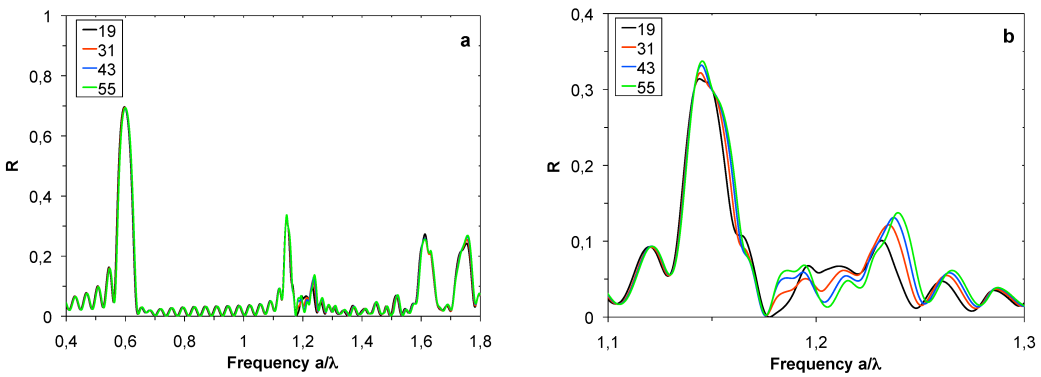

Fig. 6.4 Reflection spectra for a polystyrene opal with absorption ($\varepsilon_r = 2.4964$, $\varepsilon_i = 0.02$ in the dielectric regions) for different numbers of plane waves in the 2D plane. The opal consists of N = 15 layers on silica glass ($\varepsilon_{SiO2} = 2.1025$) and each sphere is discretized with five layers in the non-overlapping regions ($N_{nov} = 5$) and five layers in the overlapping regions ($N_{ov} = 5$).

UNIVERSITAT ROVIRA I VIRGILI
DESIGN AND MODELLING OF PHOTONIC CRYSTALS WITH ANISOTROPIC COMPONENTS
Joaquin Cos Córcoles
ISBN:978-84-693-9433-5/DL:T.69-2011

First, the dependence of the transmittance spectra with the number of plane waves is studied, which determines the accuracy with which the structure can be defined in the *x*-*y* plane. In the high-energy region, this number has to be sufficiently large to efficiently describe all the cylinders, especially in the overlap region where they are the smallest. In Fig. 6.4 the reflectance is shown as a function of a/λ along the {111} direction of the opal on a silica glass substrate ($\varepsilon_{SiO2} = 2.1025$) for *NPW = 19*, *31*, *43*, and *55* plane-waves. The spectra comparison (Fig. 6.4b for details) indicates that NPW = *31* is sufficient for the convergence. In particular, there is a critical region around $a/\lambda = 1.2$ where a lower number of plane-waves causes a distortion of the spectral features.

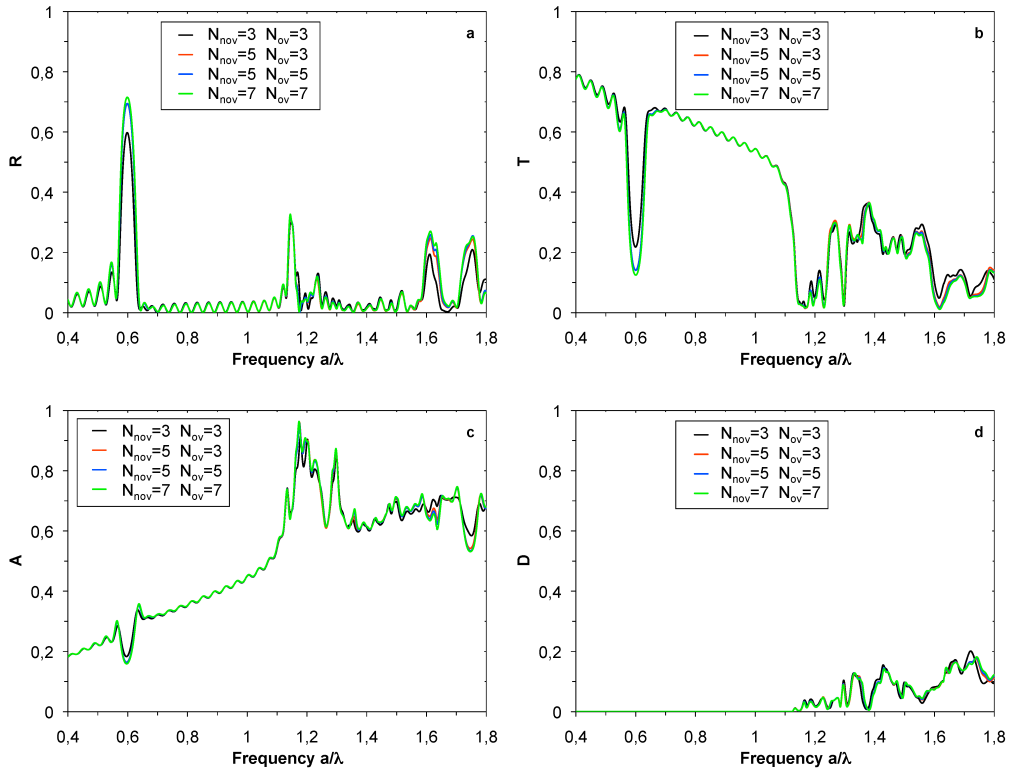

Fig. 6.5 a) Reflectance, b) transmittance, c) absorption, and d) diffraction spectra for a polystyrene opal with absorption absorption ($\varepsilon_r = 2.4964$, $\varepsilon_i = 0.02$ in the dielectric regions) for different discretization numbers N_{nov}, N_{ov} in the non-overlapping and overlapping regions, respectively. The opal consists of N = 15 layers on silica glass ($\varepsilon_{SiO2} = 2.1025$). The number of plane waves is NPW = 31.

UNIVERSITAT ROVIRA I VIRGILI
DESIGN AND MODELLING OF PHOTONIC CRYSTALS WITH ANISOTROPIC COMPONENTS
Joaquin Cos Córcoles
ISBN:978-84-693-9433-5/DL:T.69-2011

The second parameter of the study is the number *N* of discretization cylinders in which each sphere is subdivided. It is interesting to notice that, in general, at lower energies, even a small number of cylinders can give good results in the calculation of the opal band-structure and optical properties. In particular, this depends on the refractive index contrast and on whether the opal is direct or inverse [Balestreri-2006]. Since the computational time scales linearly with the total number of layers, it is important to find the right trade-off with the required accuracy. Fig. 6.5 shows the reflectance (R), transmittance (T), absorption (A) along the {111} direction and diffraction (D) for the direct opal structure on glass for different value of N_{nov} and N_{ov}. The diffraction spectra represents the intensity of light diffracted in all directions, except the {111} direction and it is calculated as

$$D = 1 - R - T - A. \qquad (6.2)$$

It can be concluded that a subdivision of *5* cylinders in the non-overlapping region and *5* cylinders in the overlapping region is sufficient to guarantee a good convergence.

In the following, all the optical spectra are calculated with *NPW = 31* and $N_{nov} = N_{ov} = 5$, as these values can guarantee a good reliability of the results.

6.3 Study of the diffraction effects on the high-energy region

In this section it is shown that the internal diffraction of the light is responsible for many of the features that characterize the high-energy spectral region of an opal. In particular, a complete description of its optical properties through the calculation of the transmittance, reflectance, absorption, and diffraction spectra for opals made of several layers is presented. As the number of layers is increased from *3* to *18*, the diffraction effects, and thus the features in the high-energy region, become stronger. The calculations of the optical spectra are done by considering two different kind of

UNIVERSITAT ROVIRA I VIRGILI
DESIGN AND MODELLING OF PHOTONIC CRYSTALS WITH ANISOTROPIC COMPONENTS
Joaquin Cos Córcoles
ISBN:978-84-693-9433-5/DL:T.69-2011

substrate: silica glass and air, in order to understand the role of the diffraction cut-off on the spectral features. In all the simulations, the numbers of discretization layers and plane waves determined in the previous section to guarantee the convergence are considered. It is considered a TE-polarized incident light, as for these structures, along the {111} direction, there is no difference between TE and TM spectra.

Figs. 6.6a-f show the optical properties for an opal structure made of (a) *3*, (b) *6*, (c) *9*, (d) *12*, (e) *15*, and (f) *18* layers of spheres with $\varepsilon_r = 2.4964$ and $\varepsilon_i = 0.02$ in air. A free standing structure in air is considered. Although it is a non realistic case, this hypothesis allows us to study the optical properties of the opal in the high-energy region between $a/\lambda = 1.2$ and $a/\lambda = 1.6$ when there is no diffraction outside the structure, as this interval is below the air diffraction cut-off (around $a/\lambda = 1.6$).

As the number of layers increase, absorption is observed, in particular at those energy values that correspond to photonic resonance associated with the presence of diffraction in the opal structure. Indeed, when the incident light is scattered at larger angles in the structure by the spheres, this results in an increase of the photon dwelling time in the opals so that the probability that the light is absorbed is higher.

UNIVERSITAT ROVIRA I VIRGILI
DESIGN AND MODELLING OF PHOTONIC CRYSTALS WITH ANISOTROPIC COMPONENTS
Joaquin Cos Córcoles
ISBN:978-84-693-9433-5/DL:T.69-2011

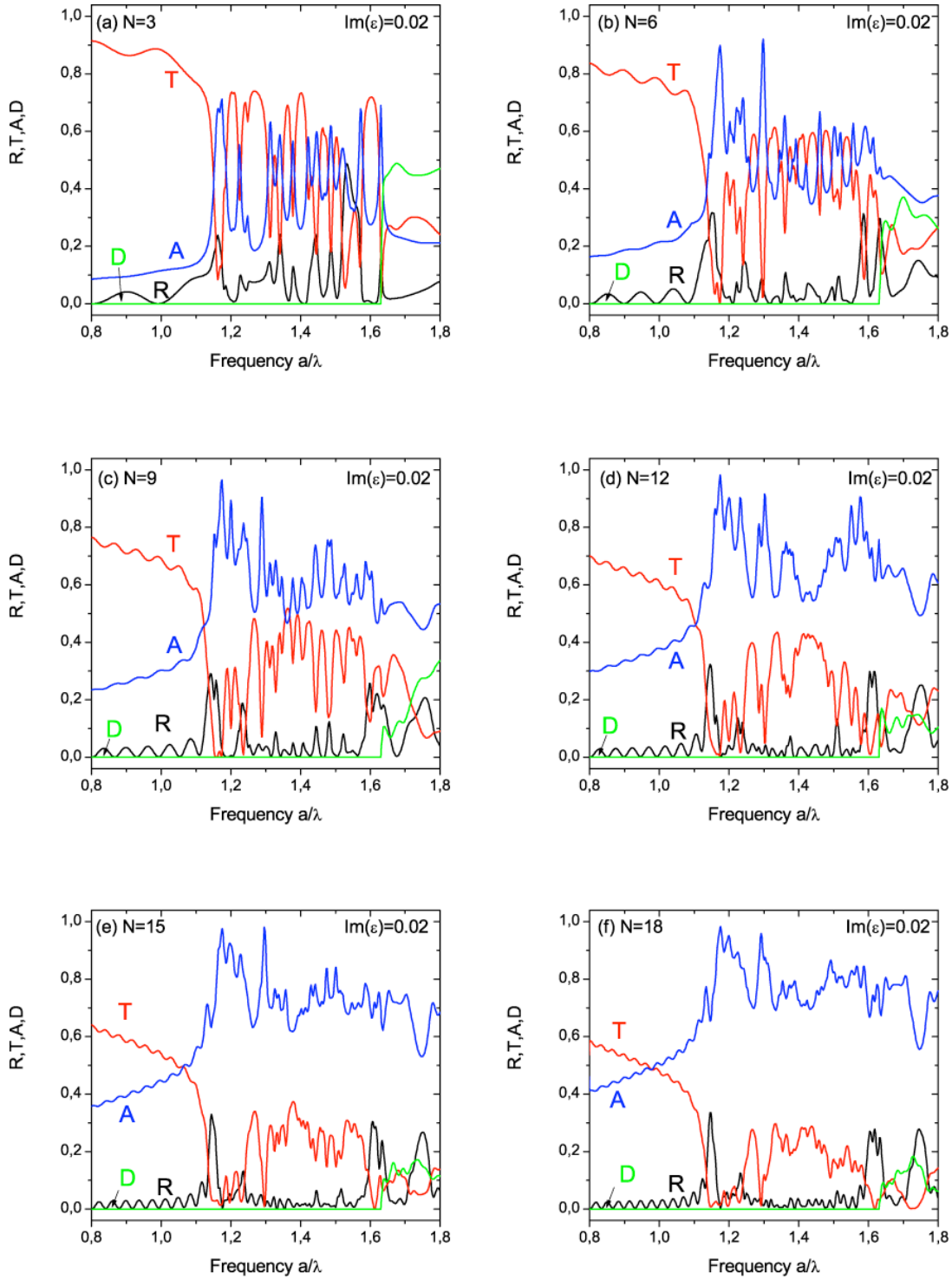

Fig. 6.6 Optical spectra for a polystyrene opal with absorption (ε_r = 2.4964, ε_i = 0.02 in the dielectric regions for different number of layers N. The opal is on air. The number of plane waves is NPW = 31 and the number of discretizations are N_{nov} = 5, N_{ov} = 5 in the non-overlapping and overlapping regions, respectively.

UNIVERSITAT ROVIRA I VIRGILI
DESIGN AND MODELLING OF PHOTONIC CRYSTALS WITH ANISOTROPIC COMPONENTS
Joaquin Cos Córcoles
ISBN:978-84-693-9433-5/DL:T.69-2011

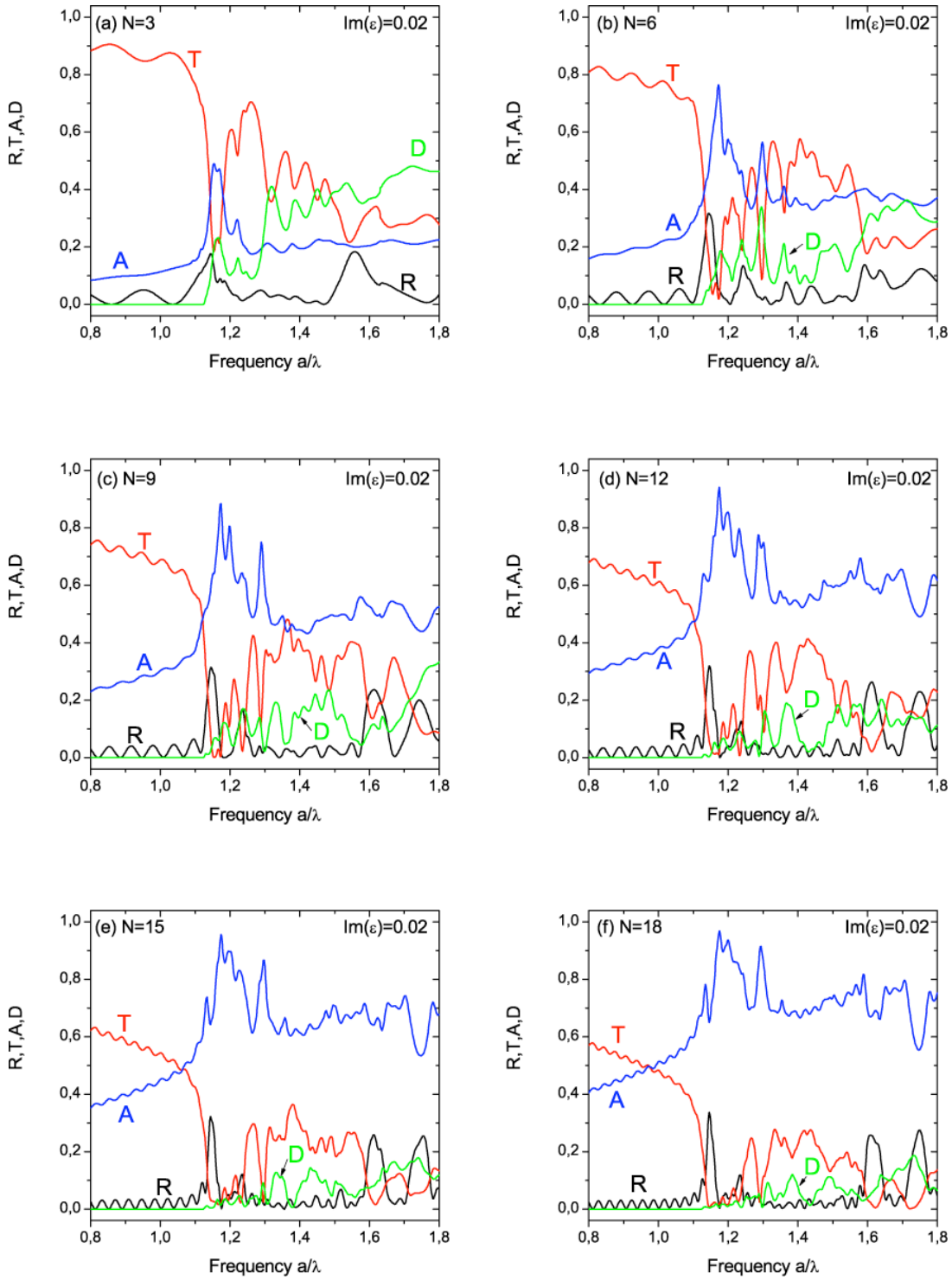

Fig. 6.7 Optical spectra for a polystyrene opal with absorption (ε_r = 2.4964, ε_i = 0.02 in the dielectric regions) for different number of layers N. The opal is on silica glass (ε_{SiO2} = 2.1025). The number of plane waves is NPW = 31 and the number of discretizations are N_{nov} = 5, N_{ov} = 5 in the non-overlapping and overlapping regions, respectively.

UNIVERSITAT ROVIRA I VIRGILI
DESIGN AND MODELLING OF PHOTONIC CRYSTALS WITH ANISOTROPIC COMPONENTS
Joaquin Cos Córcoles
ISBN:978-84-693-9433-5/DL:T.69-2011

In Fig. 6.7, the optical properties of the same structures are reproduced but in this case considering silica glass ($\varepsilon_{SiO2} = 2.1025$) as substrate media. In this case, the diffraction of the glass interacts with the light because the diffraction cut off is in the range of the first optical structure (diffraction for air starts around $a/\lambda = 1.6$ while diffraction for silica glass starts around $a/\lambda = 1.1$). However, from *9* layers the four features do not change qualitatively because there are enough opal layers to neglect the effect of the glass substrate. Comparing Figs. 6.6 and 6.7, we can observe that for a high enough number of layers (e. g. at $N = 12$) there are no important differences in the reflectance and absorption spectra in the region of the four structures, in both cases the four features have similar shape and height. There is a match between maxima on diffraction and minima on transmission. This absence of differences between Figs. 6.6 and 6.7 for a sufficient number of layers demonstrate that the effects of the diffraction inside the opals negate the effects related to the substrate.

In order to study the internal diffraction of the opals and its effect on the absorption, the electromagnetic field distribution is compared in the region where internal diffraction of the opals places an important role and the region where the internal diffraction of the opal does not place an important role. In particular, we want to highlight the role of diffraction in the absorption enhancement observed in the second band-gap region (see Figs. 6.6 and 6.7). Fig. 6.8 shows the field distribution in the *xz* plane (according to the notation adopted in Fig. 6.2) for a TE-polarized incident plane wave at $a/\lambda = 0.7$ (Fig. 6.8a) and $a/\lambda = 1.3$ (Fig. 6.8b). In the region where the wavelengths are high enough to consider the behaviour of the opal structure as a one-dimensional system (e.g. at $a/\lambda = 0.7$) no appreciable diffraction effect is observed, and the field distribution is mainly characterized by an interference pattern along the *xz* plane. On the contrary, for wavelengths above the diffraction cut-off inside the opals (e. g. at $a/\lambda = 1.3$) the electric field is propagated along other directions beside the *xz* plane. This propagation produces an increase of the average optical path, which together with the high concentration of the electric field inside the opals, leads to an absorption increase that is independent of the structure substrate (see Fig. 6.6b and Fig. 6.7b), and thus it can be associated with the diffraction in the opal. Figs. 6.8c-d

UNIVERSITAT ROVIRA I VIRGILI
DESIGN AND MODELLING OF PHOTONIC CRYSTALS WITH ANISOTROPIC COMPONENTS
Joaquin Cos Córcoles
ISBN:978-84-693-9433-5/DL:T.69-2011

demonstrates the absence (for Fig. 6.8c) or presence (for Fig. 6.8d) of the diffraction. These two figures represent the in-plane Fourier components' amplitudes at the center of the opal structure (corresponding to $z = 5.5$) for $a/\lambda = 0.7$ and $a/\lambda = 1.3$ respectively. As expected, for $a/\lambda = 0.7$ the electric field is concentrated in the first Fourier component, that corresponds to the field propagation at $k = 0$. On the contrary, for $a/\lambda = 1.3$ the electric field is not concentrated in the first Fourier component and there are more Fourier components, which correspond to a propagation in different directions allowed by the in-plane lattice symmetry, and must be taken into account in the electric field propagation.

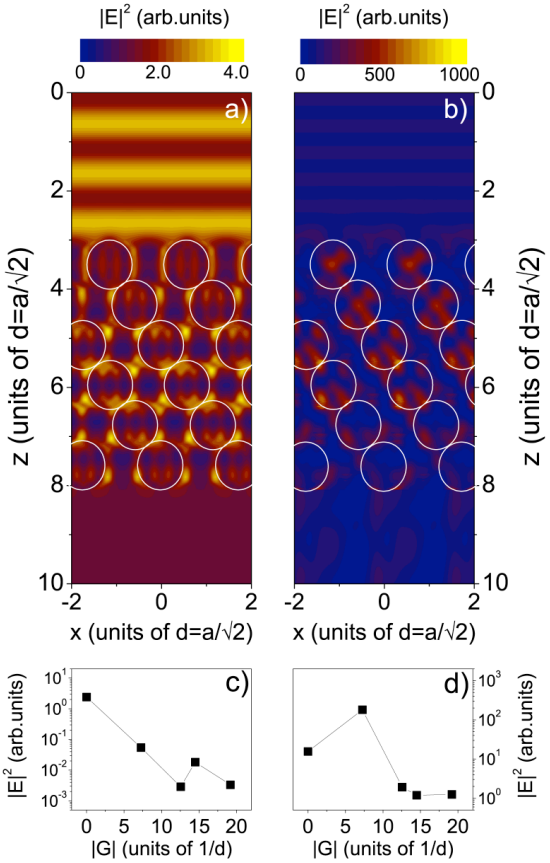

Fig. 6.8 Square of the electric field in real space (xz according to previous notations of Fig. 2) for a polystyrene opal with absorption ($\varepsilon_r = 2.4964$, $\varepsilon_i = 0.02$ in the dielectric regions) at a) $a/\lambda = 0.7$ and b) $a/\lambda = 1.3$. Fourier amplitudes of plane-wave expansion space at c) $a/\lambda = 0.7$ and d) $a/\lambda = 1.3$. The opal is composed by $N = 6$ layers on silica glass ($\varepsilon_{SiO2} = 2.1025$). The number of plane waves is NPW = 31 and the number of discretizations are $N_{nov} = 5$, $N_{ov} = 5$ in the non-overlapping and overlapping regions, respectively.

UNIVERSITAT ROVIRA I VIRGILI
DESIGN AND MODELLING OF PHOTONIC CRYSTALS WITH ANISOTROPIC COMPONENTS
Joaquin Cos Córcoles
ISBN:978-84-693-9433-5/DL:T.69-2011

6.4 Characterization of amorphous silicon/magnesia based direct opals with tunable optical properties

In this section, the experimental reflectance spectra of the opal microstructures obtained in [Pallavidino-2010] are compared with the calculated ones using the scattering matrix approach in order to evaluate the quality of the opaline replicas. Three samples are studied, corresponding to the three main processes of fabrication proposed in [Pallavidino-2010]: synthesis of the silica nanospheres (silica opal), magnesiothermic treatment of the opals (magnesized opal) and HCl wet chemical etching (porous silicon opal).

Experimental measures were obtained by specular reflectance spectroscopy operating in quasi-backscattering configuration (12.5^o with respect to the {111} direction of the fcc structures) [Pallavidino-2010].

Scattering effects and disorders are described either by introducing an imaginary part of the refractive index or by using an artificial Gaussian smoothing of the theoretical spectra [Dorado-2007; Balestreri-2006].

In the calculations, the sample was composed of *15* opal layers with a stacking sequence ABC, ABC,… on a silica glass substrate ($n = 1.45$). The diameter of the spheres is *340 nm*.

In the first sample an opal made of Silica ($n = 1.4$) spheres surrounded by air ($n = 1$) is analyzed. For the theoretical spectrum *31* plane waves are considered. Each sphere is subdivided in *5* cylinders for non-overlapping region and *5* cylinders for overlapping region (therefore each sphere is discretized in *15* cylinders). In order to take into account scattering and disorder effects, an imaginary part $\varepsilon_i = 0.02$, independent of the energies is introduced in the Silica dielectric function. In Fig. 6.9 from left to right it is plotted the band diagram, the measured reflectance spectrum at quasi-normal incidence, and the calculated spectrum at normal incidence.

UNIVERSITAT ROVIRA I VIRGILI
DESIGN AND MODELLING OF PHOTONIC CRYSTALS WITH ANISOTROPIC COMPONENTS
Joaquin Cos Córcoles
ISBN:978-84-693-9433-5/DL:T.69-2011

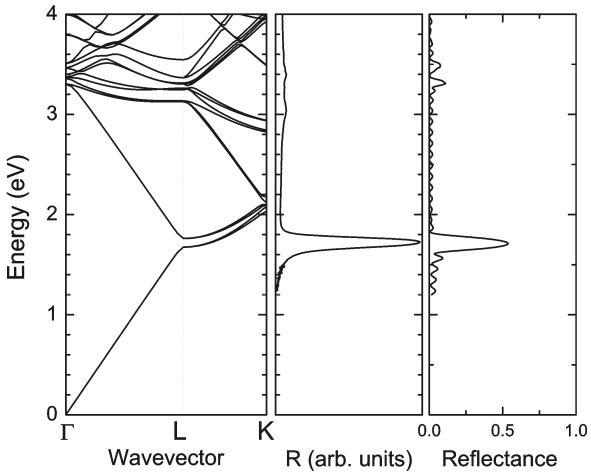

Fig. 6.9 (From left to right) Band diagram, experimental Reflectance spectrum measured at quasi-normal incidence (R), and the corresponding theoretical spectrum at normal incidence for a Silica (n = 1.4) spheres in air (n = 1). Calculated spectrum has been obtained for 15 layers of spheres, the number of plane waves is NPW = 31 and the number of discretizations are N_{nov} = 5, N_{ov} = 5 in the non-overlapping and overlapping regions. In order to take into account scattering and disorder effects we introduce an imaginary part ε_i = 0.02 in the silica dielectric function.

The width and position of the main stop-band region (first pseudo-gap at L point) agree with those of the experimental curve. In the theoretical spectrum there are also two features at *3.32 eV* and *3.46 eV*. They may correspond to the pseudo-gaps on the band distribution for silica opal (without dispersion and absorption) in the **Γ-L** direction and to two weak features of the experimental spectra. These high-energy features can be considered as a fingerprint of the good periodicity and stacking order [Nair-2007] of the opals. The differences on the energy position of these features for experimental and calculated spectra may simply be a consequence of having neglected the silica dispersion in the calculation.

UNIVERSITAT ROVIRA I VIRGILI
DESIGN AND MODELLING OF PHOTONIC CRYSTALS WITH ANISOTROPIC COMPONENTS
Joaquin Cos Córcoles
ISBN:978-84-693-9433-5/DL:T.69-2011

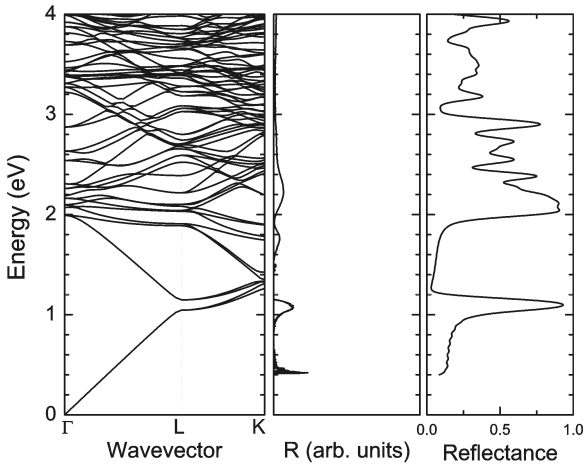

Fig. 6.10 (From left to right) Band diagram, experimental Reflectance spectrum measured at quasi-normal incidence (R), and the corresponding theoretical spectrum at normal incidence for a a-Si/MgO (n = 2.35) opal structure. Calculated spectrum has been obtained for 15 layers of spheres, the number of plane waves is NPW = 43 and the number of discretizations are N_{nov} = 9, N_{ov} = 9 in the non-overlapping and overlapping regions. In order to take into account scattering and disorder effects we introduce an artificial Gaussian smoothing of variance $\sigma a/(2\pi c) = 0.03$ in the theoretical spectrum.

The second case analyzed corresponds to the amorphous silicon magnesized ($n = 2.35$) opal structure. In this case, *43* plane waves are considered. Each sphere is discretized in *9* cylinders for the non-overlapping region and *9* cylinders for each overlapping region (therefore, each sphere is discretized in *27* cylinders). The scattering effects are considered by introducing an artificial Gaussian smoothing of variance $\sigma a/(2\pi c) = 0.03$ in the theoretical spectrum. Fig. 6.10 shows, from left to right, the band diagram, the measured reflectance spectrum at quasi-normal incidence, and the calculated spectrum at normal incidence.

The main stop-band appears at the same energy level $E = 1.1$ *eV* for experimental and theoretical results. High energy features at *1.78 eV* and *2.2 eV* of the experimental spectrum are shifted to high energies in calculated spectrum, as the material dispersion is not considered. Absorption is neglected in the calculated spectrum as well and it explains the presence of the rest of the high energies features. By comparing the simulated spectrum with the band diagram, the high-energy structures can be linked to the regions of the band diagram where pseudogaps are near to appear.

UNIVERSITAT ROVIRA I VIRGILI
DESIGN AND MODELLING OF PHOTONIC CRYSTALS WITH ANISOTROPIC COMPONENTS
Joaquin Cos Córcoles
ISBN:978-84-693-9433-5/DL:T.69-2011

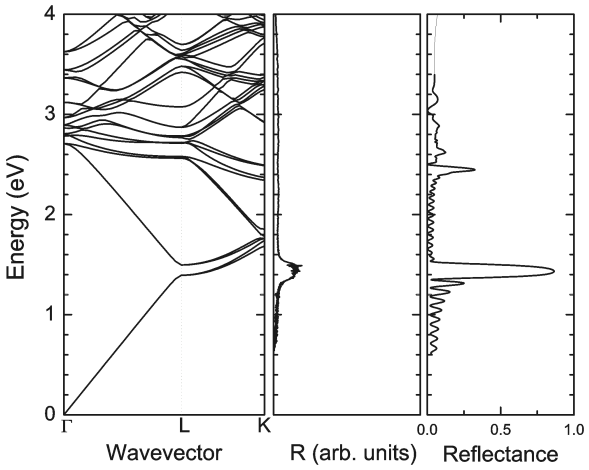

Fig. 6.11 (From left to right) Band diagram, Experimental reflectance spectrum measured at quasi-normal incidence, and the corresponding theoretical spectrum at normal incidence for the porous silicon (n = 1.72) spheres. Calculated spectrum has been obtained for 15 layers of spheres, the number of plane waves is NPW = 31 and the number of discretizations are N_{nov} = 5, N_{ov} = 5 in the non-overlapping and overlapping regions In order to describe absorption and dispersion effects of nanoporous silicon, we used the Maxwell-Garnett model to describe the porous materials.

Finally, the case of the porous silicon (*n = 1.72*) structure obtained after *20* minutes of HCl etching is studied. In this case, an oxidation process actuated by the HCl aqueous solution, which yields a highly oxidized porous silicon skeleton, is taken into account. In order to describe the absorption and dispersion effects of nanoporous silicon, the well-known Maxwell-Garnett model is used to describe the porous materials. The best agreement between experimental and calculated reflectance spectra for the *340 nm* etched opals is obtained for a structure with *73.7%* SiO_2 and *26.3%* air volume fractions, for which the refractive index value is *n = 1.72* at the energy *E = 1.4 eV*. A discretization in *5* cylinders of the non-overlapping region and *5* cylinders for each overlapping region and *31* plane-waves are considered (i. e. each sphere is discretized in *15* cylinders). Fig. 6.11 shows, from left to right, the band diagram, the experimental reflectance spectrum measured at normal incidence, and the corresponding theoretical spectrum. The main stop-band appears at energy (*E = 1.45 eV*) for both experimental and theoretical spectra. Although the material absorption and dispersion are considered, a high-energy feature appears in the

UNIVERSITAT ROVIRA I VIRGILI
DESIGN AND MODELLING OF PHOTONIC CRYSTALS WITH ANISOTROPIC COMPONENTS
Joaquin Cos Córcoles
ISBN:978-84-693-9433-5/DL:T.69-2011

theoretical spectrum. This spectrum feature may correspond to the region between *2.6 eV* and *2.8 eV* of the band diagram where the refractive index dispersion is not considered (we expect the pseudogaps to appear at higher energies).

6.5 Conclusions

An approach based on the scattering matrix method for the analysis of opal structures has been developed. This approach is based on the description of the spheres as a stacking of cylinders. In contrast with previous works, this approach allows to subdivide the overlapping region in more than one cylinder. This feature is allowed by the scattering matrix approach that is suitable for any unit cell geometry because it does not require inversion symmetry, and consequently the borum-nitride lattice can be employed for the description of the layers at the overlapping region.

This approach has been applied for two studies, a theoretical study of the high-energy features of opals and a characterization of three samples corresponding to the three main processes of the fabrication.

On one hand, it is demonstrated that the internal diffraction of the opals is the responsible for the presence of the features in the high-energy region. In this region, maxima in transmission and minima in absorption are linked and cause the existence of the features. From a sufficient number of opal layers, the different substrates (air or silica glass) do not present qualitatively differences for the spectra in the high-energy region (where appear four features) because the diffraction inside the opals and the high concentration of the electric filed inside the opals generate an absorption enhancement. Differences between optical propagation in the first and second band-gap regions has been reported in order to confirm the diffraction effects.

UNIVERSITAT ROVIRA I VIRGILI
DESIGN AND MODELLING OF PHOTONIC CRYSTALS WITH ANISOTROPIC COMPONENTS
Joaquin Cos Córcoles
ISBN:978-84-693-9433-5/DL:T.69-2011

On the other hand, the experimental spectra of three samples corresponding to a silica opal, a magnesized opal and a porous silicon opal have been compared with the calculated ones by the scattering matrix approach. The scattering effect and disorders have been taken into account considering an imaginary part of the dielectric or applying an artificial Gaussian smoothing of the theoretical spectra.

In all the cases the main stop-band appears at the same energy level for the theoretical and experimental spectra. In the case of the secondary features, they can be linked to the regions of the band diagram, where dispersion and absorption are not considered, in the Γ-L direction where pseudogaps are near to appear.

UNIVERSITAT ROVIRA I VIRGILI
DESIGN AND MODELLING OF PHOTONIC CRYSTALS WITH ANISOTROPIC COMPONENTS
Joaquin Cos Córcoles
ISBN:978-84-693-9433-5/DL:T.69-2011

Chapter 7

Summary and conclusions

The work presented in this thesis has dealt with the following subjects:

- Development of computer implementations of numerical methods for analyzing dispersion and transmission characteristics of anisotropic photonic crystals.
- Analysis of the basic characteristics of anisotropic one- and two-dimensional structures based on silicon photonic crystals and anisotropic materials, both perfect and with defects.
- Proposal and optimization of functional devices based on these structures, such as optical equalizers, switches or tunable waveguides.
- Development of a scattering matrix formalism-based numerical approach for the analysis of the optical response of opals.

UNIVERSITAT ROVIRA I VIRGILI
DESIGN AND MODELLING OF PHOTONIC CRYSTALS WITH ANISOTROPIC COMPONENTS
Joaquin Cos Córcoles
ISBN:978-84-693-9433-5/DL:T.69-2011

Since many potential applications of anisotropic photonic crystals are based on the dynamically tunable shift of the forbidden band gap or the resonance, the main attention has been paid to the analysis of dispersion and transmission characteristics. Nevertheless, due to the varied kind of structures it is not possible to face the study up with a single method. Thus, we have chosen widely used techniques for the investigation of each kind of photonic crystal. The basics of these methods have been outlined in Chapter 3. Transmission properties of one-dimensional tunable photonic crystals have been analyzed by an anisotropic transfer matrix method, while dispersion and transmission characteristics of two-dimensional tunable photonic crystals have been studied by means of plane-wave expansion and finite-differences time-domain methods.

Chapter 4 is devoted to the analysis of the transmission properties of tunable Fabry-Perot interferometer structures composed of alternating layers of silicon and liquid crystal. In particular, the tuning of the resonant wavelengths and the associated transmittance has been studied for two structures. This tuning is provided by mean of two independent liquid crystal optical axis orientations in both structures. The tuning of wavelength depends on the relative orientation between the liquid crystal optical axes, while the relative transmittance level of the two resonances depends on the difference between the liquid crystal optical axis orientation and the polarization axis. The first structure is a single-cavity Fabry-Perot where the liquid crystal optical axes at the mirrors and cavity are independent. The second structure corresponds to a double-cavity Fabry-Perot where the two cavities are made of liquid crystal, and their optical axes are independent. We have demonstrated that both structures can be applied as an optical two-channel equalizer that permits tuning the two resonances and their relative amplitude levels.

In the case of the single-cavity Fabry-Perot a tuning capability of *28 nm* can be achieved as a function of the relative orientation between the LC optical axes. For this device, *complete* equalization is achieved only where the two liquid crystal optical axes are parallel for all the orientations. The worst case corresponds to a difference of *45°* in

UNIVERSITAT ROVIRA I VIRGILI
DESIGN AND MODELLING OF PHOTONIC CRYSTALS WITH ANISOTROPIC COMPONENTS
Joaquin Cos Córcoles
ISBN:978-84-693-9433-5/DL:T.69-2011

the optical axes orientation, in which the transmittance of the unblocked channel has a minimum of *78.58%* (first resonance blocked) and *82.91%* (second resonance blocked).

In the case of the double-cavity Fabry-Perot a tuning capability of *39 nm* can be achieved as a function of the relative orientation between the LC optical axes. For this device, *complete* equalization is achieved for all the liquid crystal optical axis orientations. As a particular case, for perpendicular optical axes, the two resonances become degenerated at *1.560 μm* and both polarizations are completely transmitted. However, due to the mismatch between the refractive index of the isolator and the cavities, spurious resonances appear within the gap.

In chapter 5 we have studied and analyzed two-dimensional tunable devices based on liquid crystal and silicon. The first devices are tunable filters, based on photonic crystals without defects and with anisotropic components. We have studied the optimization of the bandgap width by changing the radius of the scatterers. We have been studied two reciprocal structures, a silicon photonic crystal with holes filled with liquid crystal and a photonic crystal composed by silicon rods surrounded by liquid crystal. For the first structure, the TE bandgap appears between the 1^{st} and 2^{nd} band and it has a 60^o periodicity with the LC optical axis orientation, α. A variation of *1.4%* of the bandgap can be obtained. Results also shown that the maximum bandgap depends very slightly on the radius of the LC cylinders. For the second structure, the TE bandgap appears between the 4^{th} and 5^{th} band for LC optical axis orientations between 0^o and 24^o and between 36^o and 60^o it has a 60^o periodicity with the LC optical axis orientation, α. A maximum bandgap width ($\Delta\omega a/2\pi c = 0.0087$) is obtained for a normalized radius of $R/a = 0.220$.

For both structures, we have also demonstrated by means of the field distributions that the change in the band gap limits depends not only on the field confinement in the LC but also on the field distribution symmetry.

We have proposed to apply these structures to an electro-optical switch, where the radius of the cylinders can be chosen to modulate the duty cycle of the switch, this is: the range of angles where the gap is closed.

UNIVERSITAT ROVIRA I VIRGILI
DESIGN AND MODELLING OF PHOTONIC CRYSTALS WITH ANISOTROPIC COMPONENTS
Joaquin Cos Córcoles
ISBN:978-84-693-9433-5/DL:T.69-2011

The second part of this chapter has been devoted to the analysis of tunable waveguides. Firstly, we have employed the plane-wave expansion method and a supercell formulation to study the tunability range of a silicon photonic crystal waveguide where a line of scatterers filled by liquid crystal acts as the core of the waveguide. Secondly we have developed a methodology for the study of the practical implementation of tunable waveguides based on silicon photonic crystals with liquid crystal-infiltrated pores.

For the analysis of the tunability range of the waveguide, the device is based on a Si-based photonic waveguide with a triangular lattice and a line of scatterers in the direction **Γ-K** infiltrated with E7 liquid crystal. The structure is modelled by the definition of a *7x1* supercell for the plane-wave expansion method. We have studied the optimization of this structure varying the size of the defect scatterers and studying the position in frequency of two guided modes.

Maximum and minimum values of the frequency of the guided modes appear for the liquid crystal optical axis orientations of $\alpha = 0^o$ and $\alpha = 90^o$. For the first guided mode there are maximum in the tunability range for $R_{def}/a = 0.420$ for the **Γ**-point and $R_{def}/a = 0.360$ for the **K**-point. For the second guided mode there are maximum in the tunability range for $R_{def}/a = 0.360$ for the **Γ**-point and $R_{def}/a = 0.500$ for the **K**-point. The field distributions for the two guided modes and for the optimal radii show a good confinement of the modes in the waveguide and high field concentration in the regions of high refractive index, corresponding to the silicon.

For the development of a methodology for the study of the practical implementation of tunable waveguides based on silicon photonic crystals with liquid crystal-infiltrated pores, by means of the FDTD method we have obtained the transmission properties of the waveguides depending on the liquid crystal optical axis orientation. Then, applying the plane-wave expansion method and a supercell formulation we have demonstrated that the differences in the transmission properties are due to a small gap between the two guided modes that opens or closes, allowing or

UNIVERSITAT ROVIRA I VIRGILI
DESIGN AND MODELLING OF PHOTONIC CRYSTALS WITH ANISOTROPIC COMPONENTS
Joaquin Cos Córcoles
ISBN:978-84-693-9433-5/DL:T.69-2011

denying the transmission of the optical beam, depending on the optical axis orientation.

Maximum and minimum transmission values for each frequency are calculated by means of the analysis of the propagation of a wide-band pulse as a function of the liquid crystal optical axis. Two regions with a maximum difference between the maximum and minimum transmission can be observed. The first region corresponds to the frequencies near $\omega a/2\pi c = 0.357$ (and can be related to the low limit of the gap) while a second region corresponds to frequencies near $\omega a/2\pi c = 0.412$. The dependence of the transmission of a monochromatic pulse of frequency $\omega a/2\pi c = 0.412$ with the angle shows a region between 30^o and 55^o where the transmitted pulse is rejected, while for the rest of orientations the pulse is transmitted. Dispersion relations of the guided modes for the same structure show that the low or high transmission of a given frequency depends on the aperture or closure of a gap between the two guided modes. For $\alpha = 0^o$ it can be seen that the two modes are degenerated and thus, there is no frequency gap between them. Instead, for $\alpha = 50^o$, the degeneration is broken as an effect of the liquid crystal orientation. The difference of the two distributions is remarkable, and this opens a gap between the two modes

Finally, chapter 6 shows how the optical response of opals can be modelled with an approach based on the scattering matrix formalism. Firstly, we demonstrate that the internal diffraction of the opals is responsible for the presence of the features in the high-energy region by comparing the optical response of different number of layer opals stacked in a glass or in the air. Secondly, we have compared the experimental spectra of several samples of opals with the calculated ones using our approach. The scattering effect and disorders have been taken into account considering the imaginary part of the dielectric or applying an artificial Gaussian smoothing of the theoretical spectra.

UNIVERSITAT ROVIRA I VIRGILI
DESIGN AND MODELLING OF PHOTONIC CRYSTALS WITH ANISOTROPIC COMPONENTS
Joaquin Cos Córcoles
ISBN:978-84-693-9433-5/DL:T.69-2011

7.1 Outlook

There are many possibilities for a future work. In the author's opinion, one of the most interesting is the application of this tuning capability to the design of electro-optical devices based in anisotropic photonic crystals.

On one-dimensional structures advances must be oriented to the design of quasi-periodic photonic crystals with anisotropic components in order to develop devices based on this kind of photonic crystals but with tunable properties. Additionally, the computer implementation of the anisotropic transfer matrix method could be modified in order to consider the absorption and dispersion of the material. This implementation would provide us with more realistic models of the simulated devices. Finally, taking advantage of the differences and the tunability of the two resonances of the Fabry-Perot interferometers, devices with a variable speed of light could be proposed for non-linear applications.

For the two-dimensional case, the combination of the dispersion relations obtained by plane-wave expansion method and the transmission properties obtained by the FDTD method provide us with a powerful tool for the design and optimization of more complex active or dynamical devices as multiplexers, filters, switches,… where applying the idea of having two independent liquid crystal optical axes used in the one-dimensional photonic crystals, the polarizations of the light could be split or the transmission of two wavelengths could be equalized.

Additionally, the substitution of silicon by nonlinear materials or the use of high birefringence liquid crystals can be studied in order to amplify the effect of anisotropy of the liquid crystal.

On the three-dimensional case, we have established a starting point for the analysis of anisotropic 3D photonic crystals, with the developing of the scattering matrix approach for isotropic opals. In this case it is clear that the work should continue with the extension of this approach to the anisotropic case and the employing of it for the design of tunable devices based on anisotropic 3D photonic crystals.

UNIVERSITAT ROVIRA I VIRGILI
DESIGN AND MODELLING OF PHOTONIC CRYSTALS WITH ANISOTROPIC COMPONENTS
Joaquin Cos Córcoles
ISBN:978-84-693-9433-5/DL:T.69-2011

References

[Adams-2005] M. Adams, G. A. De Rose, M. Loncar, A. Scherer, "Lithographically fabricated optical cavities for refractive index sensing", *Journal of Vacuum Science and Technology B* **23** 3168-3173, (2005).

[Alagappan-2006] G. Alagappan, X. W. Sun, M. B. Yu, and D. den Engelsen, "Symmetry properties of two-dimensional anisotropic photonic crystals", *Journal of the Optical Society of America A* **23** 2002-2013, (2006).

[Alagappan2-2006] G. Alagappan, X. W. Sun, P. Shum, M. B. Yu, and M. T. Doan, "One-dimensional anisotropic photonic crystal with a tunable bandgap", *Journal of the Optical Society of America B* **23** 159-167, (2006).

[Andreani-2008] L. C. Andreani, A. Balestreri, J. F. Galisteo-López, M. Galli, M. Patrini, E. Descrovi, A. Chiodoni, F. Giorgis, L. Pallavidino, and F. Geobaldo, "Optical response with threefold symmetry axis on oriented microdomains of opal photonic crystals", *Physical Review B* **78** 205304, (2008).

[Arriaga-2008] J. Arriaga, L. Dobrzynski, and B. Djafari-Rouhani, "Electrotunable band gaps of one- and two-dimensional photonic crystal structures based on silicon and liquid crystals", *Journal of Applied Physics* **104** 063108, (2008).

UNIVERSITAT ROVIRA I VIRGILI
DESIGN AND MODELLING OF PHOTONIC CRYSTALS WITH ANISOTROPIC COMPONENTS
Joaquin Cos Córcoles
ISBN:978-84-693-9433-5/DL:T.69-2011

[Ashcroft-1976] N. W. Ashcroft and N. D. Mermin, *Solid State Physics*, (Saunders College, Philadelphia, USA, 1976).

[Baier-Saip-1995] J J. A. Baier-Saip, 0. Bostanjoglo, H. J. Eichler, and R. Macdonald, "Voltage dependence of microsecond switching in a nematic optical phase modulator", *Journal of Applied Physics* **78**(5) 3020-3025, (1995).

[Balestreri-2006] A. Balestreri, L. C. Andreani, and M. Agio, "Optical properties and diffraction effects in opal photonic crystals", *Physical Review E* **74** 036603, (2006).

[Berenger-1996] J.P. Berenger, "Perfectly matched layer for the FDTD solution of wave-structure interaction problems", *IEEE Transactions on Antennas and Propagation* **44** 110-117, (1996).

[Bowley-2001] C. C. Bowley, P. A. Kossyrev, G. P. Crawford, and S. M. Faris, "Variable-Wavelength Switchable Bragg Gratings Formed in Polymer-Dispersed Liquid Crystals," *Applied Physics Letters* **79** 9-11, (2001).

[Busch-1999] K. Busch and S. John, "Liquid-crystal photonic-band-gap materials: The tunable electromagnetic vacuum", *Physical Review Letters* **83** 967-970, (1999).

[Bushyager-2006] N. Bushyager, and M. M. Tentzeris, *MRTD* (*Multi resolution time-domain*) *method in electromagnetics*, (Morgan & Claypool, Florida, 2006).

[Chutinan-2002] A. Chutinan, M. Okano, and S. Noda, "Wider bandwidth with high transmission through waveguide bends in two-dimensional photonic crystal slabs", *Applied Physics Letters* **80** 1698, (2002).

[Chutinan-2004] A. Chutinan, and S. John, "Diffractionless optical networking in an inverse opal photonic band gap micro-chip", *Photonics and Nanostructures* **2** 41-49, (2004).

[Cuesta-Soto-2004] F. Cuesta-Soto, A. Martínez, J. García, F. Ramos, P. Sanchis, J. Blasco, and J. Martí, "All-optical switching structure based on a photonic crystal directional coupler", *Optics Express* **12** 161-167, (2004).

UNIVERSITAT ROVIRA I VIRGILI
DESIGN AND MODELLING OF PHOTONIC CRYSTALS WITH ANISOTROPIC COMPONENTS
Joaquin Cos Córcoles
ISBN:978-84-693-9433-5/DL:T.69-2011

[Demus-1998] D. Demus, J. W. Goodby, G. W. Gray, H. W. Spiess, and V. Vill, *Handbook of liquid crystals*, (Vol. 2A, Wiley, New York, 1998).

[Dorado-2007] L. A. Dorado, R. A. Depine, and H. Miguez, "Effect of extinction on the high-energy optical response of photonic crystals" *Physical Review B* **75** 241101, (2007).

[Dubey-2007] R. S. Dubey and D. K. Gautamh, "Photonic bandgap analysis in 1D porous silicon photonic crystals using transfer matrix method", *Optoelectronics and Advanced Materials - Rapid Communications* **1**(9) 436 - 441, (2007).

[Espinosa-1998] V. Espinosa, F. Silva, G. J. de Valcárcel and E. Roldán, "Class-B two-photon Fabry-Perot laser", *Optics Communications* **155** 292-296, (1998).

[Fan-2001] S. H. Fan, P. R. Villenueve, J. D. Joannopoulos, H. A. Haus, "Loss-induced on/off switching in a channel add/drop filter", *Physical Review B* **64** 245302, (2001).

[Faraon-2008] A. Faraon, D. Englund, D. Bulla, B. Luther-Davies, B. J. Eggleton, N. Stoltz, P. Petroff, and J. Vuckovic, "Local tuning of photonic crystal cavities using chalcogenide glasses", *Applied Physics Letters* **92** 043123, (2008).

[Fink-1998] Y. Fink, J. N. Winn, S. Fan, C. Chen, J. Michel, J. D. Joannopoulos, E. L. Thomas, "A dielectric omnidirectional reflector", *Science* **282** 1679-1682, (1998).

[Gennes-1993] P. G. Gennes, and J. Prost, *The physics of liquid crystals*, (Oxford science publications, 1993).

[Gilardi-2010] G. Gilardi, R. Asquini, A. d'Alessandro, and G. Assanto, "Widely tunable electro-optic distributed Bragg reflector in liquid crystal waveguide", *Optics Express* **18** 11524-11529, (2010).

[Guo-2004] D G Guo, R M Lin, and W J Wang, "Modelling and optimization of a Fabry-Perot microcavity for sensing applications", *Journal of Optics A* **6** 1027-1035, (2004).

UNIVERSITAT ROVIRA I VIRGILI
DESIGN AND MODELLING OF PHOTONIC CRYSTALS WITH ANISOTROPIC COMPONENTS
Joaquin Cos Córcoles
ISBN:978-84-693-9433-5/DL:T.69-2011

[Ha-2001] Y. K. Ha, Y. C. Yang, J. E. Kim, H. Y. Park, C. S. Kee, H. Lin, and J. C. Lee, "Tunable omnidirectional reflection bands and defect modes of a one-dimensional photonic band structure with liquid crystals", *Applied Physics Letters* **79** 15-17, (2001).

[Heavens-1965] O. S. Heavens, *Optical properties of thin solid films*, (Dover, New York, 1965).

[Hecht-2002] E. Hecht, A. Zajaz *Optics*, (Adison-Wesley, Reading, 1974).

[Hirabayashi-1993] K. Hirabayashi, H. Tuda, and T. Kurokawa "Tunable liquid crystal Fabry-Perot interferometer filter for wavelength-division multiplexing communication systems", *Journal of Lightwave Technology* **11**(12) 2033-2043, (1993).

[Hughes-2009] S. Hughes and P. Yao, "Theory of quantum light emission from a strongly-coupled single quantum dot photonic-crystal cavity system", *Optics Express* **17** 3322-3330, (2009).

[Inoue-2004] K. Inoue, and K. Ohtaka, *Photonic crystals: Physics, fabrication and applications*, (Springer, New York, 2004).

[Intoni-2009] F. Intonti, S. Vignolini, F. Riboli, M. Zani, D. S. Wiersma, L. Balet, L. H. Li, M. Francardi, A. Gerardino, A. Fiore, and M. Gurioli, "Tuning of photonic crystal cavities by controlled removal of locally infiltrated water", *Applied Physics Letters* **95** 173112, (2009)

[Jin-2002] J. Jin, *The finite element method in electromagnetics*, (Wiley, New York, 2002).

[Joannopoulos-1995] J. D. Joannopoulos, S. G. Johnson, J. N. Winn, and R. D. Meade, *Photonic crystals: Molding the flow of light*, (Princeton Univ. Press, Princeton, New Jersey 1995).

[John-1987] S. John, "Strong localization of photons in certain disordered dielectric superlattices", *Physical Review Letters* **58** 2486-2489, (1987).

UNIVERSITAT ROVIRA I VIRGILI
DESIGN AND MODELLING OF PHOTONIC CRYSTALS WITH ANISOTROPIC COMPONENTS
Joaquin Cos Córcoles
ISBN:978-84-693-9433-5/DL:T.69-2011

[Karakali-2009] T. Karacali, M. Alanyalioglu, and H. Efeoglu, "Single and double Fabry-Perot structure based on porous silicon for chemical sensors", *IEEE Sensors Journal* **9** 1667-1672, (2009).

[Kitahara-2004] H. Kitahara, M. W. Takeda, M. Iida, M. Tani, M. Watanabe, and K. Sakai, "Reflection Losses of Finite Periodic Photonic Crystals", *Laser Optics* **14**(5) 654-659, (2004).

[Kittel-1953] C. Kittel, *Introduction to solid state physics*, (Wiley, New York, 1953).

[Knabe-2010] S. Knabe, N. Soleimani, T. Markvart, and G. H. Bauer, "Efficient light trapping in a fluorescence solar collector by 3D photonic crystal", *Physica Status Solidi - Rapid Research Letters* **4** 118-120, (2010).

[Knight-1998] J. C. Knight, J. Broeng, T. A. Birks, and P. St. J. Russell, "Photonic Band Gap Guidance in Optical Fibers", *Science* **282** 1476- 1478, 1998.

[Ko-1988] D. Y. K. Ko, and J. R. Sambles, "Scattering-matrix method for propagation of radiation in stratified media: attenuated total reflection studies if liquid crystals", *Journal of the Optical Society of America A* **5** 1863-1866, (1988).

[Kopperschmidt -2001] P. Kopperschmidt, "Tunable band gaps in electro-optical photonic bi-oriented crystals", *Applied Physics B* **73** 717-720, (2001).

[Lei-2010] P. H. Lei, S. H. Wang, F. S. Juang, Y. H. Tseng, and M. J. Chung, "Effect of SiO_2/Si_3N_4 dielectric distributed Bragg reflectors (DDBRs) for Alq_3/NPB thin-film resonant cavity organic light emitting diodes", *Optics Communications* **283** 1933-1937, (2010).

[Leonard-2000] S. W. Leonard, J. P. Mondia, H. M. van Driel, O. Toader, S. John, K. Busch, A. Birner, U. Gösele, and V. Lehmann, "Tunable two-dimensional photonic crystals using liquid crystal infiltration", *Physical Review B* (*Rapid Communication*) **61** 2389-2392, (2000).

UNIVERSITAT ROVIRA I VIRGILI
DESIGN AND MODELLING OF PHOTONIC CRYSTALS WITH ANISOTROPIC COMPONENTS
Joaquin Cos Córcoles
ISBN:978-84-693-9433-5/DL:T.69-2011

[Li-2005] X. Li, and Z. Liu, "Bending and branching of acoustic waves in two-dimensional phononic crystals with linear defects", *Physics Letters A* **338** 413-419, (2005).

[Li-2010] Y. G. Li, and R. M. Almeida, "Simultaneous broadening and enhancement of the 1.5 μm photoluminescence peak of Er^{3+} ions embedded in a 1-D photonic crystal microcavity", *Applied Physics B* **98** 809-814, (2010).

[Liscidini-2008] M. Liscidini, D. Gerace, L. C. Andreani, and J. E. Sipe, "Scattering-matrix analysis of periodically patterned multilayers with asymmetric unit cells and birefringent media", *Physical Review B* **77** 035324, (2008).

[Liu-2004] Y. G. Li, and R. M. Almeida, "Tunable photonic crystal waveguide coupler with nematic liquid crystals", *IEEE Photonics Technology Letters*, **16**(8) 1849-1851, (2004)

[Liu-2005] C. Y. Liu, L. W. Chen, "Tunable field-sensitive polarizer using hybrid conventional waveguides and photonic crystal structures with nematic liquid crystals", *Optics Communications* **256** 114-122, (2005).

[Liu-2006] C. Y. Liu, L. W. Chen, "Tunable channel drop filter in a two-dimensional photonic crystal modulated by a nematic liquid crystal", *Journal of Nanomaterials* **2006** 52946, (2006).

[Luan-2001] P. G. Luan and Z. Ye, "Two dimensional photonic crystals", *Condensed Matter* **1** 0105428, (2001).

[Maksymov-2006] I. S. Maksymov, L. F. Marsal and J. Pallarès, "An FDTD analysis of nonlinear photonic crystal waveguides", *Optics and Quantum Electronics* **38** 149-160, (2006).

[Mandatori-2003] A. Mandatori, C. Sibilia, M. Centini, G. D'Aguanno, M. Bertolotti, M. Scalora, M. Bloemer, and C. M. Bowden, "Birefringence in one-dimensional finite photonic bandgap structure", *Journal of the Optical Society of America B* **20**(3) 504-513, (2003).

UNIVERSITAT ROVIRA I VIRGILI
DESIGN AND MODELLING OF PHOTONIC CRYSTALS WITH ANISOTROPIC COMPONENTS
Joaquin Cos Córcoles
ISBN:978-84-693-9433-5/DL:T.69-2011

[Mao-1994] Z. M. Mao and W. P. Huang, "Analysis of polarization rotation in periodically loaded rib waveguide by transfer matrix method", *Journal of Lightwave Technology* **12** 768-773, (1994).

[Maune-2005] B. Maune, J. Witzens, T. Baehr-Jones, M. Kolodrubetz, H. Atwater, A. Scherer, R. Hagen, and Y. Qiu, "Optically triggered Q-switched photonic crystal laser", *Optics Express* **13** 4699-4707, (2005)

[Mazzoleni-1995] C. Mazzoleni, and L. Pavesi "Application to optical components of dielectric porous silicon multilayers", *Applied Physics Letters* **67** 2983-2985, (1995).

[Meade-1991] R. D. Meade, K. D. Brommer, A. M. Rappe, and J. D. Joannopoulos, "Photonic bound states in periodic dielectric materials", *Physics Review B* **44** 13772-13774, (1991).

[MEEP-2010] A. F. Oskooi, D. Roundy, M. Ibanescu, P. Bermel, J. D. Joannopoulos, and S. G. Johnson, "MEEP: A flexible free-software package for electromagnetic simulations by the FDTD method", *Computer Physics Communications* **181** 687-702, (2010).

[Mekis-1996] A. Mekis, J. C. Chen, I. Kurland, S. Fan, P. R. Villeneuve, and J.D. Joannopoulos, "High transmission through sharp bends in photonic crystal waveguides", *Physical Review Letters* **77** 3787-3790, (1996).

[Mingaleev-2004] S. F. Mingaleev, M. Schillinger, D. Hermann, and K. Busch, "Tunable photonic crystal circuits: concepts and designs based on single-pore infiltration", *Optics Letters* **29** 2858-2860, (2004).

[Nair-2007] R. V. Nair, and R. Vijaya, "Observation of higher-order diffraction features in self-assembled photonic crystals" *Physical Review A* **76** 053805, (2007).

[Ortega-1999] B. Ortega, J. Capmany, and J. L. Cruz, "Wavelength division multiplexing all-fiber hybrid devices based on Fabry-Perot's and gratings", *Journal of Lightwave Technology* **17** 1241-1247, (1999).

UNIVERSITAT ROVIRA I VIRGILI
DESIGN AND MODELLING OF PHOTONIC CRYSTALS WITH ANISOTROPIC COMPONENTS
Joaquin Cos Córcoles
ISBN:978-84-693-9433-5/DL:T.69-2011

[Ozaki-2003] R. Ozaki, T. Matsui, M. Ozaki, and K. Yoshino, "Electrically color-tunable defect mode lasing in one-dimensional photonic-band-gap system containing liquid crystals", *Applied Physics Letters* **82** 3593-3595, (2003).

[Ozaki-2005] R. Ozaki, M. Ozaki, and K. Yoshino, "Light propagation analysis and high-speed electro-optic switching in one-dimensional photonic crystal with nematic liquid crystal defect layer", *Electronics and Communications in Japan* **88** 46-53, (2005).

[Ozaki-2007] R. Ozaki, H. Moritake, K. Yoshino, and M. Ozaki, "Analysis of defect mode switching response in one-dimensional photonic crystal with a nematic liquid crystal defect layer", *Journal of Applied Physics* **101** 033503, (2007).

[Painter-1999] O. Painter, R. K. Lee, A. Scherer, A. Yariv, J. D. O'Brien, P. D. Dapkus, I. Kim, "Two-Dimensional Photonic Band-Gap Defect Mode Laser", *Science* **284** 1819-1821, (1999).

[Pallavidino-2010] L. Pallavidino, M. Liscidini, A. Virga, A. Chiodoni, E. Descrovi, J. Cos, L. C. Andreani, F. Geobaldo, and F. Giorgis, "Synthesis of amorphous silicon/magnesia based direct opals with tunable optical properties" *Chemistry of Materials*, Submitted, (2010).

[Perilloux-2002] B. E. Perilloux, *Thin-film design: Modulated thickness and other stopband design methods*, (SPIE Press, 2002).

[Rayleigh-1887] J. W. Rayleigh, "On the maintenance of vibrations by forces of double frequency, and on the propagation of waves through a medium endowed with a periodic structure", *Philosophical Magazine* **24** 145-159, (1887).

[Sakoda-2001] K. Sakoda, *Optical properties of photonic crystals*, (Springer-Verlag, Berlin, 2001).

[Sánchez-Meroño-2010] A. Sánchez-Meroño, J. Arias, and M. M. Sánchez-López, "Negative group delay of reflected pulses on microstrip slabs and Bragg reflectors", *IEEE Journal of Quantum Electronics* **46** 546-553, (2010).

UNIVERSITAT ROVIRA I VIRGILI
DESIGN AND MODELLING OF PHOTONIC CRYSTALS WITH ANISOTROPIC COMPONENTS
Joaquin Cos Córcoles
ISBN:978-84-693-9433-5/DL:T.69-2011

[Santamaria-2008] D. A. Santamaria Razo, L. Pallavidino, E. Garrone, F. Geobaldo, E. Descrovi, A. Chiodoni, and F. Giorgis, "A version of Stöber synthesis enabling the facile prediction of silica nanospheres size for the fabrication of opal photonic crystals", *Journal of Nanoparticle Research* **10** 1225-1229, (2008).

[Schaadt-2007] D. M. Schaadt, O. Brandt, S. Ghosh, T. Flissikowski, U. Jahn, and H. T. Grahn, "Polarization-dependent beam switch based on an M-plane GaN/AlN distributed Bragg reflector", *Applied Physics Letters* **90** 231117, (2007).

[Schneider-2001] G. J. Schneider, S. Hanna, J. L. Davis, and G. H. Watson, "Defect modes in coaxial photonic crystals", *Journal of Applied Physics* **90** 2642-2649, (2001).

[Schuller-2005] Ch. Schuller, J. P. Reithmaier, J. Zimmermann, M. Kamp, A. Forchel, and S. Anand, "Polarization-dependent optical properties of planar photonic crystals infiltrated with liquid crystals", *Applied Physics Letters* **87** 121105, (2005)

[Song-2007] Q. H. Song, S. M. Xiao, X. C. Zhou, L. Y. Liu, L. Xu, Y. G. Wu, and Z. S. Wang, "Liquid-crystal-based tunable high-Q directional random laser from a planar random microcavity", *Optics Letters* **32** 373-375, (2007).

[Spelman-2002] J. Spelman, S. Skrien, and T. E. Parker, "Design methodology for a Fabry-Perot interferometer used as a Concentration Sensor", *Applied Optics* **41** 2847-2857, (2002).

[Sun-2007] X. Sun, X. Tao, T. Ye, P. Sue, Y.-S. Szeto, "2D and 3D electrically switchable hexagonal photonic crystal in the ultraviolet range", *Applied Physics B* **87** 267-271, (2007).

[Taflove-2000] A. Taflove and S. C. Hagness, *Computational electrodynamics: The finite-difference time-domain method*, (Artech: Norwood, MA, 2000).

[Takeda-2002] H. Takeda, and K. Yoshino, "Tunable photonic band schemes of opals and inverse opals infiltrated with liquid crystals", *Journal of Applied Physics* **92** 5658-5662, (2002).

UNIVERSITAT ROVIRA I VIRGILI
DESIGN AND MODELLING OF PHOTONIC CRYSTALS WITH ANISOTROPIC COMPONENTS
Joaquin Cos Córcoles
ISBN:978-84-693-9433-5/DL:T.69-2011

[Takeda-2003] H. Takeda, and K. Yoshino, "Tunable light propagation in Y-shaped waveguides in two-dimensional photonic crystals utilizing liquid crystals as linear defects", *Physical Review B* **67** 073106, (2003).

[Takeda-2004] H. Takeda and K. Yoshino, "TE-TM mode coupling in two-dimensional photonic crystals composed of liquid-crystal rods", *Physical Review E* **70** 026601, (2004).

[Talneau-2002] A. Talneau, Ph. Lalanne, M. Agio, and C. M. Soukoulis, "Low-reflection photonic-crystal taper for efficient coupling between guide sections of arbitrary widths", *Optics Letters* **27**(17) 1522-1524, (2004).

[Tolmachev-2007] V. A. Tolmachev, T. S. Perova, S. A. Grudinkin, V. A. Melnikov, E. V. Astrova, and Yu. A. Zharova, "Electrotunable in-plane one-dimensional photonic structure based on silicon and liquid crystal", *Applied Physics Letters* **90** 011908, (2007).

[Torrent-2008] D. Torrent, and J. Sánchez-Dehesa, "Anisotropic mass density by two-dimensional acoustic metamaterials", *New Journal of Physics* **10** 023004, (2008).

[Trifonov-2004] T. Trifonov, L. F. Marsal, A. Rodríguez, J. Pallarès, and R. Alcubilla, "Effects of symmetry reduction in two-dimensional square and triangular lattices", *Physical Review B* **69** 235112, (2004).

[Vandenbem-2006] C. Vandenbem, J.P. Vigneron, and J.M. Vigoureux, "Tunable band structures in uniaxial multilayer stacks", *Journal of the Optical Society of America B* **23** 2366-2376, (2006)

[Villar-2003] I. Del Villar, I. R. Matias, F. J. Arregui, and R. O. Claus, "Analysis of one-dimensional photonic band gap structures with a liquid crystal defect towards development of fiber-optic tunable wavelength filters", *Optics Express* **11** 430-436, (2003).

[Weiss-2005] S. M. Weiss, H. Ouyang, J. Zhang, and P. M. Fauchet, "Electrical and thermal modulation of silicon photonic bandgap microcavities containing liquid crystals", *Optics Express* **13** 1090-1097, (2005).

UNIVERSITAT ROVIRA I VIRGILI
DESIGN AND MODELLING OF PHOTONIC CRYSTALS WITH ANISOTROPIC COMPONENTS
Joaquin Cos Córcoles
ISBN:978-84-693-9433-5/DL:T.69-2011

[Whittaker-1999] D. M. Whittaker, and I. S. Culshaw, "Scattering-matrix treatment of patterned multilayer photonic structures", *Physical Review B* **60** 2610, (1999).

[Xifre-2007] E. Xifré, L.F. Marsal, J. Pallarès, and J. Ferré-Borrull, "Porous silicon omnidirectional mirrors and distributed Bragg reflectors for planar waveguide applications", *Journal of Applied Physics* **102** 063111, (2007).

[Yablonovitch-1987] E. Yablonovitch, "Inhibited Spontaneous Emission in Solid-State Physics and Electronics", *Physics Review Letters* **58** 2059-2062, (1987).

[Yablonovitch-1993] E. Yablonovitch, "Photonic band-gap structures", *Journal of the Optical Society of America B* **10** 283-295, (1993).

[Yeh-1979] P. Yeh, "Electromagnetic propagation in birefringent layered media", *Journal of the Optical Society of America* **69**(5) 742-756, (1979).

[Yoshino-1999] K. Yoshino, Y. Shimoda, Y. Kawagishi, K. Nakayama, and M. Ozaki, "Temperature tuning of the stop band in transmission spectra of liquid-crystal infiltrated synthetic opal as tunable photonic crystal", *Applied Physics Letters* **75**(7) 932-934, (1999).

[Yu-2004] L. H. Yu, K. L. Yao, and Z. L. Liu, "Electronic structures of filled tetrahedral semiconductors LiMgN and LiZnN: conduction band distortion" *Physica B* **353** 278-286, (2004).

[Zografopoulos-2007] D. C. Zografopoulos, E. E. Kriezis, B. Bellini, and R. Beccherelli, "Tunable one-dimensional photonic crystal slabs based on preferential etching of silicon", *Optics Express* **15** 1832-1844, (2007).

UNIVERSITAT ROVIRA I VIRGILI
DESIGN AND MODELLING OF PHOTONIC CRYSTALS WITH ANISOTROPIC COMPONENTS
Joaquin Cos Córcoles
ISBN:978-84-693-9433-5/DL:T.69-2011